LEPAE – Laboratory for Process, Environmental and Energy Engineering

Chemical Engineering Department

Faculty of Engineering – University of Porto

Treatment of textile effluents by Fenton-like oxidation processes with carbon-based catalysts

Dissertation presented for the Doctor of Philosophy degree in Chemical and Biological Engineering at the Faculty of Engineering of University of Porto by

Filipa Mesquita Alves Castro Duarte

Supervisor: Professor Luis Miguel Palma Madeira

Co-supervisor: Professor Francisco José Maldonado-Hódar

May 2013

Agradecimentos

Faço questão de mencionar nesta secção algumas pessoas/instituições que merecem todo o meu respeito e reconhecimento.

É obviamente o caso, em primeiro lugar, do meu orientador, o Professor Miguel Madeira, e também do meu co-orientador, Professor Francisco Maldonado-Hódar (Universidade de Granada), pela disponibilidade e apoio contínuos. Foi realmente um privilégio poder "sugar" as suas sabedorias e visões durante as longas horas de discussão. Ao Prof. Maldonado-Hódar agradeço também a hospitalidade com que me recebeu na sua cidade e nos seus laboratórios.

Ao Doutor Herney Ramirez, que me iniciou nestas "lides" e me explicou pormenorizadamente a instalação para os ensaios e o seu funcionamento. Falando de operações e instalações, não me posso esquecer do Mestre Luís Carlos Matos, que tem o dom de solucionar todos os problemas técnicos, e outros.

Ainda na esfera académica, agradeço às inúmeras pessoas que me acompanharam nestes anos, com a sua ajuda, amizade e bom humor. É o caso do Sérgio Torres, César Águia, Joana Ângelo, Vera Gonçalves, Tânia Lopes, Sílvia Coelho, Carmen Rodrigues, Cátia Oliveira, Marta Boaventura, Margarida Catarino e outros mais que sabem quem são. Uma palavra especial para o José Carlos Pires.

Gostaria de agradecer à Fundação para a Ciência e Tecnologia pela bolsa de doutoramento (SFRH/BD/44703/2008), ao CRUP pelo Projecto de Cooperação Portugal-Espanha – Acção Integrada AI-E/11, e à Fundação Calouste Gulbenkian por ter financiado parte da minha viagem a San Diego para participar no congresso AOTs-16, em 2010. Agradeço também ao LEPAE por me ter disponibilizado todos os meios e recursos para realizar o trabalho.

E como os últimos são os primeiros, aos meus amigos e à minha família. Os meus amigos, não vou enumerar, porque felizmente são muitos e bons. Vou apenas fazer referência ao grupo das K's, das bailarinas e das "Chepas". Estão no meu coração. Para a minha família, não há palavras. Vão ser sempre poucas.

Ao meu tio.

“…we have a situation…”

Preface

This PhD thesis results from research work carried out at LEPAE (Laboratory for Process, Environmental and Energy Engineering), in the Chemical Engineering Department of FEUP (Faculty of Engineering – University of Porto), throughout the period between January 2009 and March 2013, and is based on different papers published and/or submitted for publication in international journals. The work related to the preparation and characterization of materials was mostly developed at the Inorganic Chemistry Department of the Faculty of Sciences – University of Granada, Spain.

In this work different series of specific catalysts for the treatment of textile effluents by the heterogeneous Fenton-like reactions were developed. Carbon materials as supports, iron oxides as the active phase and azo-dyes as target molecules were used. The main goal was to develop a catalytic system for the continuous treatment of textile effluents by applying a fixed-bed reactor. Nevertheless, the selection of the best catalyst was carried out in batch reactors because smaller amounts of samples are required. The optimization of the process was performed using several techniques both to characterize the materials and evaluate the quality of the treated solutions.

This thesis is divided in 8 Chapters and begins with the analysis of the state of the art – Chapter 1, where the main aspects related to the pollution generated by the textile industry and the different remediation possibilities are described. The advantages of the advanced oxidation processes applied to wastewater treatment are pointed out regarding other conventional treatments, focusing mainly on the Fenton's reagent, either in homogeneous or heterogeneous phase.

In Chapter 2, details of the experimental procedure adopted are reported, with the description of the experimental set-ups and operating conditions. The characterization and analytical techniques used are also briefly described.

The optimization of the catalysts started with the selection of the most suitable activated carbon (AC) support among three different commercial samples

(Chapter 3). The influence of the morphology and textural parameters on their adsorption/catalytic behaviour is presented.

Chapter 4 deals with the influence of the iron salt precursor in the development of AC/Fe catalysts for heterogeneous Fenton-like reactions. Three different iron salts were used for impregnating the AC support selected in Chapter 3 in order to choose the best option. The iron dispersion/location in the porous structure and active phase obtained in each case were related with the adsorption/catalytic performance of the obtained catalysts.

Chapter 5 addresses particular attention to the characterization of spent samples to clarify the involved processes in the dye removal from water during the heterogeneous Fenton process. Particularly, the catalyst with the characteristics selected in Chapters 3 and 4 was analyzed before and after adsorption/oxidation runs and such results were related with the nature of oxidation products formed.

To design a continuous fixed-bed column, additional parameters such as the particle size of the support had to be optimized. So, in Chapter 6 the influence of the particle size of the AC support is evaluated using four different size ranges. Kinetic and mass-transport parameters were obtained in each case and catalytic performances related to chemical and physical properties of the materials.

The information gathered from Chapters 3 - 6 allowed the selection of the most active and stable catalyst, obtained by combination of the best support, particle size and iron precursor. Thus, in Chapter 7 the performance and stability of a column filled with the selected catalyst was tested, thus operating in continuous mode, for the degradation of a model dye and also a real textile effluent. The main operating conditions (pH, temperature and H_2O_2 dose) were optimized for the model compound. Although in the preceding Chapters it has been used Orange II as the target molecule, in this section one used the Alcian Blue as the model dye in order to shorten the reaction time.

Chapter 8 compiles the main conclusions of this thesis and perspectives / suggestions for future work.

Abstract

This thesis deals with the removal of dyes from wastewater by the heterogeneous Fenton process using activated carbons (ACs) as the iron support. In short, the Fenton's reagent is based on the generation of the powerful hydroxyl radicals by the catalytic decomposition of hydrogen peroxide by a transition metal catalyst like iron. The AC is herein used to immobilize the catalyst (iron species) avoiding the production of iron-containing sludge as it happens in the classical homogeneous Fenton process, once metals dissolved in water are also contaminants that should not be discharged into the natural water cycle.

The main goal was to implement a fixed-bed reactor able to work in continuous mode, in such a way that the catalyst should be active and stable. The study began with experiments in batch reactors (because less amounts of catalyst are required) using the azo-dye Orange II (OII) as model compound in order to optimize the catalyst and better understand the involved co-existing phenomena (adsorption and catalysis). In all runs, discoloration of dye solutions was followed continuously by the absorbance measurement; mineralization degree and leaching levels (loss of Fe from the catalyst to the solution) were evaluated by total organic carbon (TOC) and atomic absorption analyses, respectively. All catalysts were prepared to have 7 wt. % of iron (Fe/AC) and were texturally and chemically characterized by several complementary techniques.

To optimize the catalyst, the most adequate AC support was initially selected. For that, a comparison study was carried out between three commercial activated carbons: supplied by Norit, Merck and Kynol. The ACs were impregnated with iron (II) acetate and both supports and catalysts were extensively characterized. Correlations between their properties and adsorptive or catalytic performances were established. The Fe-Norit was found to be the most active catalyst, which was assigned to a best Fe dispersion favoured by its high surface area located on large micropores. These textural characteristics also favoured the OII adsorption process. Nevertheless, it was also detected that leaching is favoured by the iron dispersion, in

such a way that a compromise situation should be reached between catalytic activity (iron dispersion) and leaching.

After identifying the most promising AC support, the best iron precursor was also selected. Therefore, the AC – Norit RX 3 Extra (simply called N) – was impregnated with three different iron salts precursors: iron acetate, iron sulphate, and iron nitrate. The different interactions between the impregnating solutions and the supports led to catalysts with different textural and chemical characteristics. These properties strongly influence the different processes that contribute to the dye removal: adsorption, homogeneous Fenton process (due to leached iron) and heterogeneous Fenton-like process (on the catalysts' surface). Ferrous acetate was considered to be the best option on the basis of its activity and particularly stability. Iron in solution (or located more externally on the carbon surface) favoured the discoloration but somehow prevented the TOC removal (which also occurs by adsorption). Finally, the catalytic behaviour of the samples was correlated with the transformations on their textural and chemical characteristics after reaction.

A deeper analysis of the process was carried out using this optimized catalyst either in the catalytic or adsorption conditions (with and without H_2O_2). It was found that, in absence of H_2O_2, OII was adsorbed without degradation and complete TOC removal was reached by adsorption. In spite of the total discoloration, the complete TOC removal did not occurred after Fenton oxidation experiments, even after increasing the H_2O_2 dose. This means that the mineralization of the dye was not complete, and that the oxidation compounds formed were unable to be adsorbed by the catalyst, which was ascribed to a weaker interaction between them and the AC surface.

For operation in a fixed-bed reactor, it is also crucial to find the most suitable particle size of the AC support (due to the competition between internal mass transfer and reaction in the catalyst). The AC was milled and sieved in four ranges of particle size: powder (< 0.15 mm), 0.25 – 0.80 mm, 0.80 – 1.60 mm and pellets (ca. 3 × 5 mm, as received). Each fraction was impregnated with iron sulphate, which is a cheaper salt as compared to iron acetate. It was found that milling liberated porosity, enhancing the adsorption capacity and the adsorption rate in the smaller particles. The Fe dispersion is also favoured when decreasing the support particle size, but iron

leaching is promoted in this sense as well. The trade-off between activity and stability pointed to the intermediate size of 0.80 – 1.60 mm as the best choice.

Therefore the catalyst with the selected characteristics (Norit RX 3 Extra AC with particles' diameter in the range 0.80–1.60 mm, impregnated with iron acetate) was immobilized in a fixed-bed reactor and tested in the elimination of the dye Alcian Blue. A parametric study was carried out in order to find the best conditions of temperature (50 ºC), pH (2.5) and H_2O_2 concentration (30 mM in the feed) for discoloration and mineralization of the dye solution (0.01 mM in the feed). Afterwards, the efficiency of the catalytic system developed was proved in the treatment of a real textile effluent proceeding from the cotton dyeing sector. Under the optimized operating conditions and contact time, W_{cat}/Q, of 3.3 g.min.ml^{-1}, almost total discoloration (96.7 %) was achieved and a strong abatement of TOC (73.6 %), chemical oxygen demand (66.3 %) and biochemical oxygen demand (72.5 %) was verified (at steady state).

Resumo

Esta tese trata da remoção de corantes de águas residuais, nomeadamente de efluentes têxteis, pelo processo Fenton heterogéneo, usando-se carvões ativados (CAs) como suporte do ferro. Resumidamente, o reagente do Fenton baseia-se na produção de radicais hidroxilo (agentes com elevado potencial de oxidação) através da decomposição catalítica do peróxido de hidrogénio pela ação de um metal de transição, como o ferro. O CA é aqui usado para imobilizar o catalisador (espécies de ferro), evitando-se a geração de lamas contendo ferro, como acontece no caso do processo do Fenton clássico (homogéneo), uma vez que os metais em dissolução são também contaminantes que não podem ser descarregados diretamente nos cursos naturais de água.

O principal objetivo foi implementar um reator de leito-fixo, capaz de operar em contínuo, onde o catalisador fosse ativo e estável. O estudo iniciou-se com ensaios em reatores *batch* (onde são necessárias menores quantidades de catalisador), usando-se o corante azo *Orange II* (OII) como composto modelo, com vista a otimizar o catalisador e perceber melhor os fenómenos coexistentes envolvidos (adsorção e catálise). Em todos os ensaios, a descoloração das soluções foi seguida continuamente pela medição da absorvância; o grau de mineralização e os níveis de lixiviação (perda do ferro do catalisador para a solução) foram avaliados por análises de carbono orgânico total (COT) e de absorção atómica, respetivamente. Todos os catalisadores foram preparados de forma a terem um teor mássico de ferro de 7 % (Fe/CA) e foram caraterizados a nível textural e químico por diversas técnicas complementares.

Para otimizar o catalisador, primeiro selecionou-se o suporte de CA mais adequado. Para tal, foi levado a cabo um estudo comparativo entre três carvões ativados comerciais fornecidos pela Norit, Merck e Kynol. Os CAs foram impregnados com acetato de ferro (II), os suportes/catalisadores foram extensivamente caraterizados e posteriormente foram estabelecidas correlações entre as suas propriedades e os seus comportamentos (na catálise e na adsorção). O Fe-Norit foi considerado o catalisador mais ativo, o que foi atribuído à melhor dispersão do ferro, favorecida pela elevada área superficial do Norit, localizada nos seus

microporos largos. Estas caraterísticas também favoreceram a adsorção do OII. No entanto, foi detetado que a lixiviação é também promovida neste sentido, por isso deve ser procurada uma situação de compromisso entre atividade (dispersão do ferro) e lixiviação.

Depois de identificado o carvão ativado mais promissor como suporte, foi também selecionado o melhor precursor de ferro. Assim, o CA – Norit RX 3 Extra (N) – foi impregnado com três diferentes sais de ferro: acetato de ferro, sulfato de ferro e nitrato de ferro. As diferentes interações entre as soluções precursoras de sais de ferro e o suporte levaram à obtenção de catalisadores com distintas caraterísticas texturais e químicas. Estas propriedades têm uma forte influência nos diferentes processos que contribuem para a remoção do corante: adsorção, Fenton por via homogénea (devido ao ferro lixiviado) e processo tipo Fenton heterogéneo (na superfície do catalisador). O acetato de ferro foi considerado a melhor opção, com base na sua atividade e, particularmente, na sua estabilidade. O ferro em solução (ou localizado mais exteriormente na estrutura porosa do catalisador) favoreceu a descoloração, mas impediu de alguma forma a remoção do COT (que ocorre também por adsorção). Por último, o comportamento catalítico das amostras foi relacionado com as transformações que ocorreram nas suas características texturais e químicas induzidas pela reação de oxidação.

Usando o catalisador previamente selecionado, foi então efetuada uma análise mais profunda sobre o processo, nas condições de catálise e de adsorção (com e sem H_2O_2). Foi observado que, na ausência de H_2O_2, as moléculas de OII foram adsorvidas sem degradação e houve remoção total do COT. Apesar da total descoloração, a remoção completa do COT não foi verificada após os ensaios catalíticos, mesmo depois de se aumentar a concentração inicial de oxidante. Isto significa que a mineralização do corante foi parcial, e que os produtos de oxidação formados não foram adsorvidos pelo catalisador, o que foi atribuído a uma interação mais fraca entre estes e a superfície do CA.

Para a operação num reator de leito-fixo é também crucial otimizar o tamanho das partículas do suporte de CA (devido à competição entre fenómenos de transferência de massa e reação no catalisador). Assim, o CA foi moído e peneirado de forma a se obterem quatro diferentes gamas de tamanhos: pó (< 0.15 mm), 0.25 – 0.80 mm, 0.80 – 1.60 mm e *pellets* (com cerca de 3 × 5 mm – forma comercial).

Cada fração foi impregnada com sulfato de ferro, um sal mais barato quando comparado nomeadamente com o acetato de ferro. Verificou-se que a moagem libertou porosidade, favorecendo a capacidade e velocidade de adsorção nas partículas mais pequenas. A dispersão do ferro foi também promovida pela diminuição do tamanho das partículas do suporte, mas a lixiviação foi igualmente favorecida neste sentido. O balanço entre atividade e estabilidade apontam para o tamanho intermédio (0.80 - 1.60 mm) como a melhor escolha.

Assim, o catalisador com as características previamente selecionadas (Norit RX 3 Extra, com diâmetro de partículas na gama 0.80 – 1.60 mm, impregnado com acetato de ferro) foi imobilizado num reator de leito-fixo e testado na eliminação do corante *Alcian Blue*. Foi feito um estudo paramétrico para encontrar as melhores condições de temperatura (50 ºC), pH (2.5) e concentração de H_2O_2 (30 mM na alimentação) na descoloração e mineralização da solução de corante (0.01 mM na alimentação). De seguida, a eficiência do sistema catalítico desenvolvido foi provada no tratamento de um efluente têxtil real proveniente do tingimento de algodão. Usando as condições de operação otimizadas e um tempo de contato, W_{cat}/Q, de 3.3 $g.min.ml^{-1}$, atingiu-se, em estado estacionário, praticamente a descoloração total do efluente e uma forte redução do COT (73.6 %), da carência química de oxigénio (66.3 %) e da carência bioquímica de oxigénio (72.5 %).

Resumen

Esta Tesis Doctoral trata sobre la eliminación de colorantes de aguas residuales usando procesos heterogéneos con catalizadores de hierro soportados sobre carbones activados. De forma resumida, el reactivo Fenton está basado en la generación de radicales hidroxilos que son muy poderosos como oxidantes, formados en este caso por la descomposición catalítica del peróxido de hidrógeno por metales de transición, como el hierro. El carbón activado se usa para inmovilizar la fase activa (las especies de hierro) evitando así la etapa final de precipitación del hierro en disolución con formación de lodos, puesto que los metales en disolución son también contaminantes que no pueden ser vertidos.

El objetivo final fue el diseño y puesta a punto de un reactor de lecho fijo capaz de trabajar de forma continua, para lo que se requiere un catalizador activo y estable. El estudio comienza con experimentos en reactores discontinuos agitados, puesto que la cantidad de catalizador necesaria es mucho menor, se usa el colorante Orange II como compuesto modelo, tanto para optimizar el catalizador como para el conocimiento de los fenómenos que participan en el proceso (adsorción y catálisis). En todos los experimentos, la decoloración de la disolución del contaminante se analiza continuamente mediante medidas de absorbancia; el grado de mineralización y los niveles de Fe que pasan del catalizador sólido a la disolución se analizaron mediante medidas del carbono orgánico total (COT) y absorción atómica, respectivamente. Todos los catalizadores se prepararon al 7% en peso de Fe y fueron caracterizados físico- químicamente mediante diversas técnicas complementarias.

Para optimizar el catalizador, se seleccionó inicialmente el carbón activado (CA) más adecuado. Para ello se llevó a cabo un estudio previo entre tres CA comerciales proporcionados por Norit, Merck y Kynol. Estos CA se impregnaron con acetato ferroso y se caracterizaron tanto los soportes como los catalizadores y se establecieron correlaciones entre su comportamiento en experiencias de adsorción y catálisis con los parámetros texturales y químicos. El catalizador Fe-Norit fue el más activo debido a la mejor dispersión de la fase activa lograda gracias a su alta área superficial localizada fundamentalmente en microporos anchos. Estas características

texturales también favorecen su comportamiento en procesos de adsorción. Sin embargo, se encontró también que la pérdida de fase activa por solubilización del Fe está favorecida también por una mayor dispersión, de tal manera, que se debe adoptar una situación de compromiso entre actividad (dispersión del hierro) y lixiviación.

A continuación, se seleccionó también el mejor precursor de hierro. Por tanto, usando el CA Norit RX3 (Extra), en adelante llamado N, se prepararon catalizadores usando como precursores el acetato ferroso, el sulfato ferroso y el nitrato férrico. Las diferentes interacciones del CA con sus correspondientes disoluciones producen catalizadores con diferencias texturales y químicas. Estas propiedades influencian todos los aspectos involucrados en la eliminación del colorante mediante los materiales preparados: adsorción, procesos Fenton en homogéneo (producidos por el Fe que se solubiliza) y procesos Fenton heterogéneos (sobre la superficie del catalizador). El acetato ferroso resultó ser la mejor opción en base a su actividad y particular estabilidad. Se demostró que el hierro en disolución, y el localizado en la superficie externa de las partículas del CA, favorecen los procesos de decoloración, pero, de alguna manera, evitan la remoción del COT (incluso por procesos de adsorción). Finalmente, se caracterizaron algunas muestras usadas en reacción y se relacionó las transformaciones texturales y químicas con el comportamiento catalítico.

Usando el catalizador previamente seleccionado, se efectuó entonces un análisis más profundo sobre el proceso en las condiciones de los experimentos de catálisis y adsorción (con y sin H_2O_2). Se encontró que en ausencia de H_2O_2, el OII se adsorbe sin degradación, obteniendo una completa eliminación del COT en disolución. Sin embargo, tras los experimentos catalíticos, aunque se obtiene una rápida y total decoloración de la disolución, no se logra la eliminación total del COT. Esto pone de manifiesto que la mineralización del contaminante no es completa y que los productos de oxidación intermedios no son adsorbidos por el catalizador, lo que se debe a una menor interacción de éstos con la superficie del CA.

Para el desarrollo del reactor de lecho fijo, es crucial determinar el tamaño de partícula del CA más adecuado debido a la competición entre los procesos de transferencia interna y la reacción. El CA fue molturado y tamizado en cuatro rangos de tamaño de partícula: polvo (< 0.15 mm), 0.25 – 0.80 mm, 0.80 – 1.60 mm y pellet (aprox. 3 x 5 mm en su forma comercial). Cada una de estas fracciones se impregnó

con sulfato ferroso, dado que es un precursor más barato que el acetato, para preparar los correspondientes catalizadores. Al moler, la porosidad el CA se va liberando, de forma que aumenta la capacidad y la velocidad de adsorción en las partículas más pequeñas (menores restricciones difusionales). Por la misma razón, la dispersión del Fe se favorece también en este sentido, y con él la pérdida de fase activa por solubilización. La situación de compromiso entre actividad y estabilidad indica que la mejor opción es, por tanto, usar un tamaño intermedio (0.80 – 1.60 mm).

Por lo tanto, finalmente se preparó la cantidad necesaria del catalizador optimizado con las características seleccionadas, es decir, el soporte N con un tamaño de partícula de 0.80 – 1.60 mm, impregnado con acetato ferroso para preparar un reactor de lecho fijo, que fue usado en la eliminación del colorante *Alcian Blue* - 0.01 mM en la alimentación. Se ha llevado a cabo un estudio de los parámetros operacionales, determinando como óptimo una temperatura de 50ºC, un pH de 2.5 y una concentración de H_2O_2 de 30 mM en la alimentación continua del reactor. Se ha analizado también la eficiencia de nuestro sistema catalítico en el tratamiento de una muestra real de aguas procedentes de los efluentes de una industria textil dedicada a dar color a tejidos de algodón. En las condiciones óptimas de operación y usando un tiempo de contacto (W_{cat}/Q) de 3.3 g.min.ml^{-1}, se obtiene en estado estacionario prácticamente la decoloración total de la disolución (96.7 %) con una fuerte reducción de los valores de COT (73.6 %), de la demanda química de oxígeno (66.3 %) y de la demanda biológica de oxígeno (72.5 %).

Table of Contents

List of Figures

List of Tables

Nomenclature

a – molar absorptivity ($L.mol^{-1}.cm^{-1}$)

Abs – absorbance (dimensionless)

a_m – molecular area ($m^2.molecule^{-1}$)

A_p – area of the catalyst particle (cm^2)

b – optical path length (cm)

C – concentration ($mol.L^{-1}$)

c – dimensionless constant of BET equation

$C_{OII,s}$ – Orange II concentration at the catalyst's surface conditions ($mol.cm^{-3}$)

D_e – effective diffusion coefficient ($cm^2.s^{-1}$)

d_p – particle size (mm)

E_0 – characteristic adsorption energy ($kJ.mol^{-1}$)

E_a – activation energy ($kJ.mol^{-1}$)

k – kinetic constant ($mol^{1-n}.L^{n-1}.s^{-1}$), n – reaction order

k_{obs} – observed rate constant ($(mol.g^{-1}.s^{-1}).(cm^3.mol^{-1})^n$), n – reaction order

k_v – true rate constant ($(mol.g^{-1}.s^{-1}).(cm^3.mol^{-1})^n$), n – reaction order

L_0 – mean micropore size (nm)

m – O_2 consumption rate ($mg.g_{vss}^{-1}.h^{-1}$)

n_{AD} – homogeneity degree of the microporous system (dimensionless)

n^a – amount of gas adsorbed per adsorbent mass unit ($mol.g^{-1}$)

N_A – Avogadro number ($molecules.mol^{-1}$)

n_m^a – monolayer's capacity ($mol.g^{-1}$)

n_{obs} – apparent reaction order (dimensionless)

P – pressure (Pa)

P/P_0 – relative pressure (dimensionless)

P_0 – saturation vapour pressure (Pa)

Q – volumetric flow rate ($ml.min^{-1}$)

R – ideal gas constant ($kJ.mol^{-1}.K^{-1}$)

r – radius of the spherical catalyst particle (cm)

r_{obs} – observed reaction rate ($mol.g^{-1}.s^{-1}$)

$r_{v,s}$ – true reaction rate ($mol.g^{-1}.s^{-1}$)

S_{BET} – surface area obtained using the Brunauer-Emmett-Teller (BET) equation ($m^2.g^{-1}$)

S_{mic} – micropores' surface area ($m^2.g^{-1}$)

T – temperature (K / ºC)

V_{BJH} – mesopores' volume calculated by Barret, Joyner and Halenda method ($cm^3.g^{-1}$)

V_{gas} – adsorbed gas volume per adsorbent mass unit ($cm^3.g^{-1}$)

V_{meso} – mesopores' volume calculated by the Gurvitch's rule ($cm^3.g^{-1}$)

V_p – volume of the catalyst particle (cm^3)

W – volume of gas adsorbed (expressed as liquid) in the micropores ($cm^3.g^{-1}$)

W_0 - total micropore volume ($cm^3.g^{-1}$)

W_{cat} – amount of catalyst (g)

β – affinity coefficient (dimensionless)

η – effectiveness factor (dimensionless)

λ_{max} – characteristic wavelength (nm)

ρ_{ap} – catalyst apparent density ($g.cm^{-3}$)

ϕ_g – generalized Thiele's modulus (dimensionless)

Abbreviations

AAS – atomic absorption spectrometry

AB – Alcian Blue

AC – activated carbon

AC/Fe – activated carbon impregnated with iron

AOP – advanced oxidation process

BOD – biological oxygen demand

COD – chemical oxygen demand

FTIR – Fourier transform infrared spectroscopy

HRTEM – high resolution transmission electron microscopy

OII – Orange II

SEM – scanning electron microscopy

TG and DTG – Thermogravimetry and differential thermogravimetry

TOC – total organic carbon

TPD – Temperature-programmed desorption

XPS – X-ray photoelectron spectroscopy

XRD – X-ray diffraction

CHAPTER 1- Introduction

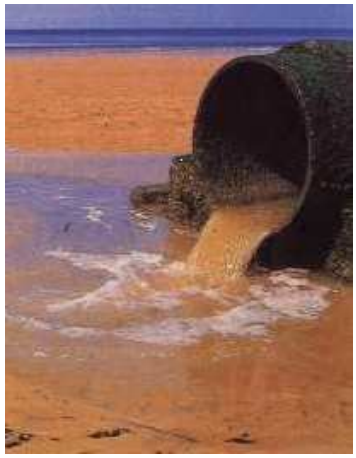

Chapter 1. Introduction

1.1. The textile industry

1.1.1. Characterization of the sector

The textile industry plays an essential role in the economy of several countries around the world since a long time ago. It is believed that textiles have risen in Egypt, India, Turkey and China and the first evidences of this fact were found thousands years BC [1]. Nowadays, the importance of textile activity worldwide grows every year, which is proved by the increase of the global fibre production, exceeding 70 million tonnes in 2009 (Figure 1.1) [2].

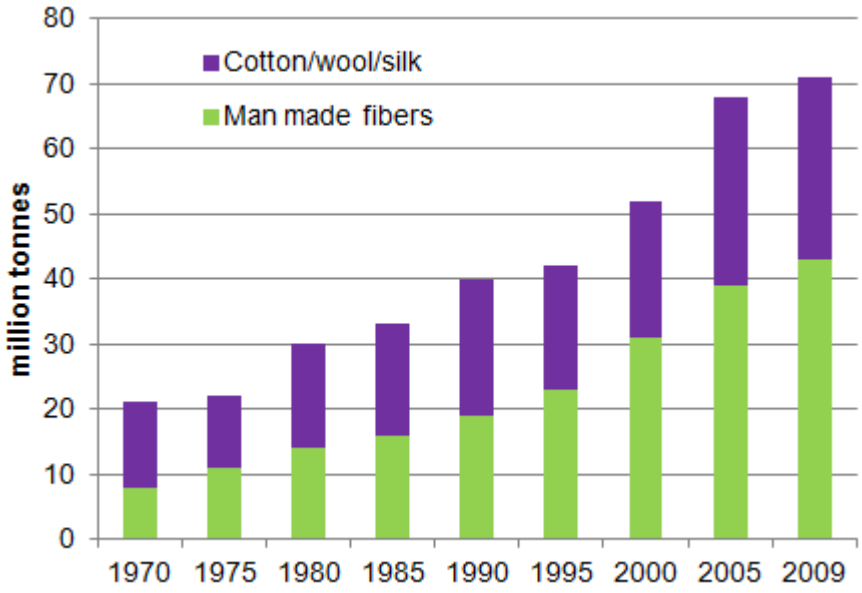

Figure 1.1 – Global fibre production since 1970 until 2009 (adapted from [2]).

China continues with its tradition on the textile industry sector, being the largest exporter of textile products, followed by the USA, Japan, Pakistan, Turkey, Taiwan and Korea [3]. Among European Union countries, Italy, Germany, France and United Kingdom are the biggest textile products exporters [3], but Portugal has also a relevant position, special taking into account the relatively small dimension of the Portuguese

economy. Actually, the textile and clothing industry has a great impact on the economy of Portugal, being one of the most important and representative industries. According to ATP (Textile and Clothing Association of Portugal) [4], the textile sector represents in Portugal (data related to 2011):

- *10 % of the total exportations;*
- *19 % of the employment in the transformation industry;*
- *8 % of the total manufacturing business volume;*
- *8 % of the manufacturing production.*

In this way, the textile industry involves in Portugal millions of Euros every year and thousands of jobs, as shown in Table 1.1.

Table 1.1 – Portuguese textile industry characterization (adapted from [4]).

	2005	**2006**	**2007**	**2008**	**2009**	**2010**	**2011**
Production (millions €)	6 756	6 749	6 733	6 147	5 687	5 782	5 220
Business Volume (millions €)	6 993	6 931	6 980	6 404	5 781	6 361	6 267
Exportations (millions €)	4 118	4 237	4 347	4 086	3 504	3 742	4 056
Importations (millions €)	2 993	3 296	3 411	3 290	3 041	3 296	3 315
Employment	201 265	186 837	180 335	168 206	157 145	150 929	147 711

In 2010, Portugal had around 70 thousand enterprises working in the sector and sub-sectors of textile and clothing industry. Some of them are vertical enterprises (covering the entire manufacturing process), but most of them are small and medium businesses working on the sub-sectors of the textile and clothing industry; they are characterized by their flexibility, efficiency, know-how and innovation [4]. This activity is typically located in the North of Portugal, namely in the Ave hydrographical bay, between Porto and Braga (see Fig. 1.2). Lisbon zone has also some textile industries and Covilhã (East of Portugal) is known by the manufacturing of wool products.

Figure 1.2 – Map of Portugal: main textile industry centres (adapted from [5]).

1.1.2. Textile manufacturing process

The raw materials in the textile industry undergo a complex cycle of production that is constituted by several stages until being transformed into the final product. Four main steps should be distinguished: yarn formation, fabric formation, wet processing and fabrication. Figure 1.3 represents a typical textile processing flowchart.

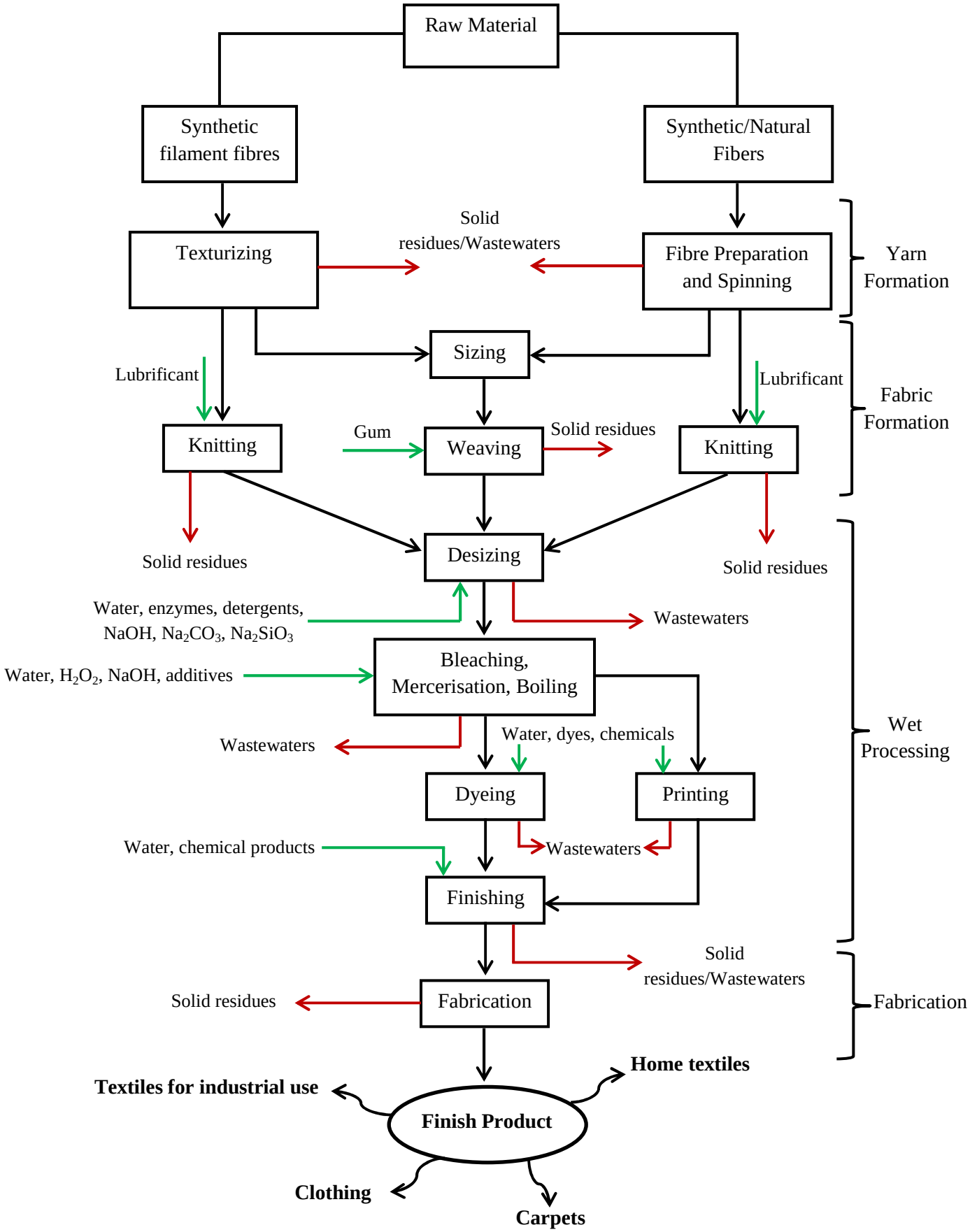

Figure 1.3 – Typical textile processing flowchart (adapted from [6]) with effluents and residues streams.

Briefly, the first stage aims to prepare the raw material for the subsequent steps. Synthetic, carded and combed fibres are produced being “spinning” – the dried mechanical process to get the yarn. The “knitting” step transforms the yarns into mesh using a lubricant to reduce friction [7] while “weaving” operation converts yarns into cloths. In this stage, a specific treatment is carried out to increase the yarn resistance, using a gum obtained from i) starch, ii) carboxymethylcellulose, iii) polyacrylates or iv) polyvinyl alcohol. The three last substances are easier to recover and reuse than starch [7]. The “desizing” is done by using an enzyme or an oxidation process when starch is used or by washing with alkaline detergents if the gum is soluble. Thereafter, several processes can be applied, such as “boiling”, “bleaching” and “mercerisation”. “Boiling” consists in a sodium hydroxide treatment at high temperatures to remove natural impurities such as waxes, alcohols and pectins; “bleaching” serves to remove the natural dye from the fibres through oxidants at high temperatures; “mercerisation” stage is only used with cotton to give it more bright and resistance by using high sodium hydroxide concentrations at low temperatures and normally adding wetting agents and/or detergents. At the end of this stage, the materials are washed to remove the excess of sodium hydroxide. The main goal of the “dyeing” step is to give colour to the knits and woven, being the choice of the dye dependent on the fibre. Here a reduction of the dye is promoted and then an oxidation process is carried out to fix the dye onto the fibre, in an alkaline medium. Then, the fibres are washed with water and detergents to remove the non-fixed dye. To obtain textile products with patterns and different colours, they follow to the “printing” phase. In the “finishing” step, the textiles are ended and tuned according to the characteristics required for the final application. Chemical or mechanical treatments can be carried out [7]. Chemical processes allow increasing the stability of the material and improving appearance and touch, making use of a wide range of chemical products (softeners, thermoplastic resins, thermosetting resins, biocides, anti-moth and anti-static reagents, etc). Mechanical finishing includes carding, cutting, shrinkage by compression and drying, etc. Finally, knits and woven go for the fabrication stage, which can take place in the same plant or in another. Here, the textiles are modelled and cut and the final product manufactured.

1.1.3. Environmental problems associated to the textile industry

The textile industry is a very important activity from the economical point of view, but it can represent a serious risk for the environment in the regions where this activity is more intensive. As it can be observed in Fig. 1.3, huge amounts of water, chemical products and additives are used in textile industry (green arrows), which have a significant negative impact on the environment after expelled as solid residues and wastewaters (red arrows).

The main problems resulting from textile activity are related to the water and air pollution, as well as to the energy consumption for raising the temperature of the baths and for drying operations. Air contamination results mainly from the emission of volatile organic compounds that come from organic solvents and the release of CO_2, SO_x and NO_x and other gases associated to the on-site burning of fossil fuels to produce thermal energy [8]. Solid residues also constitute an important environmental issue and they should be forwarded to suitable landfills to be treated, according to their characteristics and toxicity.

However, water pollution is known to be the most worrying problem associated to textile industry. Firstly, the textile manufacturing deals with huge amounts of water and that is why plants are usually located in the valleys of rivers. According to data available from the technological centre of the textile and clothing industries of Portugal (CITEVE - Centro Tecnológico das Indústrias Têxtil do Vestuário de Portugal), the water consumption in the Portuguese textile industries varies between 90,000 m^3/year and 800,000 m^3/year, which corresponds to a specific water consumption of 50 to 250 m^3/ton of textile product [8, 9]. Water consumption and generation depends however on the stage of the process.

Additionally, the intensive use of chemical reagents, most of which are non-retained in the fibres [10], together with the impurities present in the raw material, leads to the generation of tonnes of strongly polluted wastewaters throughout the textile process. The textile effluents composition depends on the different organic-based compounds, chemicals and dyes used in the industrial dry and wet-processing steps [11, 12], but are generally characterized by high temperatures and pH, intense colouration due to unfixed dyes and high organic load resulting from organic matter, mostly persistent and toxic substances [13].

Dyes are essential reagents in the dyeing and printing stages and are extensively used in textile industry. Even if used in small amounts, dyestuffs provoke coloured effluents, which are unsightly and contribute strongly to water pollution. These molecules are complex and difficult to degrade, and will be the target compounds to degrade in this work.

1.1.4. Dyes

Dyes are applied to impart colour to a substrate making use of the selective absorption of light. There is a huge variety of colours and types of dyes and they find application in a wide range of activities, from textile to food, going through paper, cosmetics and plastics' industries. Dyes can be sold in different physical forms, such as powders, granular, liquid solutions and pastes (Fig. 1.4).

Figure 1.4 – Dyes: powder form (a), pastes (b), liquid solutions (c) and granular (d).

Dyes are molecules that comprise two key components: the chromophore, responsible for the dye colour, and the functional group, auxochorome, which bonds the dye to the fibre [14-16].

The most important chromophores are azo (–N=N–), carbonyl (–C=O), methine (–CH=), nitro ($–NO_2$) and quinoid groups, and the most common auxochromes are amine ($–NH_3$), carboxyl (–COOH), sulfonate ($–SO_3H$) and hydroxyl (–OH) groups [16].

Dyes are grouped in classes taking into account their characteristics, being the most relevant classifications those related with the chemical structure and application process. In the first group one can find the azo and anthraquinones, the most common, but also triaryl-methanes, diphenyl-methanes, sulfurs, etc. Actually, azo dyes represent the largest part of the dyes production, although they constitute a serious risk for the environment and for the human health due to their high toxicity and even to their supposed carcinogenic properties [8, 17-19]. Considering the application process of dyes, they can be divided into disperse, azoic, vat, sulphur, acid, reactive, direct, mordant, metal complex and basic dyes [15]. Azo dyes are found in some of these categories, such as acid, basic, direct, disperse and azoic.

The adsorption and retention process of the dye inside the fibre can be chemical, physical or both, depending on the textile fibre and dye [15]. The adsorptive strength is controlled by several factors such as contact time, temperature, pH, the presence of auxiliary chemicals (intensively used in the dyeing stage) [14], and depends also on the fibre/dye combination. One of the biggest inconvenient related to the use of dyes is that in the most part of the cases there is not a total fixation of the dye on the fibre, yielding loss of a significant part that will integrate the produced wastewaters. Table 1.2 shows examples of different dye/fibre combinations and the respective dye losses.

Table 1.2 – Estimated unfixed dye percentages depending on the fibre/dye class combination [8, 20].

Fibre	**Dye class**	**Unfixed dye (%)**
Cellulose	Direct	5-30
	Reactive	10-50
	Sulphur	10-40
	Vat	5-20
Polyamide	Acid	5-20
Acrylic	Basic	0-5
Polyester	Disperse	0-10
Wool	Metal-complex	2-10

Thus, the dyeing stage contributes significantly to the organic load of the final textile effluent. This fact is due not only to un-fixed dyes but also to the large range of

substances used as auxiliaries in this step. Parameters like biological oxygen demand (BOD), chemical oxygen demand (COD), pH and colour intensity of textile effluents easily exceed the legal limits imposed for the direct discharge on the natural water cycle. Therefore, these effluents must be treated in order to comply with legislated standards or to decrease their toxicity and/or increase their biodegradability for subsequent biological treatment.

1.2. Textile effluents treatment processes

The current growth of environmental concerns has led to the development of technologies that fight against this problem and contribute for the air, water and soil protection and decontamination. Particularly for the wastewaters treatment, a wide range of processes were already tested or are being developed, involving physical, biological and chemical technologies, or a combination of them.

1.2.1. Conventional methods

Textile effluents can be discharged or reused after submitting them to appropriate treatments stages, being different treatments applied according to each situation. Generally, in the Portuguese textile industry, wastewaters are pre-treated and then discharged into municipal wastewater treatment plants. However, the larger textile plants manage and treat their own wastewaters.

Physical treatments like coagulation followed by flotation or sedimentation are particularly useful in the removal of solids from textile wastewaters but are inefficient in eliminating colour and dissolved organics [21]. For that, adsorption is widely used, namely on activated carbons [22, 23], which is a process significantly more efficient. However, these kind of treatments, as all the physical ones, do not promote the destruction of the pollutants and are limited to transfer them from one phase to another. So, other technologies have been developed and implemented, *e.g.* making use of microorganisms. Concerning biological processes, several approaches are found in the literature (*e.g.* [16, 23]) that use bacteria in the presence (aerobic systems) or absence

(anaerobic systems) of oxygen to remove certain pollutants. However, many of the compounds usually present in textile effluents, as is the case of several dyes, are non biodegradable and can be toxic to the microorganisms used in the biological systems, slowing or even preventing these processes.

On the other hand, chemical processes are able to overcome the limitations above mentioned, namely through catalysis, becoming a powerful tool for the oxidation of organic pollutants [24]. Particularly, recent progresses in the wastewaters treatment field yielded to the development of the so called advanced oxidation processes (AOPs) that have shown to be a promising technology, able to destroy a large range of persistent and dangerous organic pollutants [25], including dyes (*e.g.* [26-29]). Thus, the following section will be dedicated to a deeper insight of AOPs, namely in the coloured wastewaters treatment perspective.

1.2.2. Advanced oxidation processes

The increased social and political awareness for the environmental protection, namely regarding to water quality control, together with the limitations of the conventional treatments in reducing water pollution by degrading hazardous pollutants, motivated the research field of wastewaters treatment. In this way, many important progresses have been made, namely the development of advanced oxidation processes. Actually, several works have already proved the efficiency of this technology, which is able to totally or partially degrade a wide range of persistent pollutants under relatively mild conditions of temperature and pressure [25-42].

AOPs exploit the reactive power of free radicals generated by chemical reactions, electron beams, UV light or ultrasound pulses [17] to attack and destroy the contaminants. Traditionally, AOPs make use of the highly reduction potential of hydroxyl radicals ($HO^{\bullet}$), one of the strongest inorganic oxidants after elemental fluorine [43, 44]. These radicals should ideally lead to the total mineralization of the organics, i.e., oxidizing them up to carbon dioxide and water. However, chemical, photochemical and electrochemical reactions continuously generate simple (i.e. small) organic compounds such as acetic, maleic and oxalic acids, acetone or simple chloride derivates

that can persist in the treated waters [17, 44]. The scheme presented in Figure 1.5 presents the most common AOPs applied to wastewater treatments [42, 45].

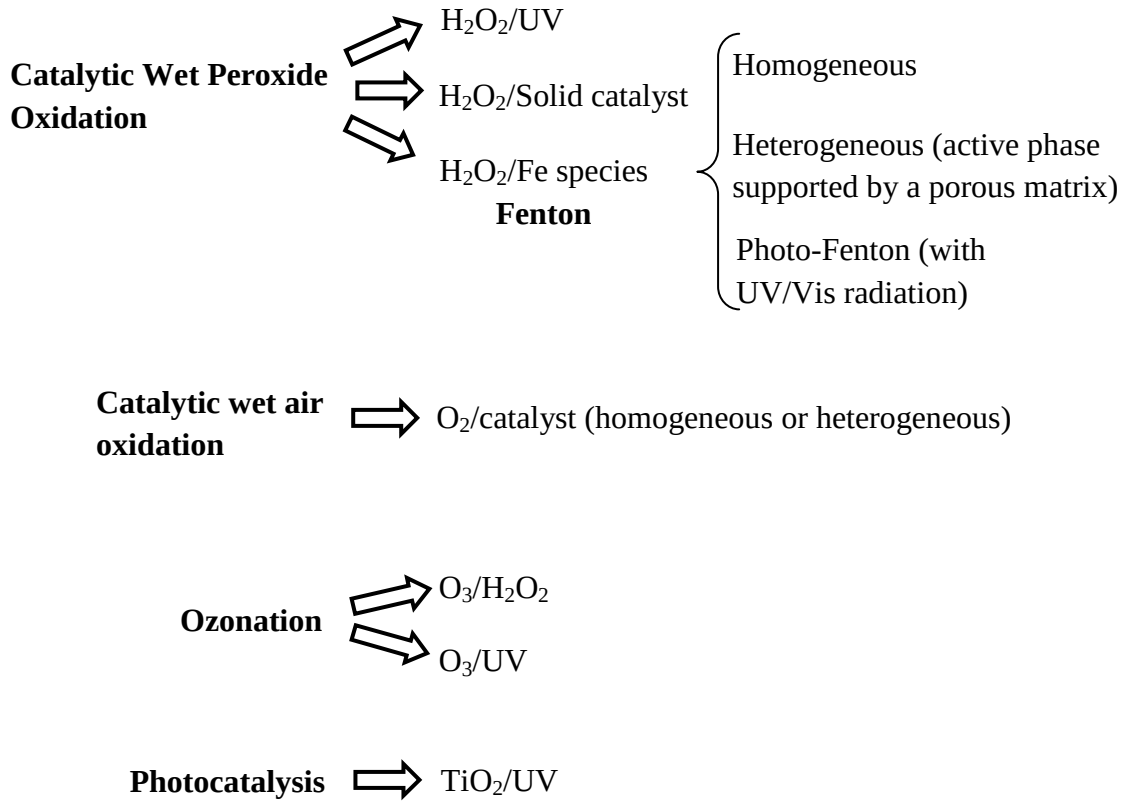

Figure 1.5 – Some relevant advanced oxidation processes for wastewaters treatment.

Every process mentioned in Figure 1.5 has advantages and disadvantages. Particularly, the processes that make use of light lead to high costs due to the equipment and electrical consumptions of UV/Vis radiation, being eventually a good option for countries with a high incidence of solar radiation, where artificial radiation sources can be substituted by the natural light. Additionally, light can be absorbed by substrate molecules rather than the oxidant, which reduces the efficiency of the process, because, although direct photolysis can produce photochemical reactions, this rarely contributes for a substantial decrease of the total organic carbon (TOC), indicative parameter of the mineralization levels [42]. AOPs based on O_3 oxidant present quite often good results in terms of contaminants elimination [46, 47], but involve complex equipments such as an ozone generator, a cooling system and pre-and post-treatment sections to dry the air fed to the ozonator and to abate the residual ozone in the off-gas, respectively [42, 48]. All

these requirements yield to expensive setups, the bigger handicap of this technology. This is also the main drawback of the catalytic wet air oxidation processes (CWAO), once they usually work under high temperature and pressure conditions, which require specific equipment and imply high costs.

On the other hand, Fenton-based processes are known for their simplicity, efficiency and low investment cost [44]. This thesis is specially focused on the use of the Fenton and Fenton-like reagent, namely the heterogeneous Fenton process, where the active phase (Fe species) is supported over a porous matrix. For this reason, the two approaches, homogeneous and heterogeneous Fenton, will be described below, as well as the basis of the photo-Fenton reaction, using UV/Vis radiation.

1.2.2.1. The homogeneous Fenton's reagent

The Fenton's reagent is probably the oldest AOP studied and applied in the wastewater field [45], and one of the most common too. The history of Fenton's process remotes to 1894, when Henry J. Fenton found that Fe (II) was able to activated H_2O_2 to oxidize tartaric acid [40]. In 1934, Haber and Weiss [49] reported that the active oxidant generated by the Fenton reaction is the hydroxyl radical ($HO^{\bullet}$), one of the most active oxidants known (E^o = 2.80 V). Since then, thousands of scientific articles about the Fenton reaction were reported, being one of the most remarkable published by Walling, in 1975 [50]. Such manuscript deals with the oxidation of organic compounds and establishes the chemical pathways of the Fenton's reagent having in mind the contemporary challenges, which relaunched the interest for this technology.

The Fenton's reagent-based process has already proved to be able to treat efficiently effluents generated in a wide range of industries such as pharmaceutical, pulp and paper, food, and cork processing, among others [51], being particularly useful in the textile activity because it promotes the easy discoloration of wastewaters from the dyeing stage. Beyond that, Fenton's treatment is applied to reduce high percentages of organic load, in terms of chemical oxygen demand (COD) or total organic carbon (TOC), and to increase biodegradability of wastewaters, reducing their toxicity by removing recalcitrant and hazardous compounds. Dependently of the final quality of treated water desired and its fate, the Fenton's process may therefore be the final step of the treatment or be followed by a conventional biological treatment.

The Fenton's reaction is based on the activation of hydrogen peroxide by Fe (II), which causes the dissociation of the oxidant, leading to the generation of highly reactive $HO^{\bullet}$ radicals in acidic medium, that attack and destroy the organic matter. Thus, this process involves an electron transfer between H_2O_2 and the iron, which acts as homogeneous catalyst [25, 52, 53]. Other transition metals can eventually be used as the active phase but, by far, the most common and active is iron [34, 44, 50].

Fenton's reagent involves several steps and a complex mechanism but can be summarized by the following equations ((1.1) to (1.7)), where *k* is the kinetic constant in each elementary step, which value varies however from author to author [54-56]:

$$Fe^{2+} + H_2O_2 \rightarrow Fe^{3+} + HO^- + HO^{\bullet} \qquad k_1 = 51\text{-}100\ M^{-1}s^{-1} \qquad (1.1)$$

$$Fe^{2+} + HO^{\bullet} \rightarrow Fe^{3+} + HO^- \qquad k_2 = 3\text{-}4.3\times10^8\ M^{-1}s^{-1} \qquad (1.2)$$

$$Fe^{3+} + H_2O_2 \rightarrow Fe^{2+} + H^+ + HO_2^{\bullet} \qquad k_3 = 0.05\text{-}0.27\ M^{-1}s^{-1} \qquad (1.3)$$

$$H_2O_2 + HO^{\bullet} \rightarrow HO_2^{\bullet} + H_2O \qquad k_4 = 1.2\text{-}4.5\times10^7\ M^{-1}s^{-1} \qquad (1.4)$$

$$H_2O_2 \rightarrow \frac{1}{2}O_2 + H_2O \qquad k_5 = 0.001\ s^{-1} \qquad (1.5)$$

$$2HO^{\bullet} \rightarrow H_2O_2 \qquad k_6 = 5.3\times10^9\ M^{-1}s^{-1} \qquad (1.6)$$

Particularly, Eq. (1.3) concerns to catalyst regeneration. The $HO^{\bullet}$ radicals are then used to attack organics non-selectively:

$$HO^{\bullet} + Org. \rightarrow Org.^{\bullet} \rightarrow \ldots \rightarrow CO_2 + H_2O \qquad k_7 = 10^7\text{-}10^{10}\ M^{-1}s^{-1} \qquad (1.7)$$

The mechanism and kinetics of the H_2O_2 decomposition by ferric and ferrous ions to produced hydroxyl radicals has been widely described and information on this field can easily be found in the literature (*e.g.* [49, 57-63]). It is generally accepted that the decomposition of H_2O_2 results from a chain of reactions that cyclically regenerate Fe^{2+} and Fe^{3+} as H_2O_2 is consumed.

Fenton reagent is known to destroy organic compounds when many conventional processes fail due to the high toxicity and/or refractory nature of the pollutants. In addition, it is an inexpensive technology, being carried out under moderate operating conditions (atmospheric pressure and temperatures close to the

room one) and does not require very specific equipment [44]. It is also noteworthy that hydrogen peroxide is safe, easy to handle, and environmentally friendly once its self-decomposition leads to non-toxic products (H_2O and O_2) - Eq. (1.5).

However, the Fenton's process is susceptible to operating conditions and parameters that may constrain the effectiveness of the process. The most important are: temperature, pH, initial pollutant concentration/organic load, initial H_2O_2 dose, concentration and nature of iron species. The focal aspects and effects of the main variables for the Fenton's process are briefly described below.

a) Effect of temperature

In general, the increase of temperature leads to the increase of the reaction rate, according to the Arrhenius law, because rate constants increase exponentially with temperature (Eq. 1.8):

$$k = k_0 \exp\left(\frac{E_a}{RT}\right) \tag{1.8}$$

where k_0 is the global constant rate, R is the ideal gas constant, E_a the activation energy and T the temperature. Thus, degradation of organics is usually promoted by increasing the temperature.

However, excessively high temperatures (typically above 50-70 ºC) should not be used in Fenton's treatment because they promote the thermal decomposition of H_2O_2 into oxygen and water (e.g. [29]), diverting the oxidant from its main function (production of hydroxyl radicals to oxidize organics) and obviously jeopardizing the treatment process.

b) Effect of pH

Fenton reactions run usually under acidic conditions (pH from 2 to 4) because it leads to the optimum rate of free radicals generation [64-67]. Walling (1975) [50] concluded that this fact is related to the requirement of H^+ ions for the H_2O_2

decomposition, which was traduced in the simplified reaction of the overall Fenton chemistry advanced by this author:

$$2Fe^{2+} + H_2O_2 + 2H^+ \rightarrow 2Fe^{3+} + 2H_2O \quad (1.9)$$

At low pH values (< 2) the Fenton's process can however be negatively affected because excessive H^+ leads to the formation of stable $H_3O_2^+$ species by consuming hydrogen peroxide, compromising Eq. (1.1) and, consequently, the formation of hydroxyl radicals [54]. On the other hand, for pH values above the optimum (pH > 4) there are parallel/undesirable effects: i) fast H_2O_2 decomposition into molecular oxygen instead of reactive species (hydroxyl radicals) [68]; ii) Fe^{3+} precipitation, and consequently, the decrease of the Fe^{2+} regeneration rate (Eq. 1.3) [10, 69].

c) Effect of H_2O_2 initial concentration

Generally, the initial H_2O_2 dose employed is higher than the stoichiometric amount required to guarantee the oxidation of the total organic load because a part of the oxidant is not transformed into active species, forming water and molecular oxygen, or is consumed in parallel reactions. However, care should be taken to avoid waste of oxidant (and money) because excess of oxidant may not contribute to improve the performance of the reaction. Actually, the initially concentration of H_2O_2 has very often an optimum value, H_2O_2 added above this limit leading to the scavenging effect, where the hydroxyl radicals are consumed in an undesirable way (Eq. 1.4) [50], contributing for the decrease of the Fenton's process efficiency [70-72] – Fig. 1.6. It is noteworthy that Eq. 1.4 shows the production of another radical, $HO_2^{\bullet}$, but its oxidation potential is significantly lower than that of the hydroxyl radical one [44, 54].

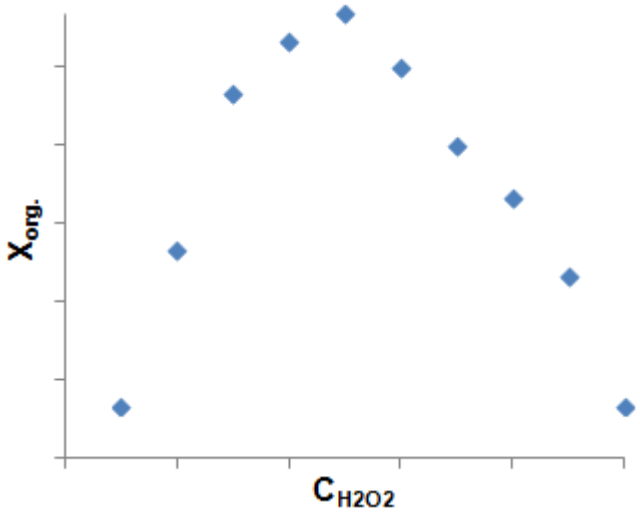

Figure 1.6 – Scheme for the illustration of the typical effect of H_2O_2 initial concentration on organics conversion by the Fenton's reagent.

d) Effect of iron concentration

As already mentioned, in the Fenton's process iron ions act as catalysts, being used to activate H_2O_2 to produced hydroxyl radicals that will subsequently attack and destroy the organic matter. In a first stage, the increase of the iron concentration leads to the increase of the oxidation rate, because more radicals are produced in the same period of time. Nevertheless, further iron doses have usually negative effects on the efficiency of the process because ferrous ion itself can be a hydroxyl radicals scavenger, promoting the reaction represented by Eq. (1.2) [50, 72-75].

Care should also be taken concerning the production of undesirable Fe-containing sludges, favoured by high Fe^{2+}/H_2O_2 ratios.

Therefore, the operating conditions should be carefully optimized, do not forgetting either the type of wastewater to handle or the final fate of the treated effluent.

1.2.2.2. The photo-Fenton's Reagent

The Fenton's process can still be improved by UV/Vis radiation thanks to the interaction of radiation with Fenton's species, which promotes additional formation of

hydroxyl radicals by the photolysis of H_2O_2 and/or Fe^{3+} species, still contributing for Fe^{2+} regeneration to feed reactions (1.1) and (1.2) [76, 77]:

$$H_2O_2 + h\nu \rightarrow 2HO^{\bullet} \quad (1.10)$$

$$Fe(HO)^{2+} + h\nu \rightarrow HO^{\bullet} + Fe^{2+} \quad (1.11)$$

This technology is widely used nowadays for wastewaters treatment. In what concerns to dyes removal, many works can be found in the literature (*e.g.* [71, 74, 78-81]), where good results are presented towards dyes elimination, mainly compared to the Fenton's reagent without radiation (dark-Fenton), once the rate of oxidation reaction is increased by the additional $OH^{\bullet}$ generation in the presence of radiation. Eventually, direct photolysis of dyes can also contribute for the increase of dyes elimination rates, if the molecules can absorb in the range of wavelengths emitted by the radiation source. However, it is noteworthy that an improvement in the discoloration rates may not mean an equal improvement in mineralization degree (i.e., breaking of the chromophores' bonds, but without further oxidation of the dyes' molecules). For that, the presence of a catalyst is usually required – photo-Fenton process.

On the other hand, it is worth mentioning that most of the works on this field use artificial UV/UV-Vis light sources, which compromises the economical viability of this technology. The use of solar radiation can be an alternative, mainly in countries with high solar radiation incidence, like Portugal and the other Mediterranean countries.

1.2.2.3. The heterogeneous Fenton's reagent

This dissertation is specially focused on the heterogeneous Fenton process. Actually, the homogeneous Fenton treatment shows to be simple and efficient to degrade a wide range of pollutants, but has an important disadvantage: the production of Fe-containing sludge (as mentioned above), contaminating the treated water with iron (typically 50-80 ppm [82]), which is significantly above the legal limit imposed by the European Union directives - 2 ppm [83]. The removal of Fe sludge implies the introduction of another stage on the treatment process, increasing significantly its complexity and cost. To overcome this problem, the heterogeneous Fenton process

arose, where the active phase (metal) is incorporated in/supported by a porous matrix. Furthermore, the heterogeneous Fenton process facilitates the recovery and reutilization of the catalyst, and seems to be less affected by pH [84].

The main principles of the homogeneous reaction are also applied here, but the whole process is naturally more complex, with the co-existence of adsorption and catalysis phenomena. However, this does not gathers consensus among researchers on this field. For example, some authors claim that the first step is the fast adsorption of H_2O_2 on the active sites, while others believe that it is the adsorption of organics' molecules. However, the followed mechanism is more or less consensual:

$$X - Fe^{3+} + H_2O_2 \rightarrow X - Fe^{2+} + HO_2^{\bullet} + H^+ \quad (1.12)$$

$$X - Fe^{2+} + H_2O_2 \rightarrow X - Fe^{3+} + OH^- + HO^{\bullet} \quad (1.13)$$

where X represents the surface of the catalyst. The first reaction involves the reduction of Fe^{+3} with the production of Fe^{2+} that are then used for the generation of the hydroxyl radicals.

Several solid materials were already tested for this application, namely clays [85-90], silica, alumina and silica-alumina [86, 91-95], zeolites [86, 91, 96-98] and activated carbon [29, 91, 99-103]. Although other materials have been tested, this work deals mainly with catalysts based on activated carbons (ACs) as iron supports. A support for the development of heterogeneous Fenton catalysts should be stable in the acidic conditions used and highly porous, should provide a good dispersion of the metal phase, with a low leaching degree (loss of the metal from the support to the solution), and offer easy accessibility to the active sites. Different aspects of activated carbons, such as low price, high porosity and surface area, stability in acid and basic media, easily tuneable surface chemistry, etc., can favour the use of ACs regarding alternative inorganic supports. A deeper insight on activated carbons and their applications, namely in the heterogeneous Fenton reaction, is presented below.

a) Activated carbons - physical and chemical properties

Activated carbons (ACs) are versatile materials with application in several areas, namely in the environmental protection field, where they are used as adsorbents,

catalyst support or catalysts on their own [104], either in gas or liquid-phase (this last concerning namely the wastewater treatment), thanks mainly to their high surface areas and highly developed porosity. Usually they are in powder, granular or pellets form (Fig. 1.7). Chemical and physical properties of activated carbons are determinant in their performances and can be easily modified according to the final goal, which is a very important advantage; among other advantages, it is also worth mentioning their low price, especially when derived from coal or agricultural by-products.

Figure 1.7 – Activated carbons in different forms.

The first stage in the preparation of activated carbons is to choose the precursor that can be any organic material, including pure reactants or many type of residues such as agricultural by-products (olive stone, coconut, wood, etc), paper or plastics (tires, bottles, etc). This choice should follow several criteria: low inorganic load, low cost, availability, mechanical and chemical stability, easy of processing, etc. In a second step, the selected precursor is treated in inert atmosphere (typically N_2) at high temperature (depending on the precursor and the intended product). This process (carbonization) increases the precursors' carbon load, but the char obtained has typically a low porosity degree. So, activation processes are needed to develop the carbon materials' porosity, which can be carried out by the called physical or chemical methods [105]. In the physical activation, there is a gasification of the material at high temperatures with oxidizing gases (O_2, H_2O, CO_2) able to react with carbon under these conditions. The

gasification typically occurs in the more disorganized (less graphitic) and reactive zones of the chemical char structure [106] and generates more porous and ordered materials, with a higher content of carbon. This method develops significantly the porosity when increasing the gasification (activation) degree, but also enlarges pore size distributions. The development of the porosity depends on the nature of the raw precursors, activating agent and experimental conditions (temperature and time of activation). In the chemical activation, a chemical reactive agent (H_3PO_4, KOH, $ZnCl_2$, etc) is impregnated in the carbon precursor material, and the mixture is then subjected to a pyrolysis process in an inert atmosphere [105, 107]. Then the material should be washed for the agent elimination and eventually neutralized. Here the agent used, the agent/material weight ratio and the temperature are the parameters with more impact on the textural characteristics of the activated carbon.

Activated carbons are microcrystalline carbons with an amorphous and anisotropic structure that has been described as "*aromatic sheets and strips, often bent and resembling a mixture of wood shavings and crumpled paper, with variable gaps of molecular dimensions between them*" [106] – Fig. 1.8. The structure's depends on the precursor and on the treatment applied.

Figure 1.8 – Representative scheme of AC structure (adapted from [108]).

ACs' pores are classified as micropores, up to 2 nm; mesopores, from 2 to 50 nm; and macropores, > 50.0 nm [106] – Fig. 1.9. Micropores provide the main contribution for the large surface area of activated carbons and for most of their strong

adsorption capacity. This kind of pores becomes filled at low relative pressures. The presence of mesopores is denounced by N_2 adsorption/desorption experiments, since capillary condensation of N_2 is produced, which leads to the appearance of a hysteresis loop during desorption. Macropores cannot be filled by capillary condensation and they are those which less contribute to the surface area [109].

Although most of the adsorption takes place in the micropores of an activated carbon, meso an macropores play also an important role in the adsorption process, once most of micropores are at the end of the larger pores (Fig. 1.9), forcing the adsorbate to pass through them.

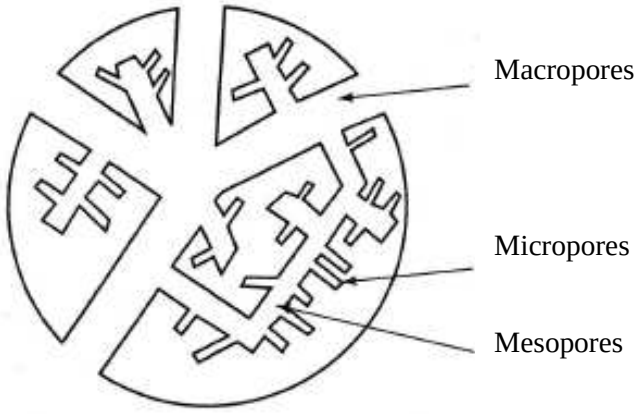

Figure 1.9 – Schematic representation of activated carbon porous structure (adapted from [109]).

The textural structure of activated carbons is not only important to their adsorption capacity but it can also influence their catalytic activity since it is related to diffusion effects, which determine the access of molecules into the active sites. In this work, ACs's textural properties are important because they are directly related to the ability of ACs to fix and disperse the iron species, which is determinant for the performance of AC/Fe catalysts in the heterogeneous Fenton reaction [29, 34].

As already mentioned, the porous structure of an activated carbon is a function of the precursor used in the preparation, the activation method followed and the extension of the activation step. Therefore, surface area, pore volume and pore size distribution may vary widely from one kind of activated carbon to another, which makes the choice of the material/preparation method truly important for the application.

For instance, whereas a microporous structure (large surface areas) can be required for gas adsorption, large micropores or mesopores can be needed for a better dispersion of the active phase and /or a better accessibility to molecules in a catalytic process.

The behaviour of activated carbons, either as adsorbents, catalysts or active phase supports, depends not only on their textural properties, but also on the chemical surface characteristics. In fact, it was already proved the decisive role of the ACs surface chemistry on adsorption and catalytic processes [104, 110].

The random and disorganised structure of ACs, with imperfect aromatic sheets, leads to saturated valences and unpaired electrons. This fact influences the adsorbent-adsorbate adsorption affinity and, on the other hand, confers catalytic activity to the surface's carbon. Moreover, ACs have significant amounts of heteroatoms, such as oxygen, nitrogen, sulphur, etc. that come from the raw material and/or are bonded during the ACs' preparation, and originates several surface functional groups [104, 106] – Fig. 1.10.

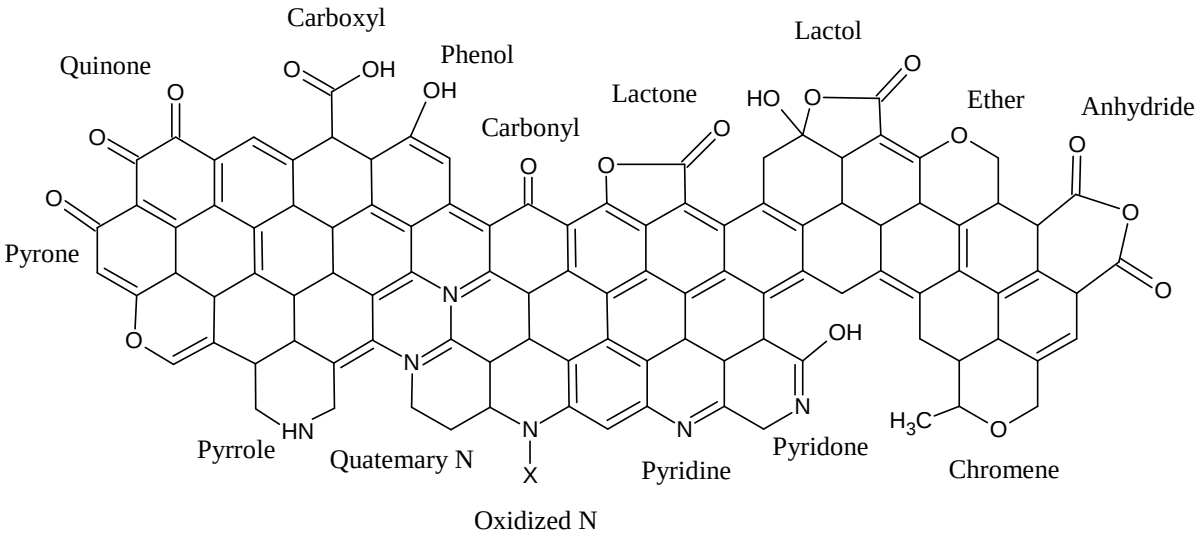

Figure 1.10 – Functional groups on activated carbons surface (adapted from [104]).

These surface groups may also be introduced by suitable treatments in the gas or liquid phase, while thermal treatments are used to remove selectively these groups [111, 112], according to the application intended. Briefly, oxidation of activated carbons with different oxidants like concentrated hydrogen peroxide (9.8 – 10 M), a saturated solution of ammonium peroxydisulphate ($(NH_4)_2S_2O_8$) or HNO_3 introduces carboxylic

acids and anhydrides, lactones and phenol groups [111-114] generating an acid material; if a basic character is required, activated carbons should be subject to H_2 treatment at high temperatures [111].

The complete physic-chemical characterization of ACs requires the use of complementary techniques due to the complexity of these materials, in terms of both textural and chemical aspects. Several techniques are available and some of them will be described later on (Chapter 2 – Experimental Section).

b) Use of activated carbons in advanced oxidation processes

As it was mentioned in the previous section, due to the specific characteristics of activated carbons, these materials can be used as catalysts on their own or as support of a metal phase, namely in the heterogeneous Fenton process.

In fact, ACs' surface is often able to decompose the hydrogen peroxide. It has been assumed that this process involves the exchange of a surface hydroxyl group with a hydrogen peroxide anion (Eq. 1.14), as described by Bansal *et al.* [115] and cited in [116] and [117]. The formed surface peroxide is regarded as having a high oxidation potential which enables the decomposition of another H_2O_2 molecule with release of O_2 and regeneration of the carbon surface [117] (Eq. 1.15).

$$AC-OH+H^{+}OOH^{-} \rightarrow AC-OOH+H_2O \quad (1.14)$$

$$AC-OOH+H_2O_2 \rightarrow AC-OH+H_2O+O_2 \quad (1.15)$$

But more important than this decomposition reaction, and in the perspective of the AOPs, it is worth nothing that H_2O_2 can be activated on the AC surface involving the formation of free radicals. It is considered that AC acts as an electron-transfer catalyst similar to the Haber-Weiss mechanism known from the Fenton reaction, where AC^+ and AC are the oxidized and reduced catalyst states, respectively [117]:

$$AC+H_2O_2 \rightarrow AC^{+}+OH^{-}+OH^{\bullet} \quad (1.16)$$

$$AC^{+}+H_2O_2 \rightarrow AC+H_2O^{\bullet}+H^{+} \quad (1.17)$$

This approach is relevant since in wastewater treatment with an AC/H_2O_2 system the attack of contaminants' bonds is made by hydroxyl radicals without requiring the use of any metallic catalyst. Therefore, the success of the treatment depends on the formation of these species.

In this way, many studies have been done in order to degrade contaminants using activated carbons combined with hydrogen peroxide (oxygen and ozone are also used, although in a smaller scale because of the advantages of using H_2O_2 already mentioned). Concerning to the treatment of textile wastewaters, namely dyes' oxidation using AC/H_2O_2 systems, some works are found in the literature, namely by Oliveira *et al.* [118], Santos *et al.* [119] and Khorramfar *et al.* [120].

However, the performance of the heterogeneous catalysis using ACs/H_2O_2 combination may be significantly improved by introducing iron (or another transition metal) particles on the AC surface to degrade contaminants by the heterogeneous Fenton process. This approach has been adopted by several authors, and, specifically regarding dyes removal, relevant works were already reported proving that this is a promising technology for the discoloration and COD abatement of textile effluents [29, 34, 91, 121, 122].

In the heterogeneous Fenton process using ACs as Fe support, the mechanism of the oxidation is a complex series of reactions, where hydrogen peroxide can be activated by the surface of the carbon and/or the metal phase; the oxidation of contaminants can occur on the active sites (after adsorption of organic molecules) and/or in solution. Additionally, adsorption without oxidation of the molecules can also happen.

Thus, physical and surface chemical properties of AC-based catalysts significantly affect their performance towards pollutants elimination. Textural characteristics are also related to the ability of AC to fix and disperse the iron, a determinant factor in the catalytic properties of this kind of materials [29, 34].

Therefore, this dissertation deals with the duality adsorption/catalysis existing in the heterogeneous Fenton reaction towards the elimination of the model azo-dye Orange II (OII), being specially focused on the development of AC/Fe catalysts. The influence of their properties, namely type of support, iron precursor nature, size of the support's particles and other parameters on the performances obtained are analysed, looking for

correlations between materials' properties and performances reached. Besides, a new insight about OII elimination by characterization of spent catalysts was also addressed in order to clarify the physic-chemical processes involved using the referred catalytic system. These experiments were carried out in *slurry* batch reactors, but the final goal was to employ a fixed-bed reactor, where the textile effluents can be treated in a continuous mode. Thus, at the end, a real textile effluent was successfully treated in a column reactor filled with the AC/Fe with the characteristics previously optimized.

References

[1] TextileAsArt.com – Antique Textiles, Woven Treasures, retrieved on August 10th 2012 from http://www.textileasart.com/weaving.htm.

[2]Adsale ATA Textile Online – Journal for Asian on Textile Apparel, retrieved on August 10th 2012 from

http://www.adsaleata.com/Publicity/Focus/lang-eng/article-3720/Article.aspx?keyword=Wool.

[3] E.O. Rocha, M.J. Sousa, M.L. Ferreira, Como evoluíram os clusters do têxtil e vestuário em Portugal durante o período de desmantelamento do acordo multi-fibras (1995-2005)?, Universidade Católica Portuguesa, Porto, 2006.

[4] ATP – Associação Têxtil e Vestuário de Portugal, retrieved on August 10th 2012 from http://www.atp.pt/gca/index.php?id=18.

[5] Mapa de Portugal, Opção PME – Negócios, retrieved on August 10th 2012 from http://www.opcaopmemais.com/home/mapa-de-portugal.

[6] Profile of the Textile Industry, U.S. Environmental Protection Agency, 1997.

[7] M.A. Silva, Indústria Têxtil e o Ambiente – Desafios actuais do Sector, Revista AEP 28, 1999.

[8] P.C.C. Faria, Catalytic Ozonation of Effluents from the Textile Industry, Ph.D. dissertation at the Faculty of Engineering of University of Porto, June 2008.

[9] Guia de Gestão Ambiental para as Indústrias Têxtil e do Vestuário - Água Industrial e Efluentes Líquidos, Associação Portuguesa de Têxteis e Vestuário, 2000.

[10] C. Rodrigues, L.M. Madeira, R.A.R. Boaventura, Treatment of textile dye wastewaters using ferrous sulphate in a chemical coagulation/flocculation process, Environ. Technol. iFirst (2012) 1–11.

[11] A.M. Talarposhti, T. Donnelly, G.K. Anderson, Colour removal from a simulated dye wastewater using a two-phase anaerobic packed-bed reactor, Water Res. 35 (2001) 425-432.

[12] A.B. dos Santos, I.A.E. Bisschops, F.J. Cervantes, Closing process water cycles and product recovery in textile industry: perspective for biological treatment, in: F.J. Cervantes, S.G. Pavlostathis, A.C. Van Haandel (Eds.), Advanced Biological Treatment Processes for Industrial Wastewaters, Vol. 1, International Water Association, London, 2006.

[13] U. Rott, R. Minke, Overview of wastewater treatment and recycling in the textile processing industry, Water Sci. Technol. 40 (1999) 137-144.

[14] D.R. Waring, G. Hallas (Eds), The Chemistry and Application of Dye, Plenum Press, New York, 1990.

[15] V.M. Correia, T. Stephenson, S.J. Judd, Characterization of textile wastewaters – A Review, Environ. Technol. 15 (1994) 917-929.

[16] A.B. dos Santos, F.J. Cervantes, J.B. Van Lier, Review paper on current technologies for decolourisation of textile wastewaters: Perspectives for anaerobic biotechnology, Bioresour. Technol. 98 (2007) 2369-2385.

[17] J.H.R. Franco, Homogeneous and Heterogeneous Oxidation of the Azo-Dye Orange II with Fenton's reagent-Based Processes, Ph.D. dissertation at the Faculty of Engineering of University of Porto, May 2008.

[18] M. Stylidi, D.I. Kondarides, X.E. Verykios, Pathways of solar light-induced photocatalytic degradation of azo dyes in aqueous TiO_2 suspensions, Appl. Catal., B 40 (2003) 271-286.

[19] C. Gomes da Silva, J.L. Faria, Degradation of an azo dye in aqueous solution by UV irradiation, J. Photochemi. Photobiol., A 155 (2003) 133-143.

[20] P. Cooper, Colour in Dyehouse Effluent, Society of Dyers and Colourists, Bradford, 1995.

[21] A. Kunz, P. Peralta-Zamora, New tendencies on textile effluent treatment, Quim. Nova 25 (2002) 78-82.

[22] N.M. Nasser, M. El-Geundi, Comparative cost of colour removal from textile effluents using natural adsorbents, J. Chem. Technol. Biotechnol. 50 (1991) 257-264.

[23] T. Robinson, G. McMullan, R. Marchant, P. Nigam, Remediation of dyes in textile effluent: a critical review on current treatment technologies with a proposed alternative, Bioresour. Technol. 77 (2001) 247-255.

[24] L. Dapeng, Q. Jiuhui, The progress of catalytic technologies in water purification: A review, J. Environ. Sci. 21 (2009) 713-719.

[25] M. Pera-Titus, V. García-Molina, M.A. Banos, J. Giménez, S. Esplugas, Degradation of chlorophenols by means of advanced oxidation processes: a general review, Appl. Catal., B 47 (2004) 219-256.

[26] S.H. Chan, T.Y. Wu, J.C. Juan, C.Y. Teh, Recent developments of metal oxide semiconductors as photocatalysts in advanced oxidation processes (AOPs) for treatment of dye waste-water, J. Chem. Technol. Biotechnol. 86 (2011) 1130-1158.

[27] H.Y. Shu, C.R. Huang, M.C. Chang, Discoloration of mono-azo dyes in wastewater by advanced oxidation process: A case study of acid red 1 and acid yellow 23, Chemosphere 29 (1994) 2597-2607.

[28] E. Kusvuran, O. Gulnaz, S. Irmak, O.M. Atanur, H.I. Yavuz, O. Erbatur, Comparison of several advanced oxidation processes for the discoloration of Reactive Red 120 azo dye in aqueous solution, J. Hazard. Mater. 109 (2004) 85-93.

[29] J.H. Ramirez, F.J. Maldonado-Hódar, A.F. Pérez-Cadenas, C. Moreno-Castilla, C.A. Costa, L.M. Madeira, Azo-dye Orange II degradation by heterogeneous Fenton-like reaction using carbon-Fe catalysts, Appl. Catal., B 75 (2007) 312-323.

[30] B. Meunier, A. Sorokin, Oxidation of pollutants catalyzed by metallophthalocyanines, Acc. Chem. Res. 30 (1997) 470-476.

[31] W.H. Glaze, J.W. Kang, Advanced oxidation processes. Description of a kinetic model for the oxidation of hazardous materials in aqueous media with ozone and hydrogen peroxide in a semi-batch reactor, Ind. Eng. Chem. Res.28 (1989) 1573-1580.

[32] S.J. Masten, S.H. Davies, The use of ozonation to degrade organic contaminants in wastewaters, Environ. Sci. Technol. 28 (1994) 180-185.

[33] O. Legrini, E. Oliveros, A.M. Braun, Photochemical processes for water treatment, Chem. Rev. 93 (1993) 671-698.

[34] F. Duarte, F.J. Maldonado-Hódar, A.F. Pérez-Cadenas, L.M. Madeira, Fenton-like degradation of azo-dye Orange II catalyzed by transition metals on carbon aerogels, Appl. Catal., B 85 (2009) 139-147.

[35] A.M. Braun, L. Jacob, E. Oliveros, C.A.O. do Nascimento, Up-scaling photochemical reactions, in: D. Volman, G.S. Hammond, D.C. Neckers (Eds.), Advances in Photochemistry, Vol. 18, Wiley, New York, 1993.

[36] W.R. Haag, C.C.D. Yao, Rate constants for reaction of hydroxyl radicals with several drinking water contaminants, Environ. Sci. Technol. 26 (1992) 1005-1013.

[37] G.R. Peyton, F.R. Huang, J.L. Burleson, W.H. Glaze, Destruction of pollutants in water with ozone in combination with ultraviolet radiation. 1. General principles and oxidation of tetrachloroethylene, Environ. Sci. Technol.16 (1982) 448-453.

[38] J.H. Ramirez, C.A. Costa, L.M. Madeira, G. Mata, M.A. Vicente, M.L. Rojas-Cervantes, A.J. López-Peinado, R.M. Martín-Aranda, Fenton-like oxidation of Orange II solutions using heterogeneous catalysts based on saponite clay, Appl. Catal., B 71 (2007) 44-56.

[39] K. Elizardo, Fighting pollution with hydrogen peroxide, J. Pollut. Eng. 23 (1991) 106-109.

[40] H.J.H. Fenton, Oxidation of tartaric acid in presence of iron, J. Chem. Soc. 65 (1894) 899-910.

[41] J. Beltran-Heredia, J. Torregrosa, J.R. Dominguez, J.A. Peres, Comparison of the degradation of p-hydroxybenzoic acid in aqueous solution by several oxidation processes, Chemosphere, 42 (2001) 351-359.

[42] R. Andreozzi, V. Caprio, A. Insola, R. Martota, Advanced oxidation processes (AOP) for water purification and recovery, Catal. Today 53 (1999) 51-59.

[43] C.P. Huang, C. Dong, Z. Tang, Advanced chemical oxidation: Its present role and potential future in hazardous waste treatment, Waste Manage.13 (1993) 361-377.

[44] R.J. Bigda, Consider Fenton chemistry for wastewater treatment, Chem. Eng. Process. 91 (1995) 62-66.

[45] H. Suty, C. Traversay, M. Cost, Applications of advanced oxidation processes: present and future, Water Sci. Technol. 49 (2004) 227-233.

[46] B. Legube, N.K.V. Leitner, Catalytic ozonation: a promising advanced oxidation technology for water treatment, Catal. Today 53 (1999) 61-66.

[47] P.C.C. Faria, J.J.M. Órfão, M.F.R. Pereira, Mineralisation of coloured aqueous solutions by ozonation in the presence of activated carbon, Water Res. 39 (2005) 1461-1470.

[48] R.G. Rice, A. Netzer, Handbook of Ozone Technology and Applications, Vol. 1, Ann Arbor Science Publishers, Butterworths, UK, 1982.

[49] F. Haber, J. Weiss, The catalytic decomposition of hydrogen peroxide by iron salts, Proc. R. Soc. London, Ser. A 147 (1934) 332-351.

[50] C. Walling, Fenton's reagent revisited, Acc. Chem. Res. 8 (1975) 125-131.

[51] P. Bautista, A.F. Mohedano, J.A. Casas, J.A. Zazo, J.J. Rodriguez, An overview of the application of Fenton oxidation to industrial wastewaters treatment, J. Chem. Technol. Biotechnol. 83 (2008) 1323–1338.

[52] F. Lücking, H. Köser, M. Jank, A. Ritter, Iron powder, graphite and activated carbon as catalysts for the oxidation of 4-chlorophenol with hydrogen peroxide in aqueous solution, Water Res. 32 (1998) 2607-2614.

[53] A. Safarzadeh-Amiri, J.R. Bolten, S.R. Cater, The use of iron in advanced oxidation processes, J. Adv. Oxid. Technol. 1 (1996) 18-26.

[54] S.F. Santos, A. Alves, L.M. Madeira, Paraquat removal from water by oxidation with Fenton's reagent, Chem. Eng. J. 175 (2011) 279-290.

[55] J.H. Sun, S.P. Sun, M.H. Fan, H.Q. Guo, L.P. Qiao, R.X. Sun, A kinetic study on the degradation of p-nitroaniline by Fenton oxidation process, J. Hazard. Mater., 148 (2007) 172–177.

[56] C. Jiang, S. Pang, F. Ouyang, J. Ma, J. Jiang, A new insight into Fenton and Fenton-like processes for water treatment, J. Hazard. Mater., 174 (2010), pp. 813–817.

[57] W.G. Barb, J.H. Baxendale, P. George, K.R. Hargrave, Reactions of ferrous and ferric ions with hydrogen peroxide, Part I. - The ferrous ion reaction, Trans. Faraday Soc. 97 (1951) 462-500.

[58] W.G. Barb, J.H. Baxendale, P. George, K.R. Hargrave, Reactions of ferrous and ferric ions with hydrogen peroxide. Part II.—The ferric ion reaction, Trans. Faraday Soc. 97 (1951) 591-616.

[59] J. De Laat, H. Gallard, Catalytic Decomposition of hydrogen peroxide by Fe (III) in homogeneous aqueous solution: Mechanism and kinetic modelling, Environ. Sci. Technol. 33 (1999) 2726-2732.

[60] J. Abbot, D.G. Brown, Kinetics of Iron-catalyzed decomposition of hydrogen peroxide in alkaline solution, Int. J. Chem. Kinet. 22 (1990) 963-974.

[61] C. Walling, A. Goosen, Mechanism of the ferric ion catalyzed decomposition of hydrogen peroxide. Effect of organic substrates, J. Am. Chem. Soc. 95 (1973) 2987-2991.

[62] F.J. Millero, S. Sotolongo, D.J. Stade, C.A. Vega, Effect of ionic interactions on the oxidation of Fe (II) with H_2O_2 in aqueous solutions, J. Solution Chem. 20 (1991) 1079-1092.

[63] B.M. Voelker, B. Sulzberger, Effects of Fulvic Acid on Fe (II) Oxidation by hydrogen peroxide, Environ. Sci. Technol. 30 (1996) 1106-1114.

[64] R.J. Watts, B.C. Bottenberg, T.F. Hess, M.D. Jensen, A.L. Teel, Role of reductants in the enhanced desorption and transformation of chloroaliphatic compounds by modified Fenton's reactions, Environ. Sci. Technol. 33 (1999) 3432-3437.

[65] F.J. Rivas, V. Navarrete, F.J. Beltran, J.F. Garcia-Araya, Simazine Fenton’s oxidation in a continuous reactor, Appl. Catal., B 48 (2004) 249-258.

[66] E. Neyens, J. Baeyens, A review of classic Fenton’s peroxidation as an advanced oxidation technique, J. Hazard. Mater. 98 (2003) 33-50.

[67] E. Neyens, J. Baeyens, M. Weemaes, B. de Heyder, Pilot-scale peroxidation (H_2O_2) of sewage sludge, J. Hazard. Mater. 98 (2003) 91-106.

[68] J. Guo, M. Al-Dahhan, Catalytic wet oxidation of phenol by hydrogen peroxide over pillared clay catalyst, Ind. Eng. Chem. Res. 42 (2003) 2450-2460.

[69] R. Oliveira, M.F. Almeida, L. Santos, L.M. Madeira, Experimental design of 2,4-diclorophenol oxidation by Fenton's reaction, Ind. Eng. Chem. Res. 45 (2006) 1266-1276.

[70] M. Rodríguez, V. Sarria, S. Esplugas, C. Pulgarin, Photo-Fenton treatment of a biorecalcitrant wastewater generated in textile activities: biodegradability of the photo-treated solution, J. Photochem. Photobiol., A 151 (2002) 129-135.

[71] L. Núnez, J.A. García-Hortal, F. Torrades, Study of kinetic parameters related to the discoloration and mineralization of reactive dyes from textile dyeing using Fenton and photo-Fenton processes, Dyes Pigm. 75 (2007) 647-652.

[72] J.H. Ramirez, C.A. Costa, L.M. Madeira, Experimental design to optimize the degradation of the synthetic dye Orange II using Fenton's reagent, Catal. Today 107-108 (2005) 68-76.

[73] L.G. Devi, S.G. Kumar, K.M. Reddy, C. Munikrishnappa, Photo degradation of Methyl Orange an azo dye by Advanced Fenton Processusing zero valent metallic iron: Influence of various reaction parameters and its degradation mechanism, J. Hazard. Mater. 164 (2009) 459-467.

[74] M.S. Lucas, J.A. Peres, Discoloration of azo dye Reactive Black 5 by Fenton and Photo Fenton oxidation, Dyes Pigm. 71 (2006) 236-244.

[75] K. Barbusinski, J. Majewski, Discoloration of azo dye acid red18 by Fenton reagent in the presence of iron powder, Polish J. Environ. Stud. 12 (2003) 151-155.

[76] J.J. Pignatello, D. Liu, P. Huston, Evidence for an additional oxidant in the photoassisted Fenton reaction, Environ. Sci. Technol. 33 (1999) 1832-1839.

[77] P.L. Huston, J.J. Pignatello, Degradation of selected pesticide active ingredients and commercial formulations in water by the photo-assisted Fenton reaction, Water Res. 33 (1999) 1238-1246.

[78] M. Neamtu, A. Yediler, I. Siminiceanu, A. Kettrup, Oxidation of commercial reactive azo dye aqueous solutions by the photo-Fenton and Fenton-like processes, J. Photochem. Photobiol., A 161 (2003) 87-93.

[79] K. Wu, Y. Xie, J. Zhao, H. Hidaka, Photo-Fenton degradation of a dye under visible light irradiation, J. Mol. Catal. A: Chem. 144 (1999) 77-84.

[80] F. Chen, Y. Xie, J. He, J. Zhao, Photo-Fenton degradation of dye in methanolic solution under both UV and visible irradiation, J. Photochem. Photobiol., A 138 (2001) 139-146.

[81] Y.H. Huang, Y. F. Huang, P.S. Chang, C.Y. Chen, Comparative study of oxidation of dye-Reactive Black B by different advanced oxidation processes: Fenton, electro-Fenton and photo-Fenton, J. Hazard. Mater. 154 (2008) 655-662.

[82] S. Sabhi, J. Kiwi, Degradation of 2,4-dichlorophenol by immobilized iron catalysts, Water Res. 35 (2001) 1994-2002.

[83] EEC List of Council Directives 76/4647.European Economic Community. Brussels, Belgium, 1982.

[84] G. Centi, S. Perathoner, M. Torre, M.G. Verduna, Catalytic wet oxidation with H_2O_2 of carboxylic acids on homogeneous and heterogeneous Fenton-type catalysts, Catal. Today 55 (2000) 61-69.

[85] J.H. Ramirez, C.A. Costa, L.M. Madeira, G. Mata, M.A. Vicente, M.L. Rojas-Cervantes, A.J. López-Peinado, R.M. Martín-Aranda, Fenton-like oxidation of Orange II solutions using heterogeneous catalysts based on saponite clay, Appl. Catal., B 71 (2007) 44-56.

[86] S. Navalon, M. Alvaro, H. Garcia, Heterogeneous Fenton catalysts based on clays, silicas and zeolites, Appl. Catal., B 99 (2010) 1-26.

[87] E.G. Garrido-Ramírez, B.K.G. Theng, M.L. Mora, Clays and oxide minerals as catalysts and nanocatalysts in Fenton-like reactions - A review, Appl. Clay Sci. 47 (2010) 182-192.

[88] J.H. Ramirez, M.A. Vicente, L.M. Madeira, Heterogeneous photo-Fenton oxidation with pillared clay-based catalysts for wastewater treatment: A review, Appl. Catal., B 98 (2010) 10-26.

[89] D. Tabet, M. Saidi, M. Houari, P. Pichat, H. Khalaf, Fe-pillared clay as a Fenton-type heterogeneous catalyst for cinnamic acid degradation, J. Environ. Manage. 80 (2006) 342-346.

[90] H. Hassan, B.H. Hameed, Fe-clay as effective heterogeneous Fenton catalyst for the discoloration of Reactive Blue 4, Chem. Eng. J. 171 (2011) 912-918..

[91] A. Rodríguez, G. Overejo, J.L. Sotelo, M. Mestanza, J. García, Heterogeneous Fenton catalyst supports screening for mono azo dye degradation in contaminated wastewaters, Ind. Eng. Chem. Res. 49 (2010) 498-505.

[92] F. Martínez, G. Calleja, J.A. Melero, R. Molina, Iron species incorporated over different silica supports for the heterogeneous photo-Fenton oxidation of phenol, Appl. Catal., B 70 (2007) 452-460.

[93] H. Lim, J. Lee, S. Jin, J. Kim, J. Yoon, T. Hyeon, Highly active heterogeneous Fenton catalyst using iron oxide nanoparticles immobilized in alumina coated mesoporous silica, Chem. Commun. 2006 (4) 463-465.

[94] C. Di Luca, F. Ivorra, P. Massa, R. Fenoglio, Alumina supported fenton-like systems for the catalytic wet peroxide oxidation of phenol solutions, Ind. Eng. Chem. Res. 51 (2012) 8979-8984.

[95] M. Xia, C. Chen, M. Long, C. Chen, W. Cai, B. Zhou, Magnetically separable mesoporous silica nanocomposite and its application in Fenton catalysis, Microporous Mesoporous Mater. 145 (2011) 217-223.

[96] M.B. Kasiri, H. Aleboyeh, A. Aleboyeh, Degradation of Acid Blue 74 using Fe-ZSM5 zeolite as a heterogeneous photo-Fenton catalyst, Appl. Catal., B 84 (2008) 9-15.

[97] M. Aleksić, H. Kušić, N. Koprivanac, D. Leszczynska, A.L. Božić, Heterogeneous Fenton type processes for the degradation of organic dye pollutant in water - The application of zeolite assisted AOPs, Desalination 257 (2010) 22-29.

[98] M. Dükkanci, G. Gündüz, S. Yilmaz, R.V. Prihod'ko, Heterogeneous Fenton-like degradation of Rhodamine 6G in water using CuFeZSM-5 zeolite catalyst prepared by hydrothermal synthesis, J. Hazard. Mater. 181 (2010) 343-350.

[99] F. Lucking, H. Koser, M. Jank, A. Ritter, Iron powder, graphite and activated carbon as catalysts for the oxidation of 4-chlorophenol with hydrogen peroxide in aqueous solution, Water Res. 32 (1998) 2607-2614.

[100] C.S. Castro, M.C. Guerreiro, L.C.A. Oliveira, M. Gonçalves, A.S. Anastácio, M. Nazzarro, Iron oxides dispersed over activated carbon: Support influence on the oxidation of the model molecule methylene blue, Appl. Catal., A 367 (2009) 53-58.

[101] A. Rey, J. Carbajo, C. Adáa, M. Faraldos, A. Bahamonde, J.A. Casas, J.J. Rodriguez, Improved mineralization by combined advanced oxidation processes, Chem. Eng. J. 174 (2011) 134-142.

[102] J.A. Zazo, J.A. Casas, A.F. Mohedano, J.J. Rodriguez, Catalytic wet peroxide oxidation of phenol with a Fe/Active carbon catalyst, Appl. Catal., B 65 (2006) 261-268.

[103] T.L.P. Dantas, V.P. Mendonça, H.J. Jose, A.E. Rodrigues, R.F.P.M. Moreira, Treatment of textile wastewater by heterogeneous Fenton process using a new composite Fe_2O_3/carbon, Chem. Eng. J. 118 (2006) 77-82.

[104] J.L. Figueiredo, M.F.R. Pereira, The role of surface chemistry in catalysis with carbons, Catal. Today 150 (2010) 2-7.

[105] H. Marsh, F. Rodríguez-Reinoso, Activated Carbon, Elsevier, 2006, Great Britain.

[106] F. Rodríguez-Reinoso, The role of carbon materials in heterogeneous catalysis, Carbon 36 (1998) 159-175.

[107] C. Moreno-Castilla, F. Carrasco-Marín, M. Victoria López-Ramón, M.A. Alvarez-Merino, Chemical and physical activation of olive-mill waste wáter to produce activated carbons, Carbon 39 (2001) 1415–1420.

[108] H.F. Stoeckli, Microporous carbons and their characterization: The present state of the art, Carbon 28 (1990) 1-6.

[109] F. Rodríguez-Reinoso, Introduction to Carbon Tecnologies, Eds. H. Marsh, E.A. Heintz, F. Rodriguez-Reinoso, Universidad de Alicante, Secretariado de Publicaciones, 1997.

[110] M.F.R. Pereira, S.F. Soares, J.J.M. Órfão, J.L. Figueiredo, Adsorption of dyes on activated carbons: Influence of surface chemical groups, Carbon 41 (2003) 811-821.

[111] J.L. Figueiredo, M.F.R. Pereira, M.M.A. Freitas, J.M.M. Órfão, Modification of the surface chemistry of activated carbons, Carbon 37 (1999) 1379-1389.

[112] C. Moreno-Castilla, F. Carrasco-Marín, F.J. Maldonado-Hódar, J. Rivera-Utrilla, Effects of non-oxidant and oxidant acid treatments on the surface properties of na activated carbon with very low ash content, Carbon 36 (1998) 145-151.

[113] C. Moreno-Castilla, M.A. Ferro-García, J.P. Joly, I. Bautista-Toledo, F. Carrasco-Marín, J. Rivera-Utrilla, Activated carbon surface modifications by nitric acid, hydrogen peroxide and ammonium peroxydissulphate treatments, Lamgmuir 11 (1995) 4386-4392.

[114] C. Moreno-Castilla, M.V. López-Ramón, F. Carrasco-Marín, Changes in surface chemistry of activated carbons by wet oxidation, Carbon 38 (2000) 1995-2001.

[115] R.C. Bansal, J.B. Donnet, F. Stoeckli, Activated Carbon, Marcel Dekker, New York, 1988.

[116] L.B. Khalil, B.S. Girgs, T.A.M. Tawfik, Decomposition of H_2O_2 on activated carbon obtained from olive stones, J. Chem. Technol. Biotechnol. 76 (2001) 1132-1140.

[117] A. Georgi, F. Kopinke, Interaction of adsorption and catalytic reactions in water decontamination processes - Part I. Oxidation of organic contaminants with hydrogen peroxide catalyzed by activated carbon, Appl. Catal., B 58 (2005) 9-18.

[118] L.C.A. Oliveira, C.N. Silva, M.I. Yoshida, R.M. Lago, The effect of H_2 treatment on the activity of activated carbon for the oxidation of organic contaminants in water and the H_2O_2 decomposition, Carbon 42 (2004) 2279-2284.

[119] V.P. Santos, M.F.R. Pereira, P.C.C. Faria, J.J.M. Órfão, Decolourisation of dye solution by oxidation with H_2O_2 in the presence of modified activated carbons, J. Hazard. Mater. 162 (2009) 736-742.

[120] S. Khorramfar, N.M. Mahmoodi, M. Arami, H. Bahrami, Oxidation of dyes from colored wastewater using activated carbon/hydrogen peroxide, Desalination 279 (2011) 183-189.

[121] M.C. Pereira, F.S. Coelho, C.C. Nascentes, J.D. Fabris, M.H. Araújo, K. Sapag, L.C.A. Oliveira, R.M. Lago, Use of activated carbon as a reactive support to produce highly active-

regenerable Fe-based reduction system for environmental remediation, Chemosphere 81 (2010) 7-12.

[122] T.D. Nguyen, N.H. Phan, M.H. Do, K.T. Ngo, Magnetic Fe_2MO_4 (M:Fe, Mn) activated carbons: Fabrication, characterization and heterogeneous Fenton oxidation of methyl orange, J. Hazard. Mater.185 (2011) 653-661.

CHAPTER 2 – Experimental Section

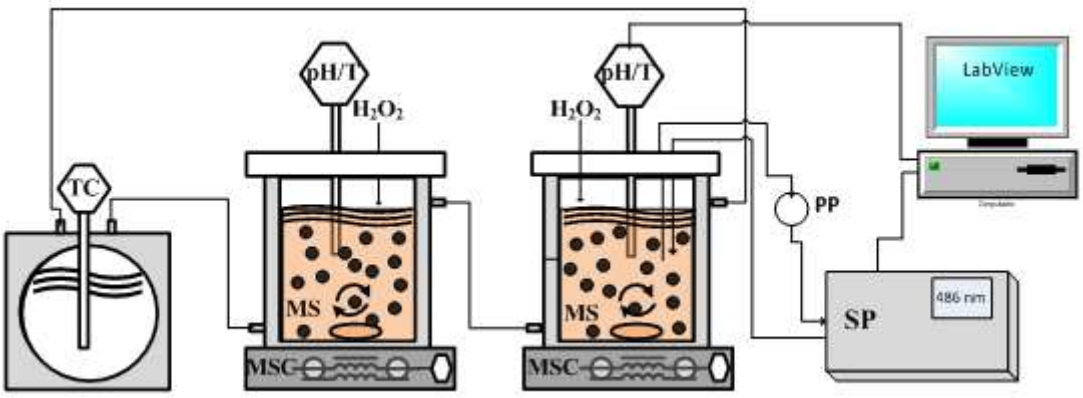

Chapter 2. Experimental Section

This section covers the methodology used in general during the whole work. However, specific materials and technical details are described in each Chapter.

2.1. Reagents

The azo-dye Orange II sodium salt (from Fluka p.a.) – OII from now on, also called Acid Orange 7, with an anionic character, was used as the model compound to be eliminated by the heterogeneous Fenton-based processes in batch reactors. OII ($C_{16}H_{11}N_2NaO_4S$) has 350.33 $g.mol^{-1}$ of molecular weight and Hsiu-Mei *et al.* [1] have reported the dimensions of the OII molecule: 0.73 nm width, 1.36 nm length and 0.23 nm of depth. Orange II in solutions presents two tautomeric forms (Fig. 2.1): the azo form, favoured in solutions with organic solvents, and the hydrazone form, which predominates in water [2, 3].

The choice of the model compound fell on this dye, once it is used in the textile industry, as well as in food, cosmetics and plastics activities, due to its low price.

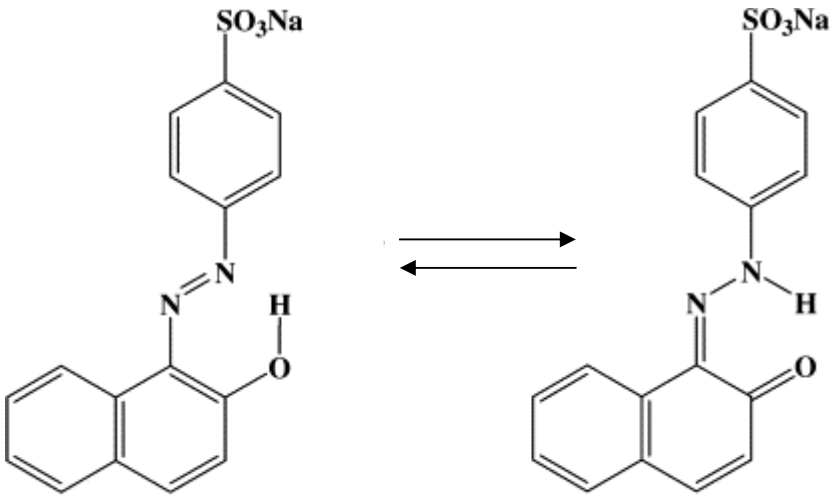

Azo form **Hidrazone form**

Figure 2.1 – Tautomeric forms of Orange II (4-(2-Hydroxy-1-naphthylazo)benzenesulfonic acid sodium salt) in solutions.

Thus, Orange II is extensively studied in the literature, particularly in what concerns to its degradation by Fenton-based processes (*e.g.* [4-12]). The OII degradation pathways and the formation of by-products are also fully described (*e.g.* [2, 3, 13-16]). It is known that benzene sulfonate and naphthoquinone are the primary by-products obtained after the oxidative attack of OII molecules. The further oxidation of naphthoquinone leads to phtalic acid [14]. Several other by-products were described, such as benzene sulphonic acid and sulphoanilic acid [2], 4-hydroxylbenzene sulphonic acid after Vis/TiO_2 degradation [3], and 2-naphtol and 2-hydroxyl-1,4-naphthoquinone [2]. The lowest molecular weight compounds found, besides phtalic acid, were oxalic, glycolic and formic acids, as well as inorganic ions [2, 13].

Concerning to iron precursors for AC/Fe catalysts preparation or for homogeneous Fenton experiments, the following salts were used: iron acetate ($Fe(C_2H_3O_2)_2$) with 95 % of purity from Aldrich, iron sulphate heptahydrate ($FeSO_4.7H_2O$) with 98% of purity from Panreac, and iron nitrate nonahydrate ($Fe(NO_3)_3.9H_2O$) with 97 % of purity from Riedel-de Haen. The oxidant used was hydrogen peroxide, 30 % (v/v), from Normapur. To stop the homogenous oxidation reactions in the samples taken along reaction time (cf. section 2.4.1), one used sodium sulphite p.a. from Riedel-de Haën.

2.2. Preparation of the AC/Fe catalysts

Commercial activated carbons (ACs) were used in adsorption experiments and in the heterogeneous Fenton processes, as iron support. Firstly, ACs were milled and sieved (when necessary) to get the desired support particle size and put in an oven at 110 ºC. Then, after dried, they were wet impregnated with the desired iron solution precursor. This solution was prepared with the amount of iron salt required to achieve 7 % by weight of iron in the final catalyst (the same iron dose used in previous works [6, 17]). The salt was dissolved in the minimum amount of distilled water (according to the salt solubility), with the help of magnetic stirring, at room temperature. Then, the iron solution was added dropwise and uniformly to the carbon, avoiding the excess of solution added. After impregnation, the sample was dried overnight in an oven at 110

°C, and finally treated for 2 hours at 300 °C under a He stream, for the iron salt decomposition.

2.3. Supports/catalysts' characterization

Textural and chemical properties of the solid materials used in the adsorption processes and heterogeneous Fenton reactions are determinant for their performances towards the dye elimination. Thus, a fully characterization of supports and catalysts is crucial and was carried out in this work. For that, several techniques were used and are briefly described below.

2.3.1. Gases adsorption

CO_2 adsorption at 273 K and N_2 at 77 K adsorption/desorption isotherms were used for the textural assessment in a Quantachrome Autosorb 1 apparatus, after sample degassing (overnight at 120 ºC and 1.3×10^{-4} Pa) and weighing.

Physical adsorption of gases is the most employed technique for the characterization of porous solids [18, 19]. Different adsorptives, like N_2, CO_2, Ar, He, CH_4, benzene, nonane, etc., can be used for this purpose, but N_2 at 77 K is the most commonly used [20]. The advantage of N_2 adsorption is that it covers relative pressures from 10^{-8} to 1, which results in adsorption in the whole range of porosity. The main disadvantage of N_2 adsorption at 77 K is that when it is used for the characterization of microporous solids, diffusional problems of the molecules inside the narrow porosity range (L_0 < 0.7 nm) may occur. To overcome this problem, the use of other adsorptives has been proposed.

CO_2 adsorption, either at 273 or 298 K, and He adsorption at 4.2 K, are two alternatives to N_2 adsorption for the assessment of the narrow microporosity. The use of He requires experimental conditions that make this technique not as available as CO_2 adsorption. Although the critical dimension of the CO_2 molecule is similar to that of N_2, the higher temperature of adsorption used for CO_2 results in a larger kinetic energy of the molecules that are thus able to enter into the narrower porosity. In this way, CO_2

adsorption has been proposed as a good complementary technique of the N_2 adsorption for the analysis of the porous texture, as it can be used to assess the narrow microporosity (L_0 < 0.7 nm), where N_2 adsorption can be kinetically restricted [21].

This technique is based on the assessment of adsorbed gas volume per adsorbent mass unit (V_{gas}) at a constant temperature (T), which depends on the relative pressure (P/P_0), i.e. the pressure in each point (P) divided by the saturation vapour pressure (P_0) of the gas [19]:

$$V_{gas} = f\left(\frac{P}{P_0}\right)T \tag{2.1}$$

Plotting V_{gas} *vs.* (P/P_0) adsorption/desorption isotherms are obtained. There are several types of isotherms that help to classify and characterize the solids, as described elsewhere [18-20].

In this work, the surface area of the materials was obtained using the Brunauer-Emmett-Teller (BET) equation (Eq. 2.2 [20] in the linear form) applied to the N_2 adsorption data, which is the most common method:

$$\frac{\frac{P}{P_0}}{n^a\left(1-\frac{P}{P_0}\right)} = \frac{1}{n_m^a c} + \frac{c-1}{n_m^a c}\frac{P}{P_0} \tag{2.2}$$

where, n^a is the amount of gas adsorbed in each point per adsorbent mass unit, n_m^a is the monolayer's capacity and c is a dimensionless constant which is related to the adsorption energy. n_m^a and c were determined by representing the first term of Eq. (2.2) *versus* (P/P_0) using the points with a linear behaviour (limited range of relative pressures), corresponding to what is considered the monolayer adsorption. The range of linearity depends on the system under analysis. Finally, the BET surface area (S_{BET}) per gram of sample was simply calculated from the n_m^a parameter using the following expression:

$$S_{BET}\left(m^2.g^{-1}\right) = n_m^a\left(mol.g^{-1}\right) \times a_m\left(m^2.molecule^{-1}\right) \times N_A\left(molecules.mol^{-1}\right) \quad (2.3)$$

where a_m is the molecular area (1.62×10^{19} m^2 for N_2) and N_A is the Avogadro number, 6.022×10^{23} molecules per mole of adsorbent.

However, it is important to be aware of the limitations of this approach, once the BET theory, as many others, is based on some hypotheses that have to be taken into account:

- Homogeneity of adsorption sites in the solid [19];
- No interaction is considered between adsorbate molecules, considering only the forces between these molecules and the adsorbent [19];
- Molecules of the first layer and those that come after are treated like equals [22];
- Condensation until a liquid film is formed occurs at adsorbate saturation pressure [23].

Therefore, S_{BET} is an apparent area in the case of non-microporous materials, which should be considered as an approximation of the real value.

Microporous structures were studied following the Dubinin-Radushkevich (DR) theory, applied to N_2 at 77 K and CO_2 at 293 K (for the narrowest micropores) adsorption data. The DR equation results from the general equation of Dubinin-Astakhov (DA), which considers the interactions between gas molecules and adsorbent sites [24]:

$$W = W_0 \exp\left[-\left(\frac{A}{\beta E_0}\right)^{n_{DA}}\right] \quad (2.4)$$

where:

- W is the volume of gas adsorbed (expressed as liquid) in the micropores at given conditions (T and $\frac{P}{P_0}$);
- W_0 is the total micropore volume;

- $A = RT\ln\left(\frac{P}{P_0}\right)$ is the adsorption potential with R being the ideal gas constant;
- n_{DA}, E_0 and β are specific parameters of the system: E_0 is a medium value of the characteristic adsorption energy, β is the affinity coefficient (β = 0.33 for N_2 and β = 0.35 for CO_2) and n_{DA} is the homogeneity degree of the microporous system.

Dubunin and Radushkevich have proposed $n_{DA} = 2$.

To obtain W_0 and E_0, Equation (2.3) with $n_{DA} = 2$ was linearized and transformed into Eq. 2.5 [18]:

$$\ln W = \ln W_0 - \left(\frac{B}{E_0}\ln\left(\frac{P}{P_0}\right)\right)^2 \quad (2.5)$$

where B is a constant of the system given by:

$$B = \frac{RT}{\beta} \quad (2.6)$$

The mean micropore size, L_0, was calculated from E_0 by applying the Stoeckli equations [25]:

$$L_0(nm) = \frac{10.8}{E_0\left(kJ.mol^{-1}\right) - 11.4} \quad \text{, when } E_0 > 20\ kJ.mol^{-1} \quad (2.7)$$

$$L_0(nm) = \frac{24}{E_0\left(kJ.mol^{-1}\right)} \quad \text{, when } E_0 < 20\ kJ.mol^{-1} \quad (2.8)$$

and the micropores' surface area was determined by Eq. (2.9):

$$S_{mic}\left(m^2.g^{-1}\right) = \frac{2000\,W_0\left(cm^3.g^{-1}\right)}{L_0(nm)} \quad (2.9)$$

Barret, Joyner and Halenda (BJH) method [26] was used to obtain the mesopore size distribution (PSD). In this case, the volume of mesopores was also calculated by this method (V_{BJH}), computed by the software of the equipment used for the gases adsorption – Quantachrome Autosorb 1. Otherwise, mesopores' volume (V_{meso}) was estimated according to the Gurvitch's rule, from the N_2 adsorption isotherms, assuming the volume of adsorbed nitrogen at P/P_0 = 0.95 ($V_{0.95}$) as the total pore volume and the micropore volume as the volume adsorbed at P/P_0 < 0.4 ($V_{0.4}$). The mesopores' volume is the volume of gas adsorbed between P/P_0 = 0.4 and P/P_0 = 0.95 ($V_{meso} = V_{0.95} - V_{0.4}$) [27]. Alternatively, the volume of mesopores can also be obtained from the difference between $V_{0.95}$ and W_0 (N_2) determined by the DR equation.

2.3.2. High resolution transmission electron microscopy (HRTEM) and scanning electron microscopy (SEM)

HRTEM was used to evaluate the iron particles' size and distribution on the catalysts, while SEM was mainly used for the morphological characterization of the materials.

These techniques are based on the interaction of a beam containing energetic electrons (20-1500 kV) [19] with the materials, providing images that give several kinds of information. The main difference between SEM and HRTEM is that SEM provides contrast due to the topology of a surface, whereas HRTEM projects all information in a two-dimensional image. One of the characteristics of using electron microscopy is that it allows obtaining local information, because the large magnification reached permits to study the sample at the nanometer scale, above 10 nm and 1 nm for SEM and HRTEM, respectively [19]. Thus, the homogeneity of the sample at large scale should be guaranteed on the basis of the analysis of many images. Complemented techniques should also be used.

In this work, SEM was complemented with micro analyses by X-rays (SEM / EDS) using a JEOL JSM 35C / Noran Voyager apparatus and the samples were observed without a previously specific treatment. For HRTEM, samples were suspended in ethanol and sonicated for 10 min. Then, the suspended particles were deposited on a carbon-coated copper grid that was introduced several times into the

suspension, “fishing” the particles. HRTEM images were acquired by a Philips CM-20 electron microscope.

2.3.3. X-ray diffraction (XRD)

XRD was used to complement TEM photos in the evaluation of the iron particle dispersion on the Fe-catalysts. Besides, this technique also gave information about the nature of iron particles.

Actually, XRD is one of the most frequently applied techniques in catalyst characterization. X-rays have wavelengths in the Å range, are sufficiently energetic to penetrate solids and are well suited to probe their internal structure. Moreover, XRD is able to solve clearly crystal structures or make the distinction between allotropic and isomorphic forms.

The basis of this technique is the diffraction phenomenon existing when a monochromatic X-rays beam focuses in a sample (Fig. 2.2) – The Bragg’s Law [28]. The XRD pattern of a powdered sample is measured with a stationary X-ray source (usually Cu Kα) and a movable detector, which scans the intensity of the diffracted radiation as a function of the angle (2θ) between the incoming and the diffracted beams. When working with powdered samples, an image of diffraction lines occurs because a small fraction of the powder particles will be oriented such that by chance a certain crystal plane (*hkl*) is at the right angle with the incident beam for constructive interference.

Amorphous phases and small particles give either broad and weak diffraction lines or no diffraction at all, with the consequence that if catalysts contain particles with a size distribution, XRD may only detect the larger ones (> 4 nm).

In this work, diffraction patterns were obtained using a Bruker D8 Advance diffractometer and a Cu Kα X-ray source (Cu Kα = 1.5406 Å), with a stepsize of 0.02 º and steptime of 2 s, i.e., scan rate of 1 º/100 s. The various iron phases in the catalysts were identified using the cards published by The Joint Committee on Powder Diffraction Standards (JCPDS) from the American Society for Testing Materials (ASTM). Nowadays, electronic resources for phase’s identification are also available.

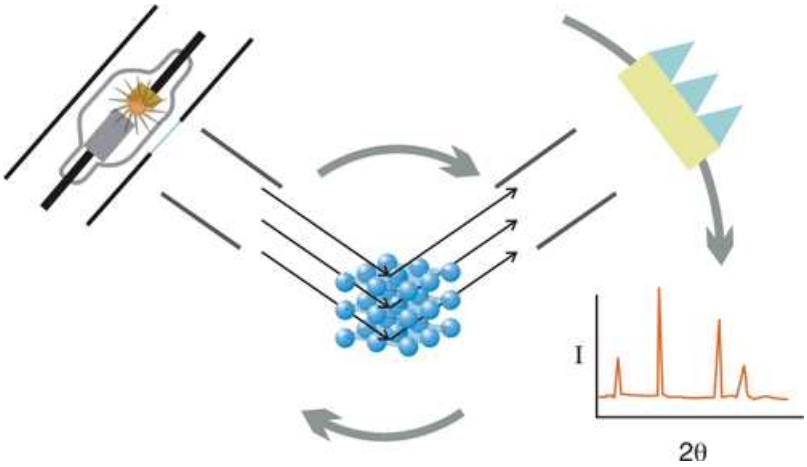

Figure 2.2 – X-ray diffraction scheme [29].

2.3.4. X-ray photoelectron spectroscopy (XPS)

XPS was specifically used for the study of the nature of the iron particles on the catalysts' surface (7-11 nm of thickness), providing information about the Fe oxidation state. This technique, as all the spectroscopies, is based on the interaction between photons emitted by an energy source and the material where they fall, and is characterized by its high surface sensibility due to the short range of the photoelectrons that are excited from the solid. Actually, the irradiation of a sample by photons with a higher energy than the binding energy of the electrons of the atoms leads to excitation of these electrons, which leave the sample with the excess of energy. This technique measures the excited electrons' kinetic energy. This is experimentally done by their deviation through electrostatic-magnetic fields, allowing the electrons with the same kinetic energy reaching the detector at a given time. This technique is illustrated in Figure 2.3.

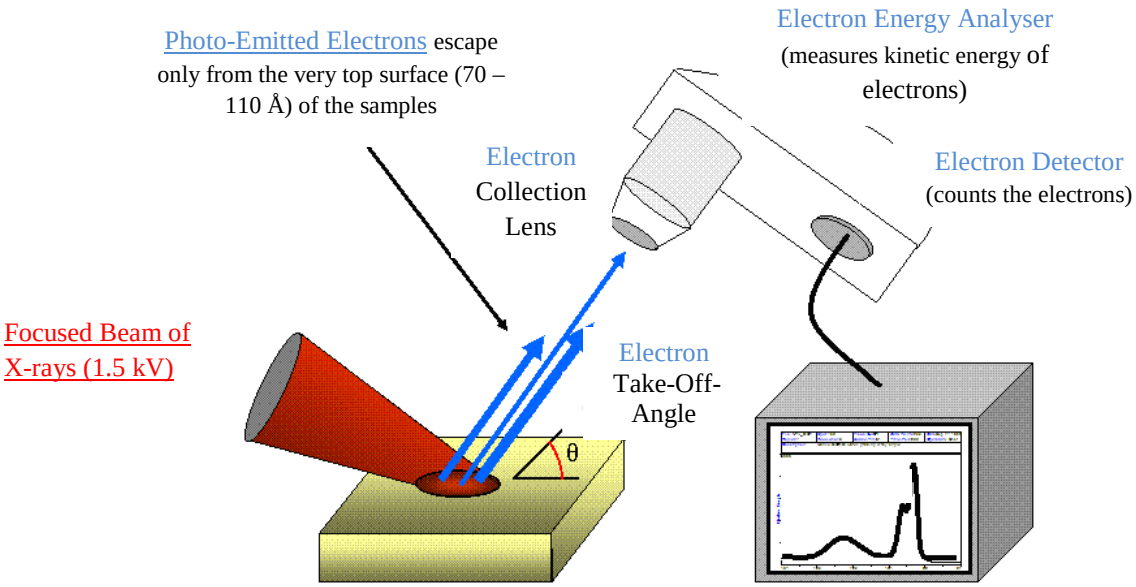

Figure 2.3 – Scheme of the X-ray photoelectron spectroscopy technique (adapted from [30]).

Because a set of binding energies is characteristic for an element, XPS can be used to analyze the composition of samples. Binding energies are not only element specific but contain chemical information: the energy levels of core electrons depend on the chemical state of the atom. In general, the binding energy increases with increasing oxidation state and also with the electronegativity of the ligands, for a fixed oxidation state.

In this work, this technique was carried out using an achromatic Al (Kα) x-ray source in an ESCALAB 200A, VG Scientific system, with the Vision and CasaXPS softwares for data acquisition and analysis, respectively.

2.3.5. Thermogravimetry

Thermogravimetry (TG) and differential thermogravimetry (DTG) in an inert atmosphere were used to look for information about the nature of the adsorbed products over the used adsorbents/catalysts and the interactions between the solids and the dye/oxidation products molecules. This is a simple technique that uses a thermobalance and the weigh variation of the sample is recorded as a function of temperature. The

differential analysis allows to observe the thermal effects during the heating that can come from the release of volatiles, fusion, phase changes, etc. [20].

TG experiments were performed in He flow (30 $cm^3.min^{-1}$ – atmospheric conditions of temperature and pressure) and a heating rate of 20 $^oC.min^{-1}$ up to 1000 ^oC using a thermobalance model TGA-50H.

TG experiments in air atmosphere allowed estimating the iron loading in AC/Fe catalysts, from the weight of ashes (by comparing to the support).

2.3.6. Temperature-programmed desorption (TPD)

Temperature programmed desorption (TPD) was used for the characterization of surface groups in carbon materials and determination of oxygen content. This technique is widely use for the surface chemical assessment of ACs, showing to be a powerful tool in this scope [31, 32].

AC materials were heated in a He flow (60 $cm^3.min^{-1}$ – atmospheric conditions of temperature and pressure) up to 1000 ^oC with a heating rate of 50 $^oC.min^{-1}$. The amount of evolved H_2, H_2O, CO and CO_2 was recorded as a function of temperature using a quadrupole mass spectrometer (Balzers, model Thermocube). The oxygen content was calculated from the amounts of CO and CO_2 evolved from the different oxygenated surface groups released while increasing the temperature. The assignation of the peaks to the different types of surface groups was carried out according to the bibliography and quantified by integration of the TPD areas. Basically, CO_2 evolved at low temperatures comes from carboxylic acids and from anhydride/lactones at higher temperatures (higher thermal stability); carboxylic anhydrides originates both CO and CO_2; CO comes also from phenols, ethers, carbonyls and quinines [31].

Table 2.1 compiles all the techniques mentioned for the AC-based materials characterization, with the respective purpose and equipment used.

Table 2.1 – Characterization techniques used along this dissertation, equipments and purposes.

Technique	Equipment	Purpose
N_2 (77 K) and CO_2 (273 K) adsorption/desorption	Quantachrome Autosorb 1	To determine textural properties(surface areas; porosity characterization)
SEM / EDS	JEOL JSM 35C / Noran Voyager	To study morphology
HRTEM	Philips CM-20 electron microscope	To evaluate iron dispersion
XRD	Bruker D8 Advance diffractometer	To evaluate iron dispersion / nature of iron particles
XPS	VG Scientific ESCALAB 200 A	To assess nature of iron particles / Fe oxidation state
TG-DTG	Shimadzu TGA-50H thermobalance	To determine iron content of AC/Fe catalysts (in air); To quantify/characterize adsorbed products
TPD	Quadrupole mass spectrometer from Balzers, Thermocube/	To study materials' surface chemistry

2.4. Adsorption and catalytic oxidation experiments

One of the focus of this thesis is to find the best AC/Fe catalyst for the elimination of the model azo-dye Orange II by the heterogeneous Fenton process, in batch reactors, for being used afterwards in a continuous fixed-bed reactor. Thus, firstly, the best commercial AC was chosen, then the most suitable iron precursor and finally the best size of AC/Fe catalyst, all of them in batch processes. During all these works/chapters, the duality adsorption/catalysis was analysed, correlations between iron catalysts and their properties were established and, inclusively, a new insight about Orange II elimination by characterization of spent AC Fenton-like catalysts was carried out.

Then, a fixed-bed reactor was implemented to analyse the ability of the selected AC/Fe to treat dye solutions, including a real textile effluent, in a continuous process.

This section describes the methodology followed.

2.4.1. Batch experiments

Tests were carried out in a jacket *slurry* batch reactor (1.5 or 0.3 L of capacity), using a 0.1 mM OII aqueous solution (prepared with distilled water) and 0.1 $g.L^{-1}$ of solid at 30 ºC and pH 3, the reference conditions for the Fenton reaction [6, 17, 33, 34]. The OII concentration used is in the range of azo-dyes' concentrations typically found in textile effluents [35-37]. The batch reactor was provided with magnetic stirring and a thermostatic bath (from Huber) to keep the temperature constant along the runs (Fig. 2.4). The initial pH 3 was set by using a 1 M sulphuric acid solution. pH and temperature were assessed by a pH-meter (WTW - Inolab pH 730), using a pH electrode with a thermocouple (WTW-SenTix 81) immersed in the solution. The time zero of the experiments was coincident with the addition of the activated carbon (for adsorption) or the solid + hydrogen peroxide (for catalysis). OII concentration in the experiments was continuously followed by visible spectrophotometry, as detailed in section 2.5.1., with the help of a flow-through cell and a peristaltic pump. This parameter, as well as the temperature and pH, were recorded, monitored and saved along the reaction time using a home developed LabView 9.0 interface. The set-up was prepared to have two experiments running simultaneously, in two parallel reactors - Fig. 2.4, in spite of on-line recording data by LabView was only possible for one experiment at a time.

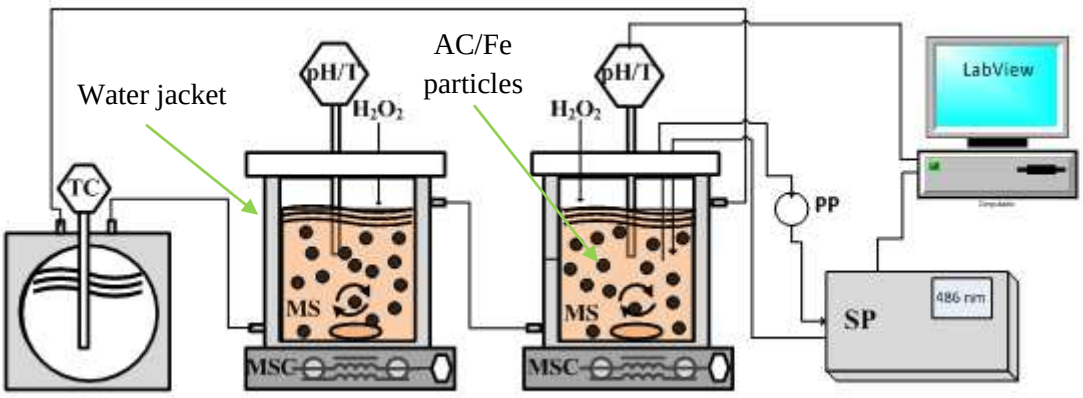

MS – Magnetic Stirrer

MSC – Magnetic Stirrer Controller

pH/T – pH-meter with thermocouple

SP – Spectrophotometer (λ = 486 nm)

PP - Peristaltic Pump

Figure 2.4 – Experimental set-up used in the batch runs.

In all oxidation experiments, samples were regularly taken and filtrated through Reeve Angel microfibre glass filter paper (pores' diameter of 0.8 μm) for total organic carbon analysis (TOC) and to determine the iron leached (iron left from the support). To guarantee the stop of the reaction in the flasks with the samples recovered, sodium sulphite was added to consume the residual H_2O_2 and the samples were kept in the fridge for later analysis.

2.4.2. Experiments in a fixed-bed reactor

A jacket borosilicate glass column with 15 mm of internal diameter and 250 mm long was used, with a piston on the top and bottom, so that any bed height could be used within the length of the column. The reactor was filled with W_{cat} = 6.63 g (10 cm) of AC/Fe catalyst; completely inert glass spheres were placed at the top and at the bottom of the column to promote a homogeneous diffusion of the solution, mainly at the entrance. A thermostatic bath (from Huber) was used to control the temperature of the column and the solutions stored in it (Fig. 2.5). Before being fed, initial pH of the H_2O_2

and dye-containing solutions was set to the desired value. The dye and hydrogen peroxide solutions were fed to the column by using a Heidolph peristaltic pump (model Pumpdrive 5001), the fed being done upwards to avoid the clogging of the column bottom fritz and of the column itself, as well as the air retention, which exits through the end fritz. Feed concentrations are the half of those in the reservoirs, counting with the dilution factor for equal flow rates of each solution; the total flow rate used was Q = 2 ml.min$^{-1,}$ checked along each experiment and being the double of dye and hydrogen peroxide flow rates. Dye concentration was followed continuously at the column outlet as in batch experiments, and also recorded by the same interface. Samples were also taken during these experiments, following the same procedure as described for batch reactors (section 2.4.1.), for the TOC and iron leaching assessment.

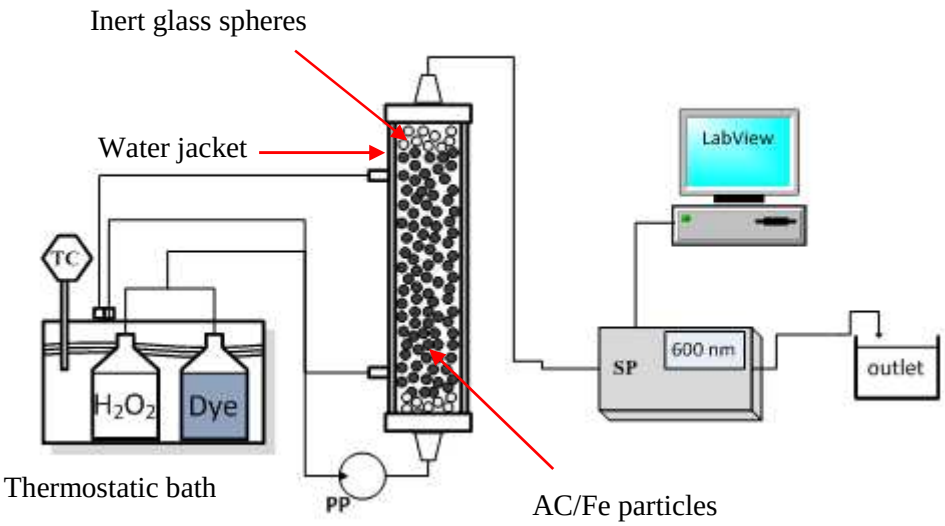

Figure 2.5 – Experimental set-up used in the continuous runs.

A parametric study was done, considering the temperature, pH of the solutions and feed H_2O_2 concentration. The stability of the AC bed was also taken into account. At the end, the selected catalytic system was applied to the treatment of a real textile effluent generated during the cotton dyeing and provided by a textile company in the North of Portugal (Barcelos) – Têxteis Luís Simões.

The three analytical techniques used – UV-Vis spectrophotometry, total organic carbon (TOC) analysis and atomic absorption – are briefly described below.

2.5. Analytical techniques

2.5.1. UV-Vis spectrophotometry

UV-Vis spectrophotometry was used to determine OII concentration along adsorption/catalytic experiments. This analytical technique exploits interactions between radiation and materials, mainly the absorption and transmission phenomena. When the incident radiation has energy that is equal to the difference between two energetic levels of molecules of the material, this energy is transferred to the material, occurring the radiation absorption, which is characteristic of each substance. By other words, each substance has its own absorption spectrum (absorbed light intensity *vs.* wavelength of the radiation), which allows its identification and can be also used to quantify it in a solution. This determination is done by the absorbance measurement - amount of light absorbed by the solution (*Abs*). The basis of this technique is the Lambert-Beer's law: the absorbance exhibited by a substance is directly proportional to its thickness *b* (optical path length) and concentration *C* [38, 39]:

$$Abs = abC \tag{2.10}$$

where *a* is a characteristic constant of the system called absorptivity when *C* is in $g.L^{-1}$, or molar absorptivity when *C* is in $mol.L^{-1}$.

Thus, experimentally, plotting *Abs vs. C* provides a calibration curve, from which is possible to determine the concentration of the compound in a solution. This should however be done within the linear calibration range. It is noteworthy that the Lambert-Beer's law has some limitations, mainly for highly concentrated solutions (where there is deviation from linearity), wide pH variations or when absorbent species don't represent the total concentration [19].

During the present experiments, absorbance was read in a Philips PU8625 UV-Vis spectrophotometer at the maximum absorbance wavelength of the studied dye, 486 nm, which is the characteristic wavelength of the Orange II molecule (Fig. 2.6) and corresponds to a region wherein interference by oxidation products does not exist [40].

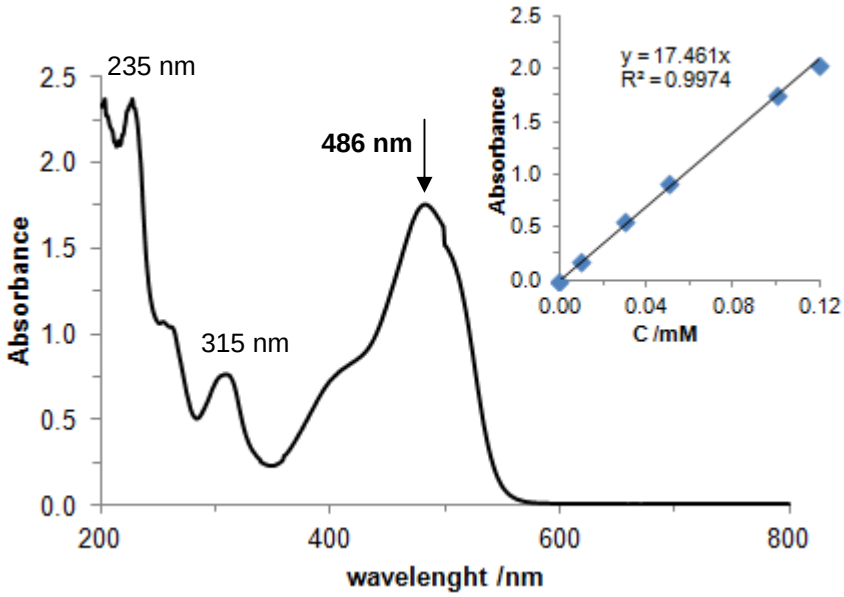

Figure 2.6 – UV-Vis spectrum of an OII solution (concentration 1×10^{-4} M), using a quartz cell, and corresponding calibration curve.

However, the main limitation of the UV-Vis to follow the advance of the reaction is that it is unable to detect intermediate species without the chromophere group, even if exhibiting absorbance in another region of the spectrum. Thus, if the oxidation of the dye is not complete to CO_2, intermediate compounds remain in the solution and are not detected by this technique. Consequently, additional tests, such as total organic carbon (TOC) analysis are needed to evaluate the mineralization degree of the parent compound oxidation.

2.5.2. Total organic carbon (TOC) analysis

Total organic carbon (TOC) assessment provides a speedy and convenient way of determining the mineralization degree of organics contamination in water and is a complementary technique of UV-Vis spectrophotometry in the evaluation of the extent of dyes degradation.

In order to evaluate the mineralization degree by total organic carbon (TOC) analyses, samples were regularly taken during the tests and filtered. Sodium sulphite in excess was added to the samples (which were kept in the fridge) to guarantee the stop of

the reaction, since this reagent consumes instantaneously the residual hydrogen peroxide. TOC analyses were done in a TOC-500A apparatus.

Briefly, after aspirating the sample, this equipment quantifies the total carbon (TC) and the inorganic carbon (IC) - the carbonate, bicarbonate and dissolved CO_2 - present in the sample, and determines the total organic carbon (TOC) by difference, which corresponds to all carbon atoms covalently bonded in organic molecules. Thus, calibration curves for total carbon and inorganic carbon were obtained. All TOC values reported are the average of at least two TC and IC measurements and only the values with a CV (coefficient of variation) < 2 % were validated.

It is expected that TOC levels decrease along Fenton-like experiments, once it corresponds to an increase in the degree of mineralization, i.e., an increase of the parent compound degradation. However, it is noteworthy that TOC removal can also occur due to adsorption of the organic compounds.

2.5.3. Atomic absorption spectrometry

Atomic absorption spectroscopy (AAS) was a very useful analytical tool in the work here developed once it allowed studying the loss of iron from the catalysts, i.e., the iron's leaching degree, by determining the iron concentration (using a UNICAM 939/959 spectrophotometer) in samples taken along the experiments. Iron leaching is a phenomenon with great importance for the whole catalytic process in wastewaters treatment, not only for environmental protection and human's health (Fe concentration of treated water has to be lower than legislated standards – 2 ppm in the UE [41]), but also in what concerns to catalysts' reutilization/stability.

To analyze iron, the samples were aspirated and subjected to a flame (2000-3000 K). As the light is absorbed in a selective way, the radiation comes from a specific source and passes through the flame into a detector (see Fig. 2.7). This apparatus measures the change of intensity of light produced by the absorption and converts it into absorbance, following the basic principles of the Lambert-Beer's law applied to AAS. Therefore, with a calibration curve (absorbance *vs.* concentration) it is possible to determine the iron amount in solution for each sample. In this work, the absorbance of

each sample was measured three times and only the values with a CV < 2 % were validated.

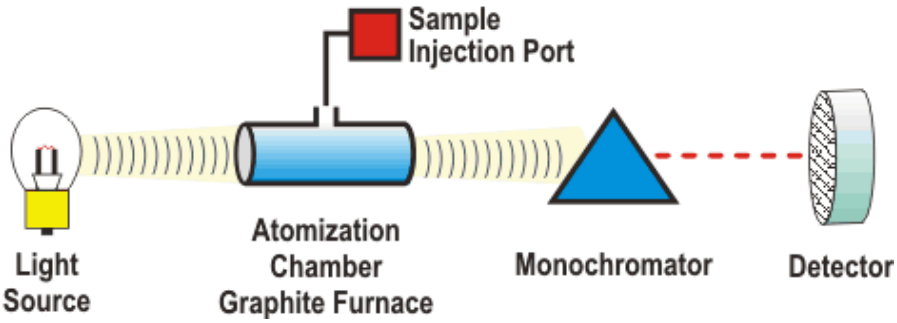

Figure 2.7 – Atomic absorption spectrometry scheme (retrieved from [42]).

References

[1] C. Hsiu-Mei, C. Ting-Chien, P. San-De, C. Hung-Lung, Adsorption characteristics of Orange II and Chrysophenine on sludge adsorbent and activated carbon fibers, J. Hazard. Mater. 161 (2009) 1384-1390.

[2] M. Stylidi, D.I. Kondarides, X.E. Verykio, Pathways of solar light-induced photocatalytic degradation of azo dyes in aqueous TiO_2 suspensions, Appl. Catal., B 40 (2003) 271-286.

[3] C. Bauer, P. Jacques, A. Kalt, Photooxidation of an azo dye induced by visible light incident on the surface of TiO_2, J. Photochem. Photobiol., A 140 (2001) 87-92.

[4] J. Feng, X. Hu, P.L. Yue, H.Y. Zhu, G.Q. Lu, Degradation of azo-dye orange II by a photoassisted Fenton reaction using a novel composite of iron oxide and silicate nanoparticles as a catalyst, Ind. Eng. Chem. Res. 42 (2003) 2058-2066.

[5] J. Bandara, C. Morrison, J. Kiwi, C. Pulgarin, P. Peringer, Degradation/decoloration of concentrated solutions of Orange II. Kinetics and quantum yield for sunlight induced reactions via Fenton type reagents, J. Photochem. Photobiol., A 99 (1996) 57-66.

[6] J.H. Ramirez, F.J. Maldonado-Hódar, A.F. Pérez-Cadenas, C. Moreno-Castilla, C.A. Costa, L.M. Madeira, Azo-dye Orange II degradation by heterogeneous Fenton-like reaction using carbon-Fe catalysts, Appl. Catal., B 75 (2007) 312-323.

[7] J. Feng, X. Hu, L.Y. Po, Discoloration and mineralization of Orange II using different heterogeneous catalysts containing Fe: A comparative study, Environ. Sci. Technol. 38 (2004) 5773-5778.

[8] J. Deng, J. Jiang, Y. Zhang, X. Lin, C. Du, Y. Xiong, $FeVO_4$ as a highly active heterogeneous Fenton-like catalyst towards the degradation of Orange II, Appl. Catal., B 84 (2008) 468-473.

[9] N. Daneshvar, S. Aber, V. Vatanpour, M.H. Rasoulifard, Electro-Fenton treatment of dye solution containing Orange II: Influence of operational parameters, J. Electroanal. Chem. 615 (2008) 165-174.

[10] J. Chen, L. Zhu, Catalytic degradation of Orange II by UV-Fenton with hydroxyl-Fe-pillared bentonite in water, Chemosphere 65 (2006) 1249-1255.

[11] J.M. Peralta-Hernández, Y. Meas-Vong, F.J. Rodríguez, T.W. Chapman, M.I. Maldonado, L.A. Godínez, Comparison of hydrogen peroxide-based processes for treating dye-containing wastewater: Discoloration and destruction of Orange II azo dye in dilute solution, Dyes Pigm. 76 (2008) 656-662.

[12] H. Zhang, Y. Li, X. Zhong, X. Ran, Application of experimental design methodology to the discoloration of Orange II using low iron concentration of photoelectro-Fenton process, Water Sci. Technol. 63 (2011) 1373-1380.

[13] N. Chahbane, D.L. Popescu, D.A. Mitchell, A. Chanda, D. Lenoir, A.D. Ryabov, K.W. Schramm, T.J. Collins, Fe^{III}–TAML-catalyzed green oxidative degradation of the azo dye Orange II by H_2O_2 and organic peroxides: products, toxicity, kinetics, and mechanisms, Green Chem. 9 (2007) 49-57.

[14] K. Vinodgopal, D. Wynkoop, P. Kamat, Environmental photochemistry on semiconductor surfaces: photosensitized degradation of a textile azo dye, acid orange 7, on TiO_2 particles using visible light, Environ. Sci. Technol. 30 (1996) 1660-1666.

[15] F. Chen, Y. Xie, J. Zhao, G. Lu, Photocatalytic degradation of dyes on a magnetically separated photocatalyst under visible and UV irradiation, Chemosphere 44 (2001) 1159-1168.

[16] M. Matsui, T. Kimura, T. Nambu, K. Shibata, Y. Takase, Reaction of water–soluble dyes with ozone, J. Soc. Dyers Colour.100 (1984) 125-127.

[17] F. Duarte, F.J. Maldonado-Hódar, A.F. Pérez-Cadenas, L.M. Madeira, Fenton-like degradation of azo-dye Orange II catalyzed by transition metals on carbon aerogels, Appl. Catal., B 85 (2009) 139-147.

[18] S.J. Gregg, K.S.W. Sing, Adsorption, Surface Area and Porosity, 2nd Ed., Academic Press INC., London, 1982.

[19] M. Faraldos, C. Goberna (Eds), Técnicas de Análises y Caracterización de Materiales, Consejo Superior de Investigaciones Científicas, Madrid, 2008.

[20] J.L. Figueiredo, F.R. Ribeiro, Catálise Heterogénea, 2nd Ed., Fundação Calouste Gulbenkian, Lisboa, 2007.

[21] D. Cazorla-Amoros, J. Alcañiz-Monge, M.A. De la Casa-Lillo, A. Linares-Solano, CO_2 as an adsorptive to characterize carbon molecular sieves and activated carbons, Langmuir 14 (1998) 4589-4596.

[22] R.M. Barrer, N. MacKenzie, D. McLeod, The adsorption method of measuring surface areas, J. Chem. Soc. (1952) 1736-1744.

[23] J.H. Singleton, G.D. Halsey, The growth of crystalline layers on foreign surfaces, Can. J. Chem. 33 (1955) 184-192.

[24] R.C. Bansal, J.B. Donnet, F. Stoeckli, Activated Carbon, Marcel Dekker inc, New York and Basel, 1988.

[25] F. Stoeckli, A. Guillot, A.M. Slasli, D. Hugi-Cleary, Microporosity in carbon blacks, Carbon 40 (2002) 211-215.

[26] E.P. Barrett, L.G. Joyner, P.P. Halenda, The determination of pore volume and area distributions in porous substances. I. Computatons from nitrogen isotherms, J. Am. Chem. Soc. 73 (1951) 373-380.

[27] C.A. Moreno-Castilla, M.A. Alvarez-Merino, M.V. Lopez-Ramon, J. Rivera-Utrilla, Cadmium adsorption on different carbon adsorbents from aqueous solutions. Effect of surface chemistry, pore texture, ionic strength and dissolved natural organic matter, Langmuir 20 (2004) 8142–8148.

[28] W.L. Bragg, The Crystalline State: Volume I. New York, The Macmillan Company, 1934.

[29] The Electron Microprobe method – Focusing electrons and diffracting X-rays, retrieved on August 20th 2012 from http://ees2.geo.rpi.edu/probe/Images/concepts/concept2.html.

[30] X-ray photoelectron spectroscopy - Wikipedia, retrieved on August 16th 2012 from http://en.wikipedia.org/wiki/X-ray_photoelectron_spectroscopy.

[31] J.L. Figueiredo, M.F.R. Pereira, M.M.A. Freitas, J.J.M. Orfão, Modification of the surface chemistry of activated carbons, Carbon 37 (1999) 1379-1389.

[32] S. Morales-Torres, F.J. Maldonado-Hódar, A.F. Pérez-Cadenas, F. Carrasco-Marín, Design of low-temperature Pt-carbon combustion catalysts for VOC's treatments, J. Hazard. Mater. 183 (2010) 814-822.

[33] S.M. Arnold, W.J. Hickey, R.F. Harris, Degradation of atrazine by Fenton's reagent: condition optimization and product quantification, Environ. Sci. Technol. 29 (1995) 2083-2089.

[34] E. Neyens, J. Baeyens, A review of classic Fenton's peroxidation as an advanced oxidation technique, J. Hazard. Mater. 98 (2003) 33-50.

[35] S.A. Ong, E. Toorisaka, M. Hirata, T. Hano, Discoloration of azo dye (Orange II) in a sequential UASB-SBR system, Sep. Purif. Technol. 42 (2005) 297-302.

[36] C.R. Corso, A.C. Almeida, Bioremediation of dyes in textile effluents by Aspergillus oryzae, Microb. Ecol. 57 (2009) 384-390.

[37] L.C. Davies, C.C. Carias, J.M. Novais, S. Martins-Dias, Phytoremediation of textile effluents containing azo dye by using Phragmites australis in a vertical flow intermittent feeding constructed wetland, Ecol. Eng. 25 (2005) 594-605.

[38] F.B. Marti, Quimica Analitica Cualitativa, 12th Ed., Paraninfo, Madrid, 1985.

[39] P. Atkins, J. de Paula, Physical Chemistry for the Life Sciences, New York, Oxford University Press, 2006.

[40] J.H. Ramirez, C.A. Costa L.M. Madeira, G. Mata, M.A. Vicente, M.L. Rojas-Cervantes, A.J. López-Peinado, R.M. Martín-Aranda, Fenton-like oxidation of Orange II solutions using heterogeneous catalysts based on saponite clay, Appl. Catal., B 71 (2007) 44-56.

[41] S. Sabhi, J. Kiwi, Degradation of 2,4-dichlorophenol by immobilized iron catalysts, Water Res. 35 (2001) 1994-2002.

[42] Atomic absorption spectrometry - ETS Laboratories, retrieved on August 20th 2012 from http://www.etslabs.com/analysis.aspx?id=VPBA

CHAPTER 3 - Influence of the characteristics of carbon materials on their behaviour as heterogeneous Fenton catalysts for the elimination of the azo dye Orange II from aqueous solutions

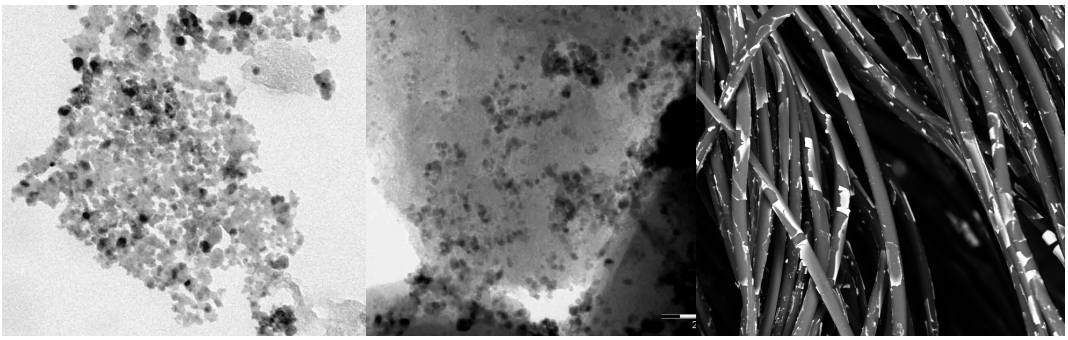

Chapter 3. Influence of the characteristics of carbon materials on their behaviour as heterogeneous Fenton catalysts for the elimination of the azo dye Orange II from aqueous solutions [*]

Abstract

Three different commercial activated carbons (ACs), Norit RX 3 Extra, Merck and Kynol, were used as Fe-supports to develop Fenton catalysts (7% wt. Fe/AC) for the elimination of the azo-dye Orange II. Both supports and catalysts were characterized by several techniques (N_2 and CO_2 adsorption, X-ray diffraction, high-resolution transmission electron microscopy). The elimination of the dye is a complex heterogeneous process with co-existence of adsorption and oxidation. Adsorption and catalytic experiments were carried out with only 0.1 $g.L^{-1}$ of solid in a *slurry* batch reactor at 30 ºC, pH 3 and initial dye concentration of 0.1 mM. The discoloration was followed continuously by the absorbance measurement; mineralization and leaching levels were evaluated by TOC and atomic absorption analyses, respectively. Correlations of ACs characteristics with their adsorptive or catalytic performances were established in order to select the best support. All the ACs are microporous materials and the OII adsorption is favoured by an increase of the micropore width. Although the carbon surface proves to be catalytically active, the main OII elimination process in pure ACs is adsorption, while for the Fe-catalyst it is determined by the Fenton oxidation. The Fe-Norit is the most active catalyst, which is associated to its high surface area located on large micropores that favours both the OII adsorption and the Fe-dispersion. However, this catalyst presented the highest tendency to the leaching. Anyway, the leaching values remain quite low even in this case (<1.7% of the total Fe), guarantying the possible reuse of the catalysts.

[*] Adapted from: F. Duarte, F.J. Maldonado-Hódar, L.M. Madeira, Appl. Catal., B 103 (2011) 109-115.

3.1. Introduction

The heterogeneous Fenton's reaction using activated carbons (AC) as catalyst's support has been shown to be a promising process in the wastewater treatment field, effectively destroying many organics (*e.g.* [1-4]). Nevertheless, the choice of the appropriate AC is not so obvious. ACs performance in the oxidation reactions depends on their physical structure (porosity and surface area) and surface chemistry [5, 6]. These parameters also determine the chemical nature and dispersion of the metal particles when used as supported catalysts, which defines the final catalytic performance [2, 3, 5]. The presence of mesoporosity permits a high metal dispersion and consequently a high catalytic activity, however, these catalysts also present the higher leaching degree [2] and thus the optimization of these parameters is a real challenge.

In this chapter, three different commercial activated carbons and their Fe-supported catalysts were tested in order to choose the best material in the elimination of the model dye Orange II (OII) by the heterogeneous Fenton process in a batch reactor. Several experiments were carried out to differentiate the adsorptive and catalytic behaviour, the homogeneous/heterogeneous character of the process and particularly the influence of textural parameters of the materials and their performances.

3.2. Materials and Methods

Three commercial activated carbons (ACs) were used as supports. The samples provided by Merck (Ref 102514 AC pure), Norit (Norit RX 3Extra) and Kynol (ACC-5092-15 Fabrics) are commercialized as granular, extruded pellets and fabrics, in that order. They will be referenced hereafter as M, N and K, respectively. Thus, N and M ACs were milled to the powder form (< 0.15 mm) and K fabrics were unravelled to fibres (15-18 μm of diameter) and cut in as small pieces as possible. All of them were used without additional treatment. Catalysts (M-Fe, N-Fe and K-Fe) were prepared following the procedure described in Chapter 2, section 2.2. FTIR and TG analysis of the supports and impregnated catalysts previously done [3] guaranteed that the precursor was decomposed by the applied pre-treatment – 2 h at 300 ºC in He

atmosphere (no acetate band was noticed in the case of the catalysts). The choice of the precursor is related to previous works [2, 3], where pure carbon aerogels were used as supports, and iron (II) acetate was selected in order to maintain the purity of the catalysts, i.e. trying to avoid the introduction of any heteroatom (N, S, Cl, etc.) with the precursor salts. Here the same precursor and loading were maintained.

Characterization of the materials was done by N_2 (at 77 K) and CO_2 (at 273 K) adsorption, HRTEM, XRD and SEM / EDS (only in the case of fibres) and according to the procedures described in Chapter 2 – section 2.3. The pH_{pzc} of the ACs supports was obtained by immersion of each sample in water previously boiled (1 g AC /10 ml water). The pH_{pzc} was measured after 48 h according to the methodology described elsewhere [7].

In either adsorption or catalytic experiments, it was used the set-up and the operating conditions described in section 2.4.1 of Chapter 2, and the evaluation of the treated solution was done by using the techniques mentioned in section 2.5 of the same Chapter (namely UV-Vis for OII dye quantification, TOC for assessing the degree of mineralization and atomic absorption spectrometry for quantifying the iron leaching level).

3.3. Results and Discussion

3.3.1. Supports and catalysts characterization

As commented, three commercial ACs were used: Norit (N), Merck (M), and Kynol (K). The N-sample is an extruded carbon and the M-support is a granulated activated carbon. Both of them (according to the supplier's data) present a significant ash content (between 2-6%). These inorganic components can contribute to the catalytic activity of the supports, because they can contain active components; as an example, the Fe-content is 300 and 500 ppm for N and M supports, respectively. However, K-support is a 100% pure AC material made directly from novoloid (phenolic) precursors.

The textural characterization of the materials was developed by the analysis of their corresponding N_2 and CO_2 adsorption isotherms at 77 K and 273 K, respectively.

Results obtained showed that all of them are essentially microporous materials with BET areas ranging between 900 - 1300 $m^2 g^{-1}$ (Table 3.1).

Table 3.1 – Textural characteristics of the supports and catalysts obtained by N_2 and CO_2 adsorption at 77 and 273 K, respectively.

Material	S_{BET} ($m^2.g^{-1}$)	V_{meso} ($cm^3.g^{-1}$)	W_0 (N_2) ($cm^3.g^{-1}$)	L_0 (N_2) (nm)	W_0 (CO_2) ($cm^3.g^{-1}$)
N	1233	0.05	0.54	1.67	0.27
N-Fe	1083	0.10	0.48	1.76	0.34
M	907	0.12	0.37	1.53	0.24
M-Fe	826	0.09	0.36	1.67	0.22
K	1307	0.08	0.53	1.26	0.47
K-Fe	1160	0.06	0.49	1.59	0.48

S_{BET}: BET surface area obtained by N_2 adsorption; V_{meso}: mesopores' volume; W_0 (N_2): micropores' volume obtained by N_2 adsorption; L_0 (N_2): mean micropores' size obtained by N_2 adsorption; W_0 (CO_2): micropores' volume obtained by CO_2 adsorption.

Kynol tissue has the largest BET area, while the M-support has the largest mesopore volume. The corresponding N_2-adsorption isotherms are shown in Fig. 3.1 and match mainly to the type I, typical of microporous materials. The adsorption occurs mainly at low pressures as a consequence of the micropore filling. Nevertheless, the shape of the isotherm knee is quite different, being broader in the case of the N-support, indicating a greater heterogeneity in the micropore size distribution, while the K-support presents a more homogeneous microporosity. The mean micropore size (L_0) progressively decreases in the sense N > M > K. Mainly in the case of M-support, adsorption at higher pressures is indicative of the presence of mesopores.

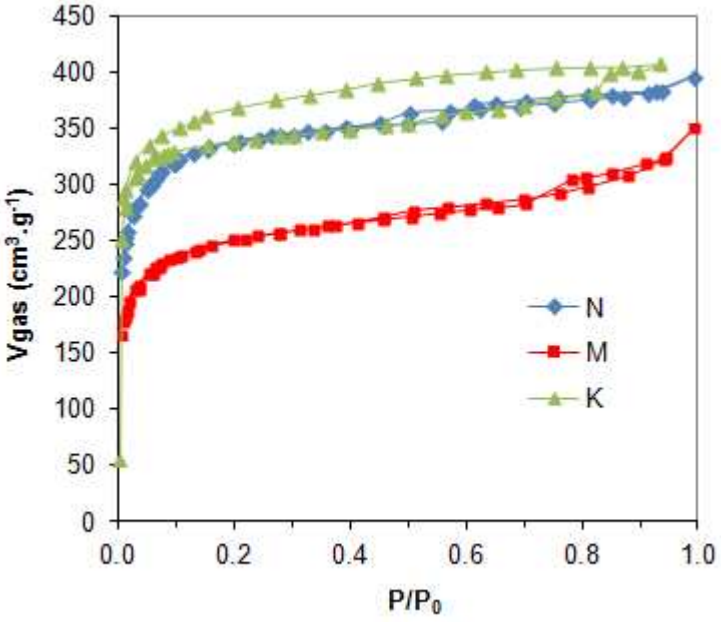

Figure 3.1– N_2 isotherms at 77 K of the AC supports used.

These results are also in agreement with the conclusions obtained when comparing the results from the CO_2 and N_2 adsorption experiments (Table 3.1). Thus, the micropore volume (W_0) accessible to both N_2 and CO_2 is quite similar in the case of K-support, while in the case of M and N-supports W_0 (N_2) > W_0 (CO_2). These results confirm a high homogeneity of the microporosity of the K-support, while N_2 condensation inside the larger micropores of N and M samples occurs. In fact, the difference between W_0 (N_2) and W_0 (CO_2) increases with L_0 because this parameter reaches values close to the mesopore limit (2 nm).

Comparing the porosity values of the supports and catalysts, it can be seen that there is a slight decrease of the surface areas and in most cases of pore volumes while L_0 increases, indicating the blocking of the pores by the Fe particles, as found by other authors [5].

The metal dispersion and chemical nature of the Fe-particles on the catalysts were studied by XRD, HRTEM and SEM/EDS. By HRTEM it was observed a good dispersion of small Fe-particles for both N and M supports (Fig. 3.2). It was difficult to analyze the K-Fe catalyst by TEM because of the lack of contrast of the fibres; nevertheless, the analysis of the sample by SEM/EDS showed iron films on different

regions of the fibres (Fig. 3.3a), indicating that the iron is not homogeneously distributed because the metal loading is not enough to develop a uniform coating on the fibre. The EDS analysis confirms the presence of iron oxides on the fibres' surface (Fig. 3.3b).

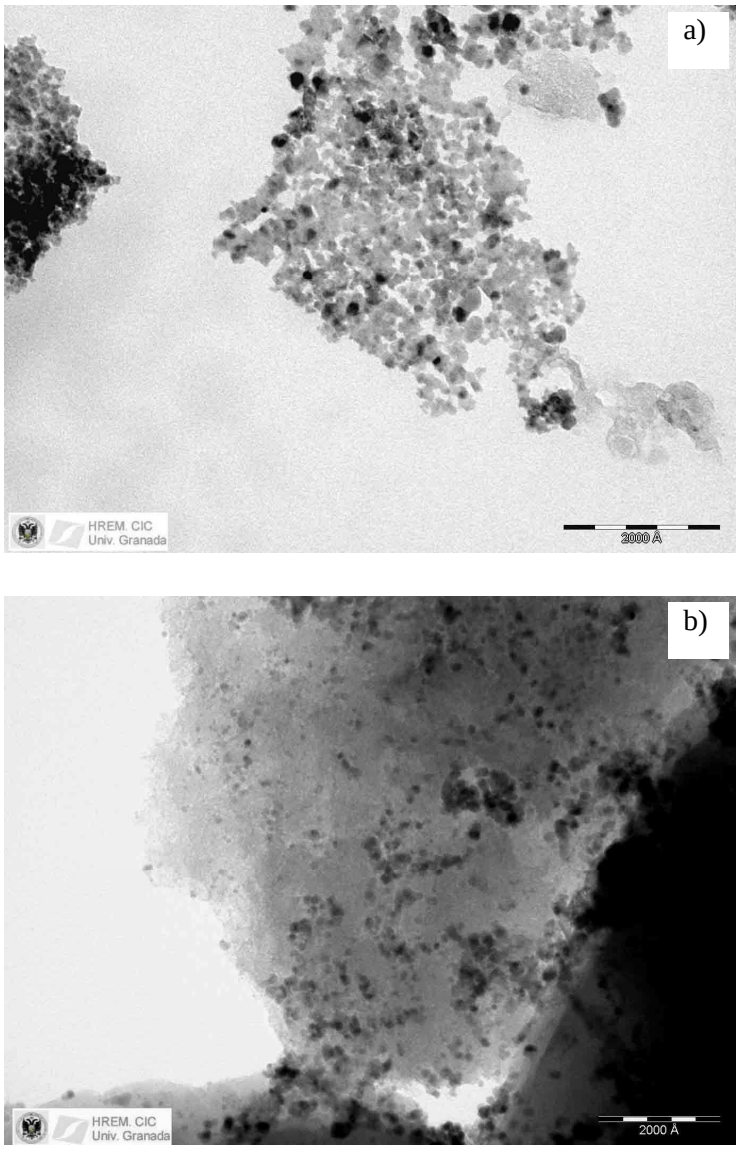

Figure 3.2 – HRTEM photos of the Fe-impregnated catalysts: N-Fe (a) and M-Fe (b).

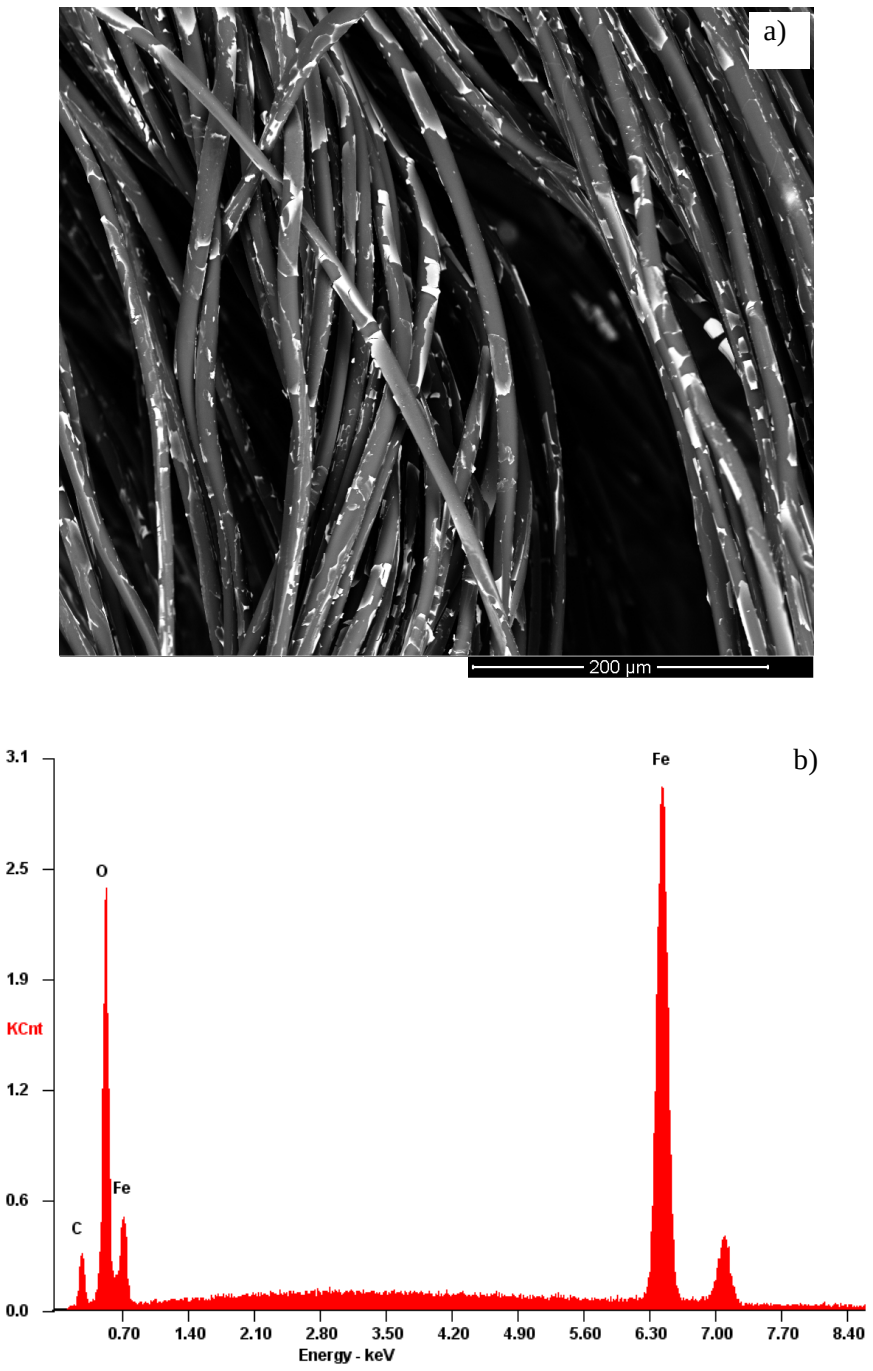

Figure 3.3 – SEM photograph of the K-Fe catalyst (a) and EDS spectrum in an iron film zone (b).

However, XRD patterns confirm that the iron particles are quite small (close to the 4 nm of limit), because the intensity of the peak associated to the iron phase is small (Fig. 3.4). Thus, even in the case of K-Fe, the formation of large three-dimensional iron particles seems to be avoided. Actually, only a wide and small diffraction peak at 2θ =

35.7 º, which corresponds to the I_{100} of γ-Fe_2O_3 (JCPDS 13-534) or Fe_3O_4 (JCPDS 88-0866), is observed. These metallic phases were also previously observed in Fe-carbon supported catalysts [2, 3]. No XRD peaks corresponding to the inorganic components of the supports were observed; nevertheless, mainly in the case of K-Fe catalyst, the XRD pattern shows two broad bands, at around 26 and 44°, corresponding to the 002 and 101 diffraction peaks of graphite, respectively.

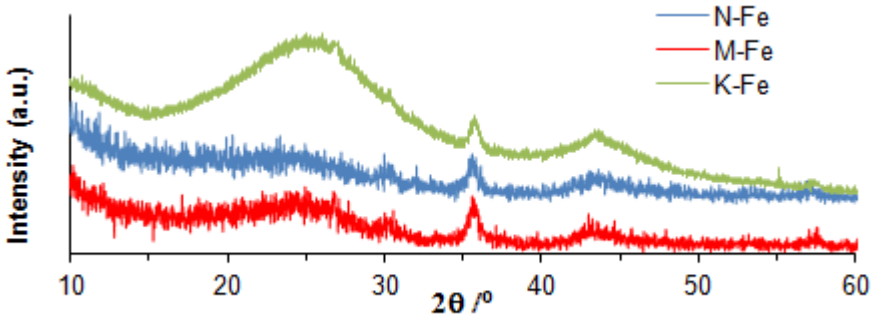

Figure 3.4 – X-ray diffraction patterns of N-Fe, M-Fe and K-Fe catalysts.

3.3.2. Elimination of Orange II from the solution

Due to the co-existence of adsorption and oxidation during the complex heterogeneous Fenton's process, as discussed along this Chapter, the adsorption phenomenon was firstly studied independently.

3.3.2.1. Performance of the ACs

ACs are typically used as adsorbents of pollutants in solution. The adsorptive behaviour of the supports is compared in Fig. 3.5. Taking into account the textural characteristics of the supports (Table 3.1) and their behaviour as OII adsorbents (Fig. 3.5), it is possible to conclude that the adsorption capacity, and also, the adsorption kinetics, is controlled mainly by the presence of large micropores in the support. Thus, in spite the BET surface vary in the sense K ≈ N > M, the low and slow adsorption

process of OII on the K-support indicates a strong restriction for the diffusion of OII into its narrower micropores. The diffusion is favoured with increasing L_0 (N_2), and thus N-support presented the highest adsorption rate and adsorption capacity favoured by the large micropore size and micropore volume. Sample M presents an intermediate behaviour between both N and K samples. Hsiu-Mei *et al.* [8] have reported the dimensions of the OII molecule: 0.73 nm width, 1.36 nm length and 0.23 nm of depth. Because the mean micropore size of K-support is 1.26 nm, adsorption could only occur in slit-shaped micropores (the molecules can enter parallel to the split edge).

The pH_{pzc} measurements indicate that N has clearly a basic surface (pH_{pzc} of 11.0), whereas M and K present pH_{pzc} values around the neutrality (pH_{pzc} are 6.8 and 7.5, respectively). The acid pH 3 used in adsorption or catalytic experiments induces in all the supports a positively charged surface (because pH < pH_{pzc}) and OII to be in the form $C_{16}H_{11}N_2OSO_3^-$ [9]. Thus, the high pH_{pzc} of sample N regarding M or K supports can also contribute to the better adsorptive behaviour of this sample, because in this sense attractive interactions between the aromatic groups of the dye and the basic carbon surface can be favoured. Dispersion forces between the electron system of the OII aromatic ring and the π band of the graphitic planes of the carbon surface are responsible for adsorption. Actually, the acidic oxygen surface groups have an inhibiting effect on adsorption because they localize electrons, removing them from the π band of the graphitic planes of the carbon, thus weakening the attractive forces [10].

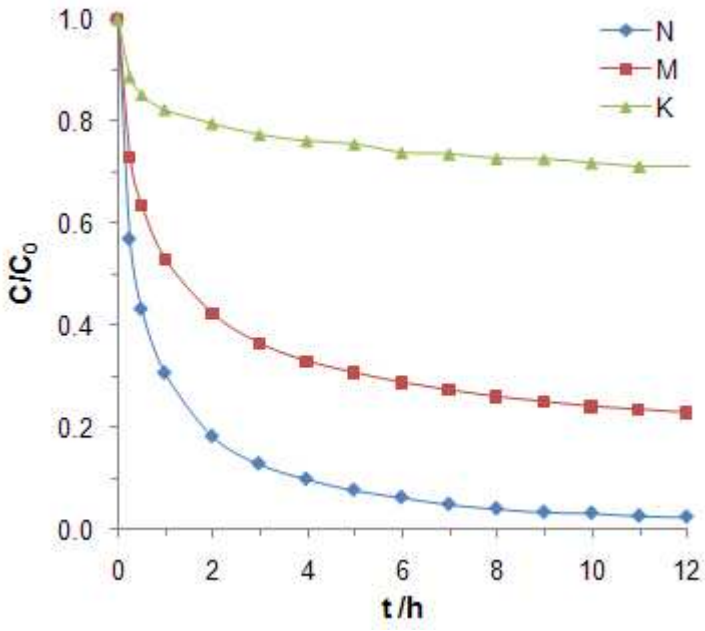

Figure 3.5 – OII adsorption profiles over the supports.

Different experiments were carried out using the N-sample, taking into account its best performance in terms of adsorption. In Fig. 3.6 is shown the adsorption process of OII on N-AC, followed by colour disappearance (TOC values revealed also a complete dye removal after the 1st cycle). The carbon was recovered, by filtration, and submitted to another adsorption experiment. This second cycle evidences that the adsorbent becomes nearly saturated after the first adsorption cycle.

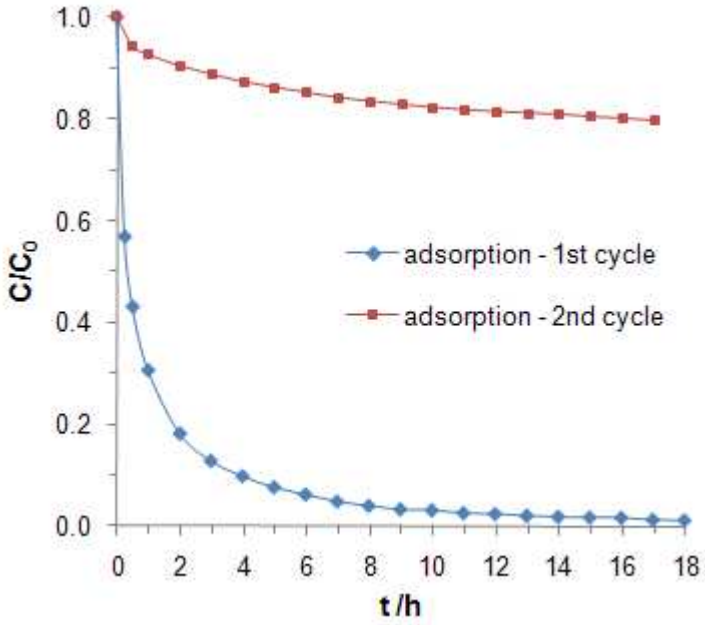

Figure 3.6 – OII adsorption on N-activated carbon in the first and second adsorption cycles.

It is also interesting to clarify if the Norit surface is catalytic active or not in the presence of hydrogen peroxide. Thus, the support was checked in the same experimental conditions that the Fe-supported catalysts – section 3.3.2.2 (6 mM H_2O_2, 0.1 mM OII, pH 3, 30 ºC, 0.1 $g.L^{-1}$ of solid). The results obtained are shown in Fig. 3.7 in comparison with the pure adsorptive behaviour. It is observed that the differences between both curves (OII removal in presence or absence of H_2O_2) are negligible. Thus, the main process leading to removal of OII from the starting solutions seems to be adsorption, even in the presence of H_2O_2.

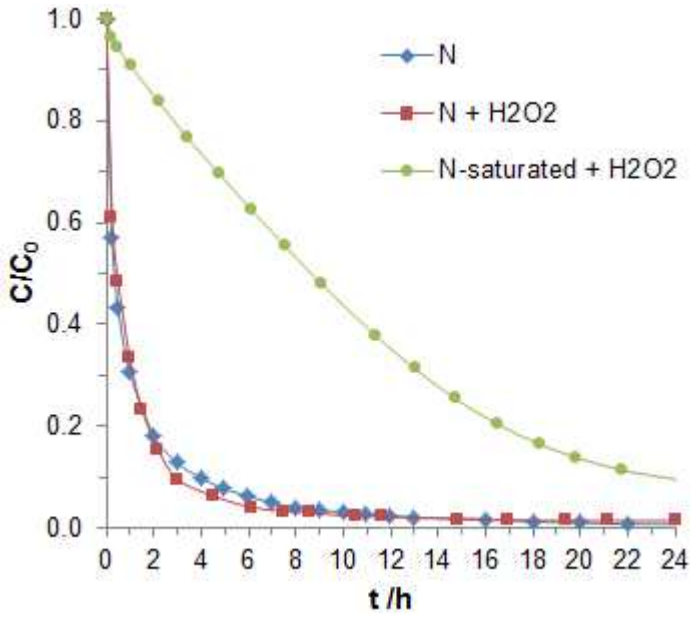

Figure 3.7 – Comparision of OII adsorption and reactive behaviour (in the presence of 6 mM of H_2O_2) for N and N-saturated samples.

To avoid the effect of the adsorption process, a sample of the N-support was saturated with OII (herein called N-saturated) and then used in the same catalytic experimental conditions. The discoloration profile is also shown in Fig. 3.7 in comparison with a fresh sample. Obviously, the discoloration kinetics is slower than when using a fresh sample, because in this case adsorption is avoided. Nevertheless, the N-saturated support removes 90 % of the dye (although only after 24 h), demonstrating that the carbon surface is catalytically active. Because the micropores are saturated, the sample only presents a small fraction of its surface free (the external surface area), which can justify the slow reaction rate observed. It is also worth of noting that H_2O_2 alone is not able to degrade this dye, i.e. the homogeneous oxidation by the oxidant alone can be neglected. Therefore, the carbon surface is clearly catalytically active: the oxidation reaction is a heterogeneous process, where H_2O_2 should be activated on the catalyst surface.

Nevertheless, it is also interesting to determine the porosity range where the oxidation reaction can take place, as well if OII should be adsorbed or degraded in solution after the formation of $OH^{\bullet}$ species on the catalyst surface. The previous

experiments showed that the reaction can at least be developed on the external surface of the AC once the microporosity is saturated.

In order to evaluate if the oxidation can be also developed inside the micropores, and consequently, the possibility of regenerating the spent adsorbents, another fraction of the N-sample was saturated with the dye and then exposed to 24 mM of H_2O_2 along 24 h. After that, the sample was recovered and a second adsorption cycle was developed. The results are shown in Fig. 3.8 in comparison with the second adsorption cycle carried out without regeneration. It is observed that the adsorption capacity increased after the treatment with H_2O_2 of the saturated adsorbent, indicating that OII can be oxidized also inside the micropores. This fact can be favoured also by the large size of the micropores of this support. Thus, the spent N-adsorbent can be regenerated by H_2O_2 treatment, which is of interest for practical applications. Regarding the oxidation mechanism, the results seem to indicate that both OII and H_2O_2 should be adsorbed and activated on the carbon surface. It is important to highlight that the effect of H_2O_2 over the porosity can be neglected, once, as H_2O_2 is not a strong oxidant, significant changes on the textural properties are not verified, even when much higher hydrogen peroxide concentrations are used [11-13].

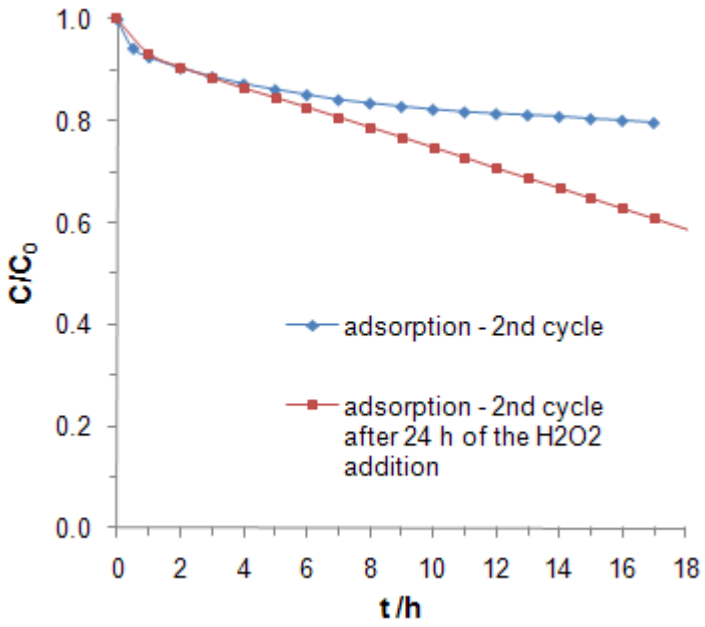

Figure 3.8 – Discoloration profiles of the 2nd cycle of OII adsorption on N support (simple) and after 24h of the addition of 24 mM of hydrogen peroxide.

3.3.2.2. Performance of Fe-AC catalysts

In all cases, Fe-AC catalysts are more active than their corresponding supports. It is well known that Fe is probably the best transition metal for activating H_2O_2 in the Fenton's process [2]. In order to choose the best catalyst in the degradation of the azo-dye OII by the heterogeneous Fenton process, catalytic tests were made using N-Fe, M-Fe and K-Fe in the experimental conditions previously described. N-Fe showed the smaller half-life time ($t_{1/2}$) value, i.e. the time required to reduce the OII concentration in 50%, and the highest TOC reduction – 61% after 24 h (Table 3.2). Thus, the N support showed also here to have the most appropriate textural properties, and the high metal dispersion reached led to the best performance towards OII removal from the solution.

Table 3.2 – Half-life times for OII discoloration, TOC removal and iron leaching obtained with the three catalysts.

Catalyst	$t_{1/2}$ **(h)**	$X_{TOC,\ 24h}$ **(%)**	$C_{Fe,\ 24h}$ **(mg.L^{-1})***
N-Fe	0.58	61	0.116 (1.65 %)
M-Fe	1.75	25	0.047 (0.67 %)
K-Fe	2.58	25	0.062 (0.89 %)

* Values between brackets refer to the percentage of Fe lost from the support.

However, N-Fe has led to the highest value of leaching, 0.116 mg.L^{-1}, whereas M-Fe and K-Fe led to 0.047 and 0.062 mg.L^{-1} of Fe, respectively, after 24 h of reaction. In a previous work [2] it was shown that the Fe-leaching on carbon supports is related with the Fe-dispersion which, on its turn, is favoured by a large external surface area associated to the presence of mesopores. In this case, the high dispersion and consequently high leaching tendency can be related to the larger values of L_0. In spite of this, N-Fe leaching level is still very low, really below the legal limits (2 ppm), guarantying its reutilization once this value represents only 1.7 % of the total iron amount supported on the carbon surface.

The worst performance of the K-Fe sample, in particular the higher $t_{1/2}$ value obtained (Table 3.2), can be also related to the absence of any inorganic components in K support (in opposition to N and M samples) and to the worst Fe dispersion in the fibres (cf. section 3.3.1).

As commented, in these experimental conditions, even with the best catalyst (N-Fe), total mineralization was not reached. Thus one tried to improve TOC removal, in this case by increasing the H_2O_2 dose, starting from the optimum one determined in a previous work [3]. However, the rate of discoloration was not enhanced (see Fig. 3.9a) and the TOC results were even progressively worst with increasing H_2O_2 concentrations up to 24 mM (Fig. 3.9b), which suggest the occurrence of a competition between H_2O_2 and OII molecules towards the active sites (in agreement with the previous results) and/or the scavenging of HO radicals by excess H_2O_2 [14]:

$$H_2O_2 + HO^{\bullet} \rightarrow HO_2^{\bullet} + H_2O \qquad (3.1)$$

However, when 24 mM of H_2O_2 are added in two steps (12 mM at t = 0 and more 12 mM at t = 10 h), mineralization of the dye was improved regarding the experiment with only one addition of 24 mM, increasing from 37 % to 54 % at the end of the runs. By this way, i.e., reducing the oxidant concentration within the batch reactor, parallel reactions like the scavenging (Eq. 3.1) are minimized and the efficiency of H_2O_2 use increased. However, TOC reduction is still low. So, it is also reasonable to consider that stable intermediates are formed that keep in solution (do not adsorb) or hinder the process to proceed (*e.g.* by pore blockage due to formation of polymeric species as found by other authors [15]).

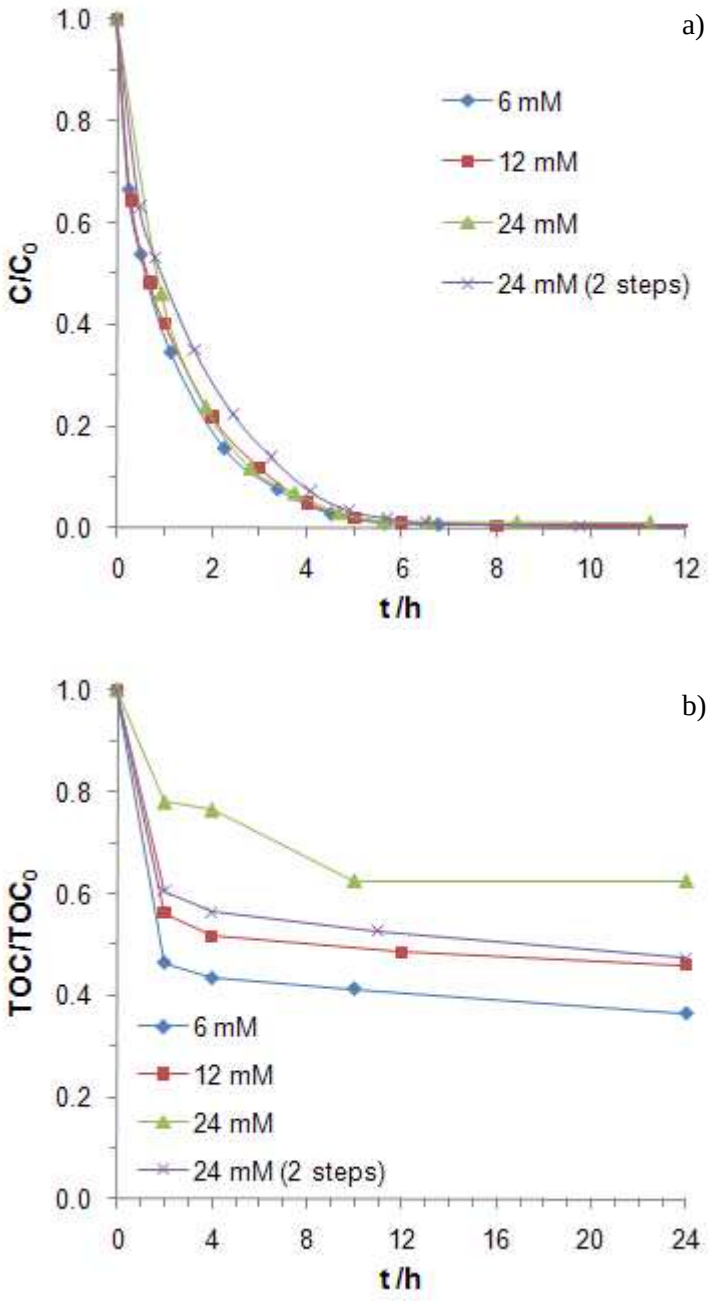

Figure 3.9 – Colour (a) and TOC (b) removal of OII catalysed by N-Fe using different H_2O_2 concentrations.

To confirm the hypothesis mentioned above, the solution after the experiment carried out with 6 mM of H_2O_2, with 39% of the TOC remained (TOC removal of 61% after 24 h of reaction) was filtered. An adsorption experiment similar to those previously described was carried out using this solution and a fresh sample of N AC. However, the TOC did not decrease, proving that this material is not able to adsorb the by-products formed. Therefore, such products seem to have a lower affinity towards the

carbon surface. In general, benzene sulfonate and naphthoquinone are the primary products of an oxidative reaction of an azo-dye of OII's family (phenyl azonaphtol family). Other by-products have been reported such as benzene sulphonic acid, sulphoanilic acid, 1,4-naphthoquinone, phthalic acid [16], quinone and 4-hydroxybenzene sulphonic acid [17]. However, and as mentioned above, the formation of small amounts of polymeric species, inaccessible to the pores of these materials or that could block porosity entrance, could also explain why TOC removal is limited.

3.3.2.3. Adsorption *vs.* catalytic activity of Norit and Norit-Fe

As previously described for the supports, adsorption and catalytic activity were studied independently and compared for N-Fe. The amount of dye adsorbed on the catalyst (Fig. 3.10) is smaller than on the support (Fig. 3.7), once Fe particles block some pores (as shown also by the BET), decreasing its adsorption capacity in such a way that in this case the catalyst is not able to remove completely the OII from the solution. However, and on the contrary to the behaviour observed in Fig. 3.7, in the presence of H_2O_2 the dye removal is clearly improved (Fig. 3.10), due to the presence of Fe - Fenton's process.

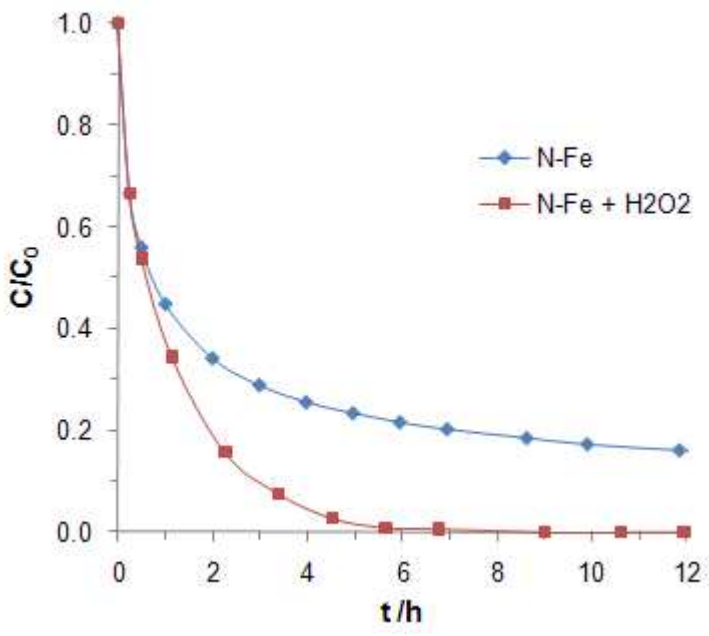

Figure 3.10 – Adsorption capacity *vs*. catalytic activity of N-Fe.

Following the same procedure previously used to evaluate the contribution of adsorption and catalysis, as well as to obtain some information about the influence of the porous texture in the process, the N-Fe sample was first used as adsorbent (in absence of H_2O_2) and, after saturation, recovered and used as catalyst. The results obtained in this experiment are shown in Fig. 3.11, in comparison with that obtained with a fresh N-Fe catalyst sample.

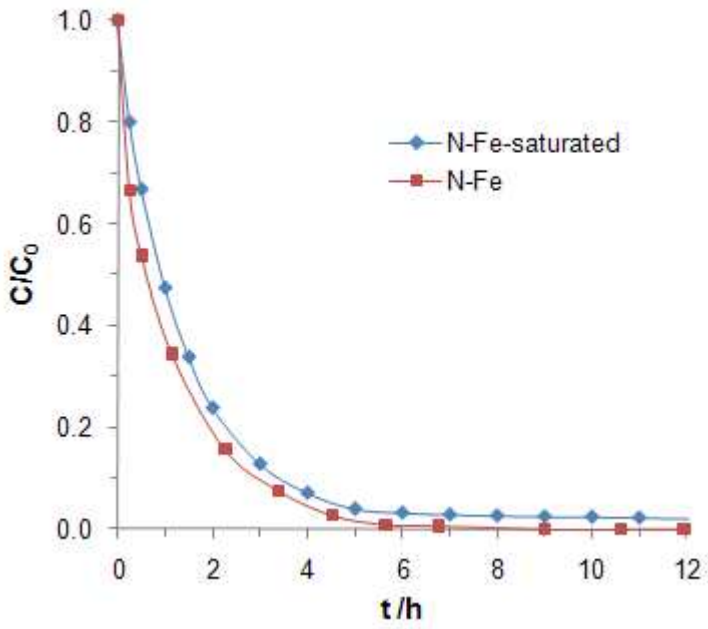

Figure 3.11 – Catalytic oxidation of Orange II using fresh and saturated N-Fe catalysts.

It is observed striking similarities, indicating that the OII removal from the solution is mainly done by the Fenton's reaction in detriment of the adsorption process (see also Fig. 3.7 for the support). Moreover, because adsorption takes place in micropores, these results also prove that after filling this porosity range with adsorbed species, the catalytic activity is not influenced. This means that the Fe-particles are not capped by the oxidation products and/or are located in the mouth of micropores, and are still available to catalyse the reaction. This fact, together with the small Fe-particle size, can justify the higher lixiviation values observed. These results also confirm that the microporosity of the support has a weak contribution to the activity of Fe-catalysts, but can contribute to the catalytic behaviour of pure supports, as previously shown.

3.4. Conclusions

Three different activated carbons (Norit, Merck and Kynol) were used to remove the azo dye Orange II from aqueous solutions. Correlations between their textural properties and their performances on the adsorptive and catalytic (Fenton oxidation) behaviour were established. All the supports are microporous and it was verified that Norit AC was the best adsorbent, with the adsorption capacity of the three supports decreasing with the decrease of the micropore size of each one in the order N > M > K.

N-support's surface showed to be catalytic active and it was possible to conclude that the oxidation reaction takes place not only on the external surface of this carbon, but also inside the micropores, which enables its regeneration by H_2O_2.

N-Fe showed to have the most appropriate textural properties, providing also a good dispersion of the metal. Concerning the catalyst's performance, N-Fe was the most active towards OII degradation, leading to 90 % of discoloration in ca. 4 h and a TOC removal of 61 % in 24 h. However, the high dispersion in this catalyst also favours the iron leaching. Comparing adsorption and catalytic activity of N-Fe, it was observed that the presence of H_2O_2 clearly improved the rate of discoloration (by means of the Fenton's process). Moreover, it was possible to prove that in the presence of the oxidant, catalytic degradation occurred in detriment of the adsorption process. Actually, unlike what happened with the support, the contribution of the microporosity to the activity of N-Fe seems not to be very relevant. The increase of the H_2O_2 concentration does not enhance the TOC removal, on the contrary, because scavenging reactions are favoured in this sense.

References

[1] F. Lucking, H. Koser, M. Jank, A. Ritter, Iron powder, graphite and activated carbon as catalysts for the oxidation of 4-chlorophenol with hydrogen peroxide in aqueous solution, Water Res. 32 (1998) 2607-2614.

[2] F. Duarte, F. J. Maldonado-Hódar, A. F. Pérez-Cadenas, L. M. Madeira, Fenton-like degradation of azo-dye Orange II catalyzed by transition metals on carbon aerogels, Appl. Catal. B: Environ. 85 (2009) 139-147.

[3] J. H. Ramirez, F. J. Maldonado-Hódar, A. F. Pérez-Cadenas, C. Moreno-Castilla, C. A. Costa, L. M. Madeira, Azo-dye Orange II degradation by heterogeneous Fenton-like reaction using carbon-Fe catalysts, Appl. Catal. B: Environ. 75 (2007) 312-323.

[4] J. A. Zazo, J. A. Casas, A. F. Mohedano, J. J. Rodríguez, Catalytic wet peroxide oxidation of phenol with a Fe/active carbon catalyst, Appl. Catal. B: Environ. 65 (2006) 261-268.

[5] A. Rey, M. Faraldos, J.A. Casas, J.A. Zazo, A. Bahamonde, J.J. Rodríguez, Catalytic wet peroxide oxidation of phenol over Fe/AC catalysts: Influence of iron precursor and activated carbon surface, Appl. Catal. B: Environ. 86 (2009) 69-77.

[6] H. Marsh, E.A. Heintz, F. Rodriguez-Reinoso, Introduction to Carbon Technologies, Universidad de Alicante, Secretariado de Publicaciones, 1997.

[7] A.F. Perez-Cadenas, F.J. Maldonado-Hódar, C. Moreno-Castilla, On the nature of surface acid sites of chlorinated activated carbons, Carbon 41 (2003) 473–478.

[8] C. Hsiu-Mei, C. Ting-Chienb, P. San-De, C. Hung-Lung, Adsorption characteristics of Orange II and Chrysophenine on sludge adsorbent and activated carbon fibers, J. Hazard. Mater. 161 (2009) 1384–1390.

[9] L. Abramian, H. El-Rassy, Chem. Eng. J. 150 (2009) 403-410.

[10] L.R. Radovic, C. Moreno-Castilla, J. Rivera-Utrilla, Carbon Materials as Adsorbents in Aqueous Solutions, in Chemistry and Physics of Carbon, Vol 27, p. 361, L.R. Radovic Editor, Marcel Dekker Inc, New York, 2000.

[11] H. T. Gomes, S. M. Miranda, M.J. Sampaio, A.M.T. Silva, J.L. Faria, Activated carbons treated with sulphuric acid: Catalysts for catalytic wet peroxide oxidation, Catal. Today 151 (2010) 153-158.

[12] M.F.R. Pereira, S.F. Soares, J.J.M. Órfão, J.L. Figueiredo, Adsorption of dyes on activated carbons: influence of surface chemical groups, Carbon 41 (2003) 811–821.

[13] S. Morales-Torres, F.J. Maldonado-Hódar, A.F. Pérez-Cadenas, F. Carrasco-Marín, Design of low-temperature Pt-carbon combustion catalysts for VOC's treatments, J. Hazard. Mater. 183 (2010) 814–822.

[14] J.H. Ramirez, F.M. Duarte, F.G. Martins, C.A. Costa, L.M. Madeira, Modelling of the synthetic dye Orange II degradation using Fenton's reagent: From batch to continuous reactor operation, Chem. Eng. J. 148 (2009) 394–404.

[15] X. Chen, G. Chen, Anodic oxidation of Orange II on Ti/BDD electrode: Variable effects, Sep. Purif. Technol. 48 (2006) 45–49.

[16] K. Vinodgopal. D. Wynkoop, P. Kamat, Environmental photochemistry on semiconductor surfaces: photosensitized degradation of a textile azo dye, acid orange 7, on TiO_2 particles using visible light, Environ. Sci. Technol. 30 (1996) 1660-1666.

[17] C. Bauer, P. Jacques, A. Kalt, Photooxidation of an azo dye induced by visible light incident on the surface of TiO_2. J. Photochem. Photobiol. A: Chem. 140 (2001) 87-92.

CHAPTER 4 - Influence of the iron precursor in the preparation of heterogeneous Fe/activated carbon Fenton-like catalysts

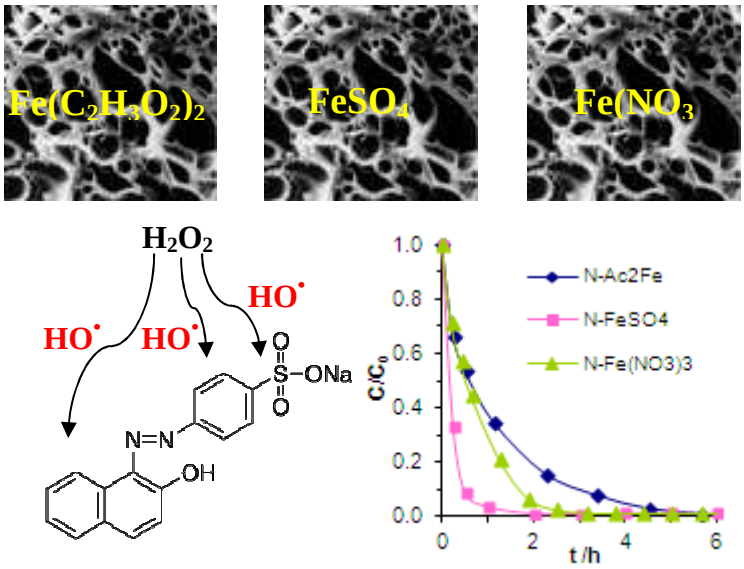

Chapter 4. Influence of the iron precursor in the preparation of heterogeneous Fe/activated carbon Fenton-like catalysts *

Abstract

In this Chapter, the influence of the iron salt precursor for the impregnation of a commercial activated carbon (AC) is evaluated in order to choose the best catalyst in the removal of the azo-dye Orange II (OII) from water by the heterogeneous Fenton-like process. Three iron salts were used: iron acetate, iron sulphate and iron nitrate, all catalysts being obtained with a content of 7 % wt. of iron (Fe/AC) after pre-treatment at 300 ºC. The characterization of fresh and used materials was done by different techniques (N_2 and CO_2 adsorption, X-ray diffraction, X-ray photoelectron spectroscopy, high-resolution transmission electron microscopy and thermal programmed desorption). The three catalysts presented different textural properties and distinct iron dispersions, along with different locations of the metal in the pore structure, thus leading to quite different materials for the envisaged application because those properties strongly influence the different processes that contribute to the dye removal: adsorption, homogeneous Fenton process (due to leached iron) and heterogeneous Fenton-like process (on the catalysts' surface). Iron in solution (or located more externally on the carbon surface) favours the discoloration but can somehow prevent the TOC removal (which also occurs by adsorption). The catalytic behaviour of the samples was correlated with the transformations on their textural and chemical characteristics. Ferrous acetate seems to be the best option for the precursor to use on the basis of the activity and particularly stability of its corresponding catalyst (i.e., possibility of catalyst reutilization due to low leaching).

* Adapted from: F. Duarte, F.J. Maldonado-Hódar, L.M. Madeira, Appl. Catal., A 458 (2013) 39-47.

4.1. Introduction

As it has been mentioned, in heterogeneous advanced catalytic oxidation, ACs can be very useful because they are able to support the metallic catalyst particles in an active and stable way, having high porosity, high surface area and relatively low cost. Performance of ACs as supports depends on their textural characteristics, surface chemistry, ability to disperse and fix the active phase, and also on the accessibility of the reagents towards the active sites. All these aspects, as well as the behaviour of the AC-based catalyst, depend on the metal to be dispersed. Different transition metals have already been used as the active phase in heterogeneous Fenton's oxidation employing ACs [1, 2], but iron is the most common, being also cheap and very active. The iron species can be introduced on the support by impregnation with an iron precursor salt. However, the nature of the iron precursor might have a crucial role in the final catalyst obtained, as long as it affects the above-mentioned catalyst properties.

In this Chapter, the previously selected AC (Norit RX 3 Extra) was impregnated with three different iron precursors: iron acetate, iron sulphate and iron nitrate in order to choose the best catalyst for the removal of the azo dye Orange II from an aqueous solution by the heterogeneous Fenton-like process.

4.2. Materials and Methods

Norit RX 3 Extra was milled and sieved to get particles in the powder form (< 0.15 mm). Three identical fractions of AC powder were separated and each one was impregnated with a different iron salt aqueous solution to obtain 7% wt of iron load as described in Chapter 2 – section 2.2. Thus, the catalysts, herein called N-Ac_2Fe, N-$FeSO_4$ and N-$Fe(NO_3)_3$, were obtained by using iron acetate, iron sulphate and iron nitrate, respectively, as salt precursor. In other works it was shown that after this thermal treatment both iron acetate and iron sulphate were decomposed – [3] (Chapter 3) and [4] (Chapter 6), respectively. Decomposition temperature of iron (III) nitrate is known to be the lowest among the three iron salts, so the thermal treatment applied was also effective in this case.

The materials were characterized by N_2 (at 77 K) and CO_2 (at 273 K) adsorption, X-ray diffraction (XRD), X-ray photoelectron spectroscopy (XPS), high resolution transmission electron microscopy (HRTEM) and temperature programmed desorption (TPD). For further details please consult Chapter 2, section 2.3.

Catalytic and adsorption experiments were carried out in a batch *slurry* reactor according to Chapter 2 – section 2.4.1. In the oxidation reactions, 6 mM of H_2O_2 (ratio of 1.43 regarding the stoichiometric amount) was used. The treated solution was evaluated by using the techniques also previously exposed (UV-Vis spectrophotometry for the dye quantification, TOC analysis for assessing the removal of organic carbon and atomic absorption spectrometry for measuring the iron leaching from the support) – Chapter 2, section 2.5.

4.3. Results and Discussion

4.3.1. Characterization of fresh samples

N_2 adsorption/desorption isotherms for the support (N) and for the three catalysts impregnated with the different iron salts (N-Ac_2Fe, N-$FeSO_4$ and N-$Fe(NO_3)_3$) are shown in Fig. 4.1. As observed, after impregnation the iron particles lead to a partial blockage of the porosity, in agreement with other works ([3, 4] – Chapters 3 and 6 and [5]), decreasing the N_2 adsorption capacity (cf. Table 4.1). However, in the case of N-$Fe(NO_3)_3$, this blockage is only noticed in the microporosity range. In fact, the NOx formed by decomposition of the iron nitrate can induce certain gasification of the micropores' walls, leading to a pore widening as denoted by the L_0 (N_2) values – Table 4.1, favouring the N_2 adsorption at high relative pressures (Figure 4.1). Nevertheless, all the isotherms have the same shape, corresponding mainly to a type-I isotherm, with a great amount of N_2 adsorbed at low P/P_0 values (adsorption in the micropores). There is however an important heterogeneity in the microporosity, denounced by the large knee of the isotherms. The samples also have some mesopores, detected both by the small hysteresis cycle and the slope of the isotherm after micropore's saturation. Complementary CO_2 adsorption was used to characterize the narrowest microporosity

[6]. Table 4.1 shows that the volume of micropores determined by nitrogen adsorption is larger than the one determined by CO_2 adsorption, i.e. W_0 (N_2) > W_0 (CO_2), indicating the absence of diffusional restrictions and the occurrence of N_2 condensation inside the larger micropores and/or mesopores.

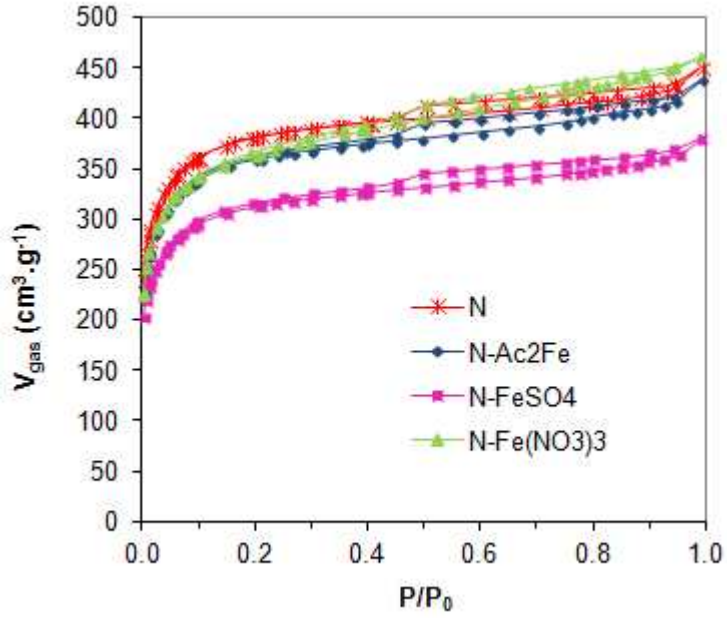

Figure 4.1 – N_2 adsorption/desorption isotherms for the AC support and for the three different catalysts.

Table 4.1 – Textural characteristics of the support (N) and of the three different catalysts.

Sample	S_{BET} m^2.g^{-1}	L_0 (N_2) nm	W_0 (N_2) cm^3.g^{-1}	S_{mic} (CO_2) m^2.g^{-1}	L_0 (CO_2) nm	W_0 (CO_2) cm^3.g^{-1}
N	1405	1.70	0.62	1173	0.81	0.48
N-Ac_2Fe	1328	1.74	0.58	763	0.83	0.32
N-$FeSO_4$	1160	1.75	0.51	758	0.89	0.35
N-$Fe(NO_3)_3$	1347	1.79	0.59	1033	0.77	0.40

S_{BET}: BET surface area obtained by N_2 adsorption; L_0 (N_2): mean micropores' size obtained by N_2 adsorption; W_0 (N_2): micropores' volume obtained by N_2 adsorption; S_{mic} (CO_2): micropores' surface area obtained by CO_2 adsorption; L_0 (CO_2): mean micropores' size obtained by CO_2 adsorption; W_0 (CO_2): micropores' volume obtained by CO_2 adsorption.

The decrease of N_2 adsorption capacity after impregnation was more evident in the case of the N-$FeSO_4$ catalyst (Figure 4.1), which presents the smaller BET surface

area and micropore volume (W_0 (N_2)) (Table 1). This catalyst also presents a strong pore blockage of the narrower microporosity (W_0 (CO_2)). In the case of the N-Ac_2Fe sample, the decrease of the W_0 (CO_2) value is also significant (from 0.48 to 0.32 $cm^3.g^{-1}$) but only a small variation of the S_{BET} area concerning the AC support was detected. The smaller textural transformations in both meso/micropore range occurred with the N-$Fe(NO_3)_3$ catalyst. This means that depending on the iron precursor used the iron particles are located at different ranges of porosity causing significantly different textural changes. The results previously exposed indicate that in the case of the N-Ac_2Fe sample iron particles are mostly inside (or in the mouth) of the smaller micropores, preventing the gas adsorption in this range of porosity and leading to a more important decrease of the narrowest microporosity, given by W_0 (CO_2). Regarding the N-$FeSO_4$ catalyst, it seems that iron particles are mostly distributed over bigger micropores/mesopores once S_{BET} significantly decreased. In the case of N-$Fe(NO_3)_3$ sample, iron particles appear not to be large enough to produce significant pore blockage, indicating a good dispersion of the metal phase on the AC surface (or that the iron particles almost did not enter into the porosity).

TEM and XRD techniques were used to evaluate the dispersion and nature of the iron species in the catalyst samples. HRTEM photos (Figure 4.2) show how the iron dispersion varies, which is in the sense: N-$Fe(NO_3)_3$ > N-Ac_2Fe > N-$FeSO_4$, Fe particles bigger than 100 nm being visible for the latter sample. These results are in agreement with those obtained by XRD (Figure 4.3). Indeed, the XRD pattern of the N-$Fe(NO_3)_3$ catalyst seems to confirm as being the most well dispersed sample, where the size of iron particles is below the detection limit of the technique (4 nm). The N-Ac_2Fe catalyst exhibits a slightly worse iron dispersion, being now the XRD peaks noticed, in spite of being not intense. The assignment of the peaks is however a hard task, because different oxides, allotropic forms and mixture of species can be present. In this case, a small and width diffraction peak at 2θ = 35.7 º, corresponding to the I_{100} of γ-Fe_2O_3 (JCPDS 13-534) or Fe_3O_4 (JCPDS 88-0866), was observed. N-$FeSO_4$ catalyst has more pronounced and narrower diffraction peaks, indicating larger iron particles. In this case, the XRD pattern pointed out the presence of a mixture of oxide-hydroxide species; the peaks at 14.2 and 25.8 º are attributed to lepidocrocite, FeO(OH) (JCPDS file 8-98), while the one at 33.1 º and the small peak at 49.5 º can be assigned to the I_{100} of hematite, α-Fe_2O_3 (JCPDS file 33-0664).

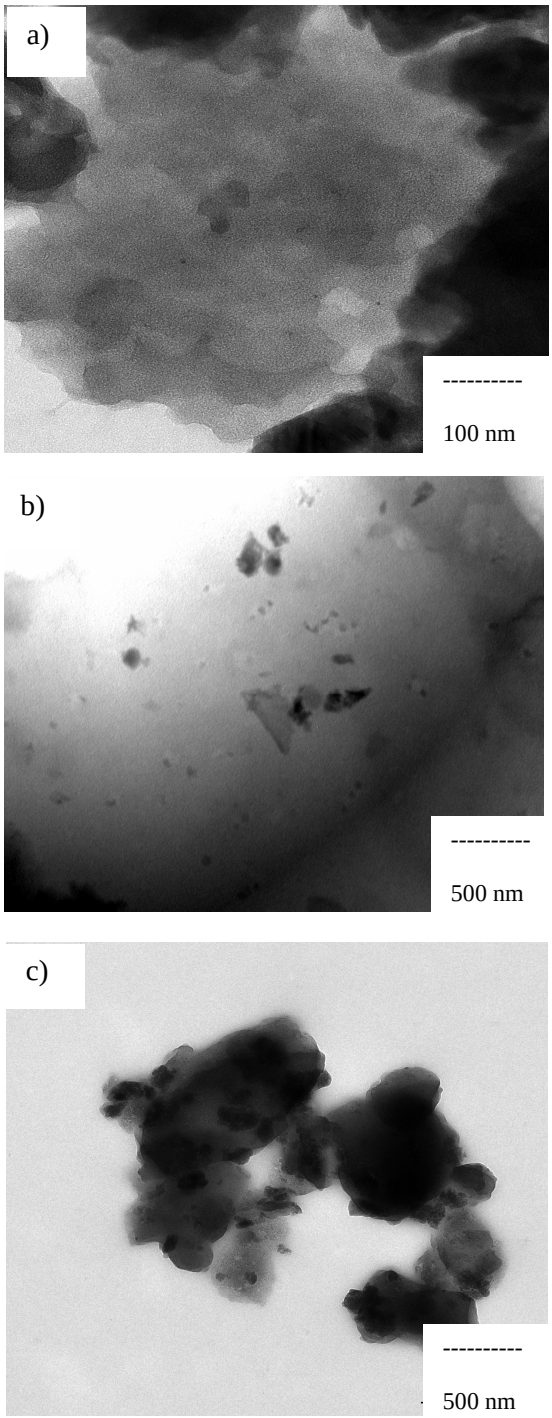

Figure 4.2 – HRTEM images of the AC impregnated with the iron nitrate (a), iron acetate (b) and iron sulphate (c).

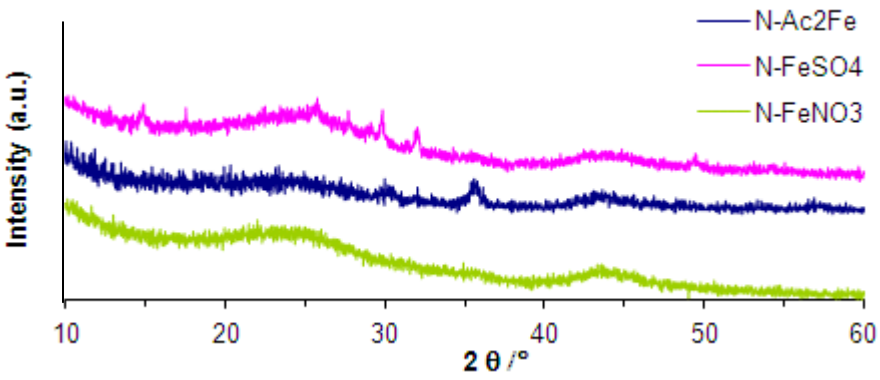

Figure 4.3 – XRD patterns of the three catalysts.

The XPS results (Table 4.2) showed a Fe-concentration effect on the carbon surface because in all the samples the percentage of iron detected is greater than the total Fe-loading (7% wt). The smaller concentration of iron detected in the case of the N-$FeSO_4$ catalyst pointed out also a worse dispersion (i.e., formation of larger particles, in agreement with above-mentioned results). On the other hand, all the catalysts showed a mixture of Fe^{2+}/Fe^{3+} species, identified after the deconvolution of the Fe 2p spectral regions at 710.7 and 712.6 eV, respectively [7-9] – Figure 4.4; so, even in the case of the N-$Fe(NO_3)_3$ sample, the Fe^{+3} species are significantly reduced by the carbon during the pre-treatment.

Table 4.2 – Surface composition of the three different catalysts by XPS.

Samples	**C** **% wt.**	**N** **% wt.**	**O** **% wt.**	**S** **% wt.**	**Fe** **% wt.**	**Fe^{2+}/Fe^{3+}**
N-Ac_2Fe	61.56	0.22	15.56	1.00	21.62	2.43
N-$Fe(NO_3)_3$	54.79	0.45	20.46	1.11	23.18	1.75
N-$FeSO_4$	61.91	0.97	19.26	1.15	16.68	3.26

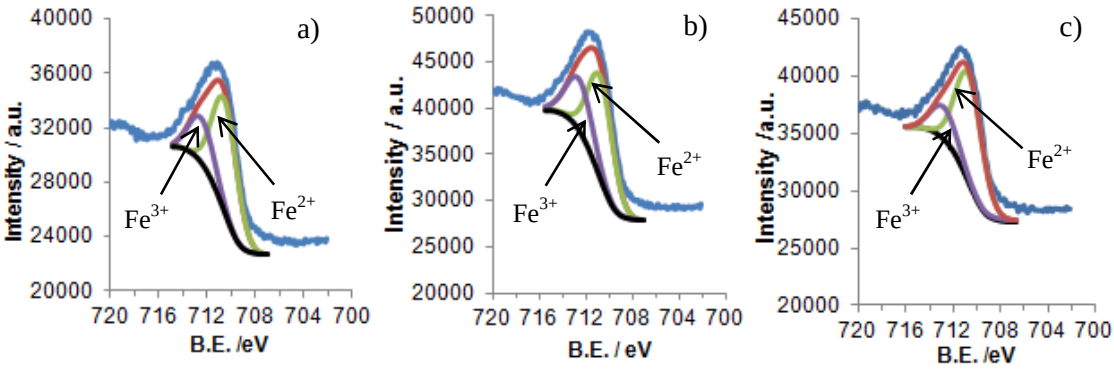

Figure 4.4 – XPS spectra and their deconvolution for the three catalysts: a) N-Ac_2Fe, b) N-$Fe(NO_3)_3$ and c) N-$FeSO_4$.

Rey *et al.* [5] pointed out the importance of the metal precursor on the characteristics of AC/Fe wet peroxide oxidation catalysts. In such work, $Fe(NO_3)_3$ (in water) and $Fe(CO)_5$ (in n-hexane) were used as precursors. In the first case, the surface Fe concentration of the final catalyst increased when increasing the surface oxygen concentration of the support, which did not happen when using the $Fe(CO)_5$ precursor. According to them, this could be the result of electrostatic interactions between negatively charged oxygen groups and Fe^{3+} hydroxocomplexes in the impregnation step when $Fe(NO_3)_3$ is used, whereas with iron pentacarbonyl iron is as Fe^0. The influence of the solvent is not discussed, but it is expected a lower dispersion in water regarding cyclohexane due to the hydrophobic character of the carbon surface. So, depending on the AC support and iron salt used, iron oxides in the final catalyst could be located internally or externally, or even a more uniform Fe distribution could be obtained. Catalytically, it was suggested that the most external Fe particles favours the H_2O_2 decomposition into O_2, which is not active for oxidation under mild experimental conditions.

In the case of this work, an identical support (Norit RX 3 Extra – N) was used for the impregnation with aqueous solutions of the different precursors, and, consequently, differences should be due to the precursor solution nature. The surface chemistry of this AC was studied by TPD (Figure 4.5). The total oxygen content determined by this technique is low - 1.8 wt.% (lower than those obtained by XPS because the catalysts present oxygen from iron oxides) - and the oxygenated surface groups evolve upon thermal treatment as CO or CO_2, depending on their chemical nature [10]. In this case, the concentration of the CO evolving groups (semiquinones,

carbonyl, etc.), which show a basic character, are predominant *versus* those CO_2 evolving groups with an acid character (carboxylic, anhydrides, lactones). The N-support presents a pH_{pzc} = 11 [3] (Chapter 3), denoting clearly the basic character of the carbon surface. However, the pH values for iron acetate, iron sulphate and iron nitrate solutions are 4.3, 3.3 and 1.3, respectively, and consequently greater interactions can be established in this sense with iron species, as well as a better fixation of acid Fe^{+3} on the basic oxygenated surface groups of the AC may occur, leading to the different catalyst's characteristics previously described.

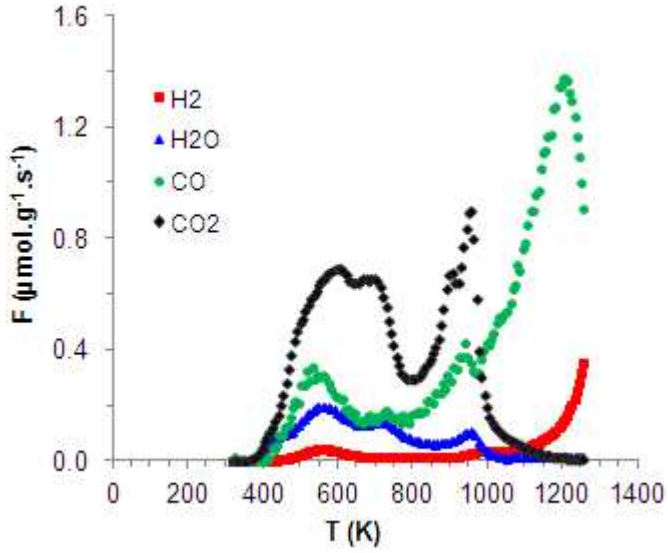

Figure 4.5 – TPD profiles obtained for N support.

4.3.2. Orange II elimination

The heterogeneous Fenton process involves a complex system of coexistent phenomena: adsorption and catalysis. So, these phenomena were analyzed in independent experiments. The pH 3 used in adsorption experiments (the same as in the catalytic ones) induces in the AC a positively charged surface (because pH < pH_{pzc} = 11). On the other hand, and as it was mentioned in Chapter 3 (section 3.3.2.1), at these pH conditions (pH 3), OII is in the mono protonated form - $C_{16}H_{11}N_2OSO_3^-$ [11, 12]. Thus, strong electrostatic attraction should exist between the positively charged AC and

the negatively charged dye molecules, increasing the adsorption capacity of the adsorbent in such conditions.

The different location and dispersion of the Fe-particles and the consequent textural transformation discussed above influence the accessibility of the dye (OII) molecules to the pores and, consequently, the adsorption processes, as denoted by Figure 4.6. In a previous work it was demonstrated that the OII adsorption on the catalysts takes place without degradation or breakage of the OII molecule [13] (Chapter 5). As observed in Figure 4.6, the OII adsorption rate decreases from the AC support to the Fe-supported catalysts in the order N > N-Ac_2Fe > N-$FeSO_4$, in agreement with the pore blockage generated by the Fe-particles, according to the results of Table 4.1. The poor adsorptive behaviour observed for N-$Fe(NO_3)_3$ should be therefore related not with the textural properties of this catalyst (which lie between those of the N support and the N-Ac_2Fe catalyst), but with a different surface chemistry induced by the different anchoring and reduction of Fe^{+3} species during pre-treatment, as previously commented.

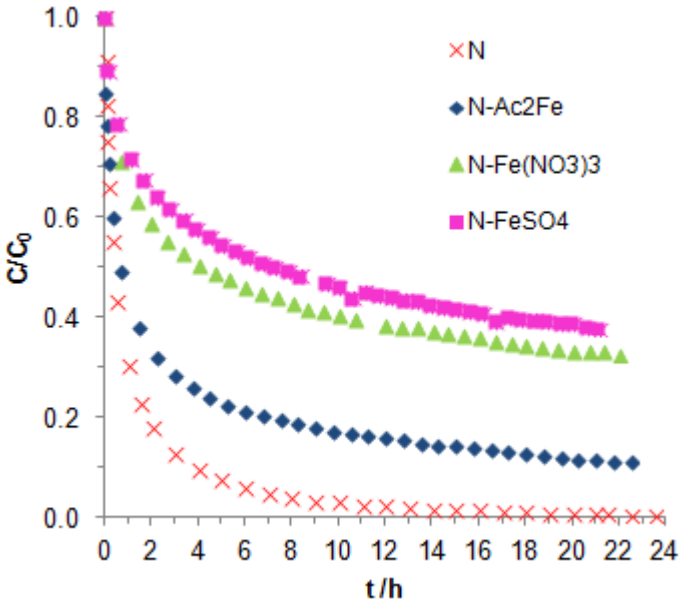

Figure 4.6 – OII elimination by adsorption using N support and the three different catalysts (C_{OII}= 0.1 mM, C_{sol}= 0.1 g.L^{-1}, T = 30º and pH 3).

For the same reasons, the different catalysts led also to different performances towards the elimination of OII dye by the heterogeneous Fenton reaction, as shown in Figure 4.7. The OII removal was studied by analyzing the solution discoloration and the

TOC values. In terms of colour removal (Figure 4.7a), it can be concluded that the process is faster using the catalyst impregnated with iron sulphate. However, the TOC removal data (Figure 4.7b) showed that the most active catalyst was N-Ac_2Fe, while N-$Fe(NO_3)_3$ presented an intermediate performance in both cases.

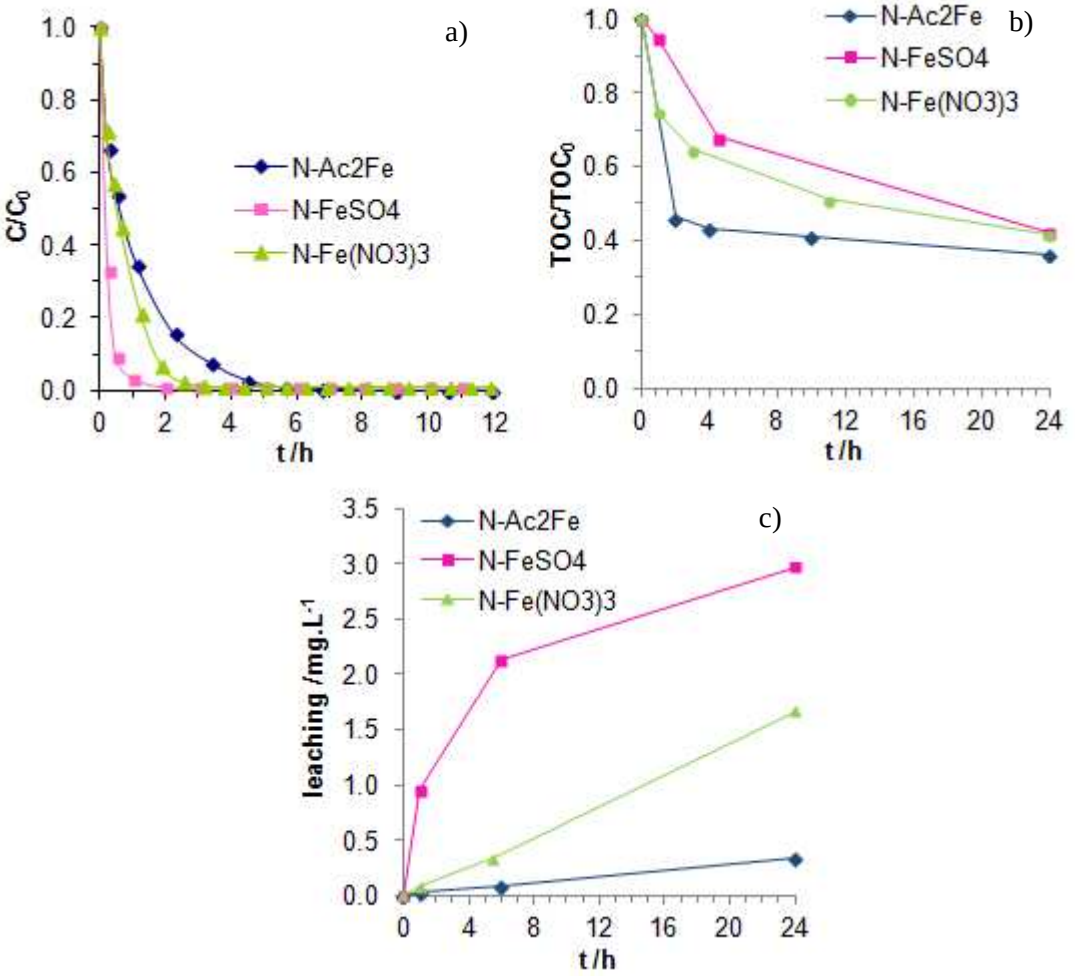

Figure 4.7 – Performance of the three different catalysts in the Fenton-like process in terms of colour removal (a), mineralization (b) and leaching (c) (C_{OII}= 0.1 mM, C_{cat}= 0.1 g.L^{-1}, C_{H2O2}= 6 mM, T = 30º and pH 3).

From the above results, one could expect a worse performance of the N-$FeSO_4$ catalyst towards OII elimination, because this sample presented the worst adsorptive performance (Figure 4.6) together with a worse iron dispersion (section 4.3.1). The results of Figure 4.7 allow concluding that in this case discoloration is carried out mainly catalytically. The iron particles located more externally in this sample (i.e., on mesopores/large micropores) favour a fast breakage of the azo bonds, which are known

to be the easiest and the first being degraded during azo dyes oxidation. The slowest performance is thus obtained with the N-Ac_2Fe catalyst, where Fe-particles are located inside the narrower micropores (more internally). However, the greater TOC removal detected in this case is favoured by both the faster adsorption and the greater activity of the best dispersed iron particles, able to degrade in a large extent the adsorbed organic products. Besides, because iron species are in this case located deeper in the solid porous structure, a higher residence time is required for the intermediates that must diffuse back towards the aqueous solution, promoting a further oxidation and thus a better TOC removal. Finally, the intermediate behaviour of N-$Fe(NO_3)_3$ seems to be related with the distribution of smaller Fe-particles more or less homogeneously throughout the internal-external surface of the catalyst, which should be highly active according to the dispersion degree; even so, it is anticipated that the most external ones should favour the azo-dye breakage and the more internal ones the TOC removal. These results pointed out the importance of the dispersion and distribution of the iron particles on the support, and are also in agreement with the results observed by Rey *et al.* [5].

In terms of stability, the N-$FeSO_4$ catalyst presented also the higher leaching levels (Fig. 4.7c). Consequently, these values should be related with the nature of the iron species and their location on the AC support; for the acetate-derived catalyst, where iron particles are mostly located inside micropores, the smaller loss of iron from the support was obtained. The low leaching level obtained in this case is important both concerning the very low iron concentration in solution (thus complying with EU standards – 2 $mg.L^{-1}$) and the possibility of reutilization of this catalyst, higher than in the other two cases. The best catalytic behaviour (in terms of TOC reduction), together with a limited leaching degree, makes the use of Ac_2Fe as precursor for Fenton catalyst development the most feasible option, in spite that this salt is relatively more expensive.

On the other hand, the results shown in Fig. 4.7 suggest that there is apparently a direct relation between dissolved/leached iron and discoloration rate for all catalysts (although opposite to the mineralization trend). To find if this effect depends on the iron salt, homogeneous and heterogeneous experiments were carried out simultaneously, i.e., the OII elimination was done by using the most stable catalyst (N-Ac_2Fe) together with each iron salt precursor in solution (C_{Fe}= 2.13 $mg.L^{-1}$). Under the same operating conditions used in Fig. 4.7, the results obtained show clearly an improvement in the colour removal rate in the presence of the dissolved iron salts (Fig. 4.8a), independently

of the salt nature. However, comparing TOC removal in the different situations (Fig. 4.8b), one can conclude that iron dissolved in the solution may somehow "prevent" the TOC reduction, being the corresponding by-products formed by the homogeneous reactions more stable and less adsorbed than those generated heterogeneously. In line with the above results, it can also be inferred that for discoloration (the first oxidation step) contributes mainly external iron (i.e. located externally on the AC surface or available in the solution), while for a good mineralization it is required that the by-products enter into the pores and that their residence time therein is long enough to suffer further oxidation. In this way, one can anticipate that the homogeneous reaction is faster than the heterogeneous one for the discoloration, but is less effective in terms of pollutant mineralization, which, in turn, reinforces the necessity to develop heterogeneous Fenton catalysts, highly active for the total mineralization, and also highly stable.

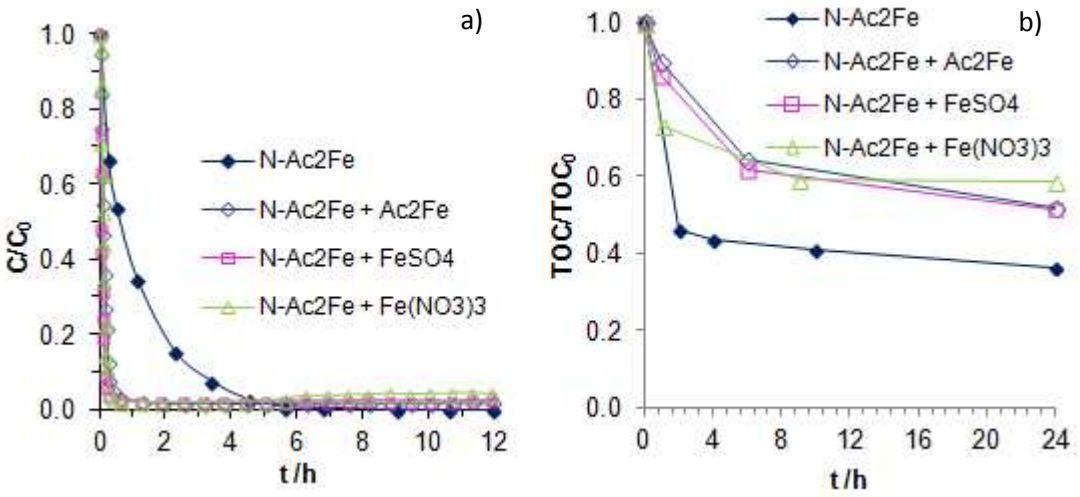

Figure 4.8 – OII degradation using N-Ac_2Fe and N-Ac_2Fe plus each iron salt as the homogeneous phase (C_{OII}= 0.1 mM, C_{cat}= 0.1 g.L^{-1}, C_{H2O2}= 6 mM, C_{Fe}= 2.13 mg.L^{-1}, T = 30º and pH 3).

4.3.3. Characterization of used samples

After the oxidation runs, the samples were characterized by N_2 adsorption/desorption at 77 K and X-ray diffraction. XRD data of the used samples (data not shown) did not evidenced significant changes as compared to the XRD patterns of the fresh ones. However, N_2 isotherms of used samples revealed interesting features after comparing to N_2 isotherms of fresh samples (Table 4.3 and Fig. 4.9). These transformations are the combined result of two factors: i) the adsorption of OII molecules and their oxidation products that induced the decrease of surface area in all cases, and ii) the iron leached from the catalysts, which liberated porosity and inherently surface area. Clearly, in the case of N-Ac_2Fe and N-$Fe(NO_3)_3$ catalysts the adsorption of organic products is preponderant, leading to an important decrease of surface area (Table 4.3). However, in the case of N-$FeSO_4$, the surface area also decreases, but textural properties undergo very small changes regarding the rest of catalysts. In this last case, the iron leaching is larger, compensating also in some extent the loss of porosity induced by adsorbed products.

The different textural transformations occurred in the catalysts are in accordance with the different catalytic performances. The stronger pore blockage corresponds to the most active catalyst in terms of TOC removal (N-Ac_2Fe) and occurs mostly in the range of large micropores (W_0 (N_2)) with a significant increase of the mean micropore width (L_0 (N_2)). In this case, the narrowest microporosity (W_0 (CO_2)) also decreases but L_0 (CO_2) is maintained, indicating that this decrease is due to the blockage of the bigger micropores that permit the access to the smaller ones. The BET surface area decrease follows the order N-Ac_2Fe > N-$Fe(NO_3)_3$ > N-$FeSO_4$, according to the TOC removal and progressive more internal localization of the Fe-particle on fresh catalysts; the opposite order, i.e. more external Fe location, favours in turn the breakage of the azo dye (and more by-products remain in solution). The stronger decrease of available surface area / pore volume can however compromise the reutilization of the N-Ac_2Fe catalyst. Different (chemical and thermal) treatments can be applied for the reactivation of the catalyst(s) [14, 15] and further studies should be carried out in order to choose the most effective one.

Table 4.3 – Textural characterization of fresh and used samples by N_2 adsorption.

Support	S_{BET} ($m^2.g^{-1}$)	L_0 (N_2) (nm)	W_0 (N_2) ($cm^3.g^{-1}$)	S_{mic} (CO_2) ($m^2.g^{-1}$)	L_0 (CO_2) (nm)	W_0(CO_2) ($cm^3.g^{-1}$)
N-Ac_2Fe fresh	1328	1.74	0.58	763	0.83	0.32
N-Ac_2Fe used	577	1.96	0.26	492	0.84	0.21
N-$FeSO_4$ fresh	1160	1.75	0.51	758	0.89	0.35
N-$FeSO_4$ used	1086	1.74	0.48	600	0.91	0.27
N-$Fe(NO_3)_3$ fresh	1347	1.79	0.59	1033	0.77	0.40
N-$Fe(NO_3)_3$ used	950	1.74	0.42	767	0.85	0.33

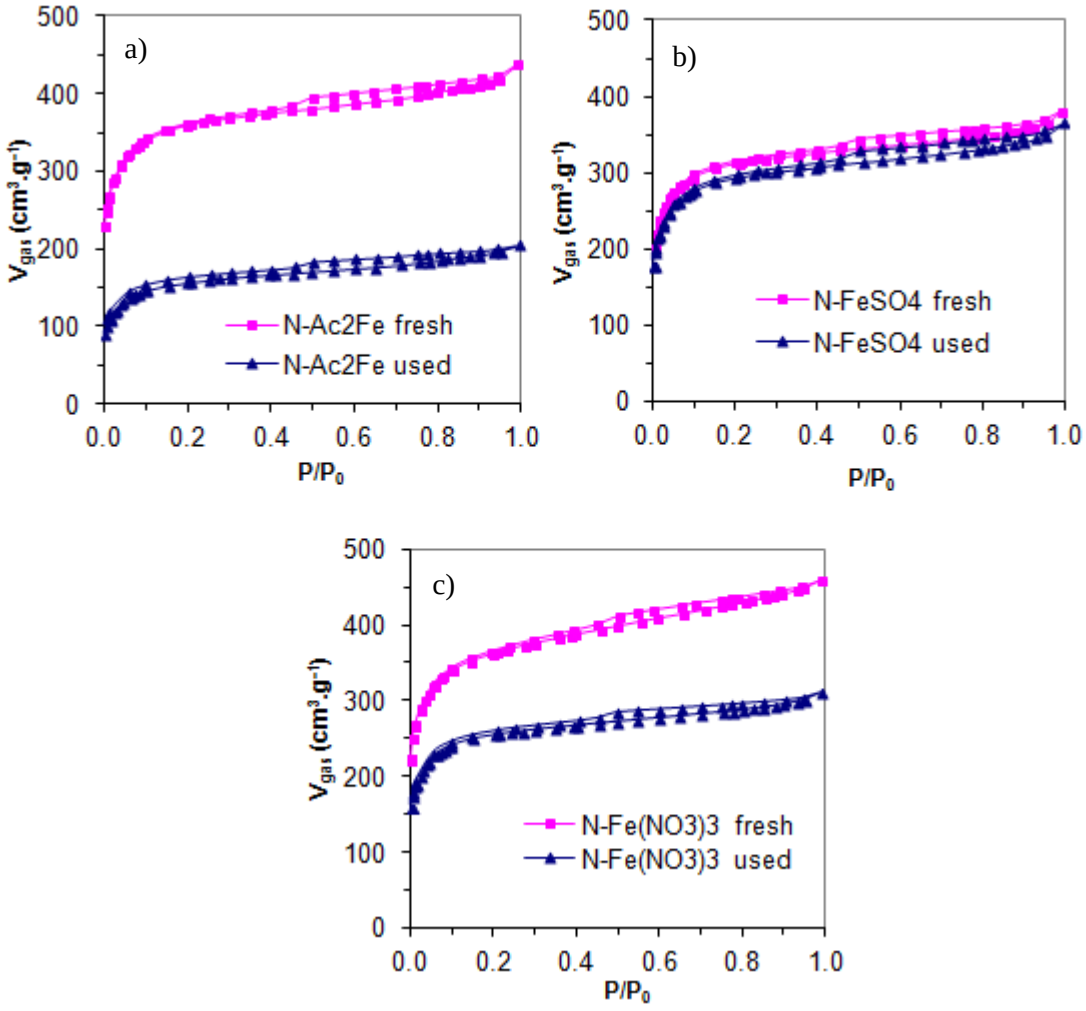

Figure 4.9 – N_2 isotherms of the three fresh and used catalysts: N-Ac_2Fe (a), N-$FeSO_4$ (b) and N-$Fe(NO_3)_3$ (c).

The used catalysts were also characterized by TPD in order to obtain information about the oxidation degree induced by the Fenton-like reactions. The results obtained are summarized in Table 4.4 and the corresponding TPD profiles compared in Figure 4.10. The samples that provided a faster and higher TOC reduction (Fig. 4.7b) led to a residue with higher oxygen content. Thus, the oxygen content, determined by TPD, decreased in the sense: N-Ac_2Fe > N-$Fe(NO_3)_3$> N-$FeSO_4$ (cf. Table 4.4). It is also important to highlight the CO/CO_2 ratios. This parameter was smaller in the case of N-Ac_2Fe, indicating a greater proportion of the most oxidized chemical species, that evolve as CO_2 (carboxylic acid, lactones, anhydrides) *vs.* those groups that evolve as CO (phenol, carbonyl, semiquinone, etc). Thus, the TPD experiments confirm the greater and deeper oxidation activity of the N-Ac_2Fe catalyst.

By analyzing the TPD profiles, it is observed that the used N-$FeSO_4$ not only presented the smaller CO_2-desorption peak, but also, that the CO_2-evolving groups are, in general, less stable (once they decompose at lower temperatures). At low temperatures (from 370 to 670 K) mainly carboxylic acids are evolved, in spite of the large tail and the smaller maximum observed, which indicates also the presence of other species such as anhydrides or lactones, more thermally stable [10]. On the contrary, the CO-desorption peaks took place in all cases at the same temperature range, indicating that, in general, the nature of the groups evolved are similar. The wide CO-desorption peak can involve also the reduction of the iron oxides particles and the smaller CO-desorption in the case of N-$FeSO_4$ is related with the greater difficulty to reduce the biggest Fe-particles detected in this case.

Thus, TPD experiments allowed concluding that the TOC removal, mainly in the case of N-Ac_2Fe catalyst, is not exclusively due to adsorption. The OII molecules are not only more adsorbed in this case, but also more deeply oxidized, yielding smaller and more acid by-products inside the pores that provoke the large decrease of the surface area after the catalytic experiments. In the case of N-$FeSO_4$ the localization of the Fe-particles on the more external surface of the AC can favour the fast breakage of the azo-bond in the OII molecule, favouring discoloration, but the sample is poorly active for mineralization. N-$FeSO_4$ catalyst presented also the larger leaching degree, which led to the faster homogeneous process, but TOC reduction was somewhat prevented, as it was also pointed out.

Table 4.4 – Oxygen content of the used catalysts obtained by TPD.

Sample	O (wt. %)	CO (μmol g^{-1})	CO_2 (μmol g^{-1})	CO/CO_2
N-Ac_2Fe used	10.5	3484	1536	2.3
N-$Fe(NO_3)_3$ used	7.9	2980	974	3.1
N-$FeSO_4$ used	5.5	2028	705	2.9

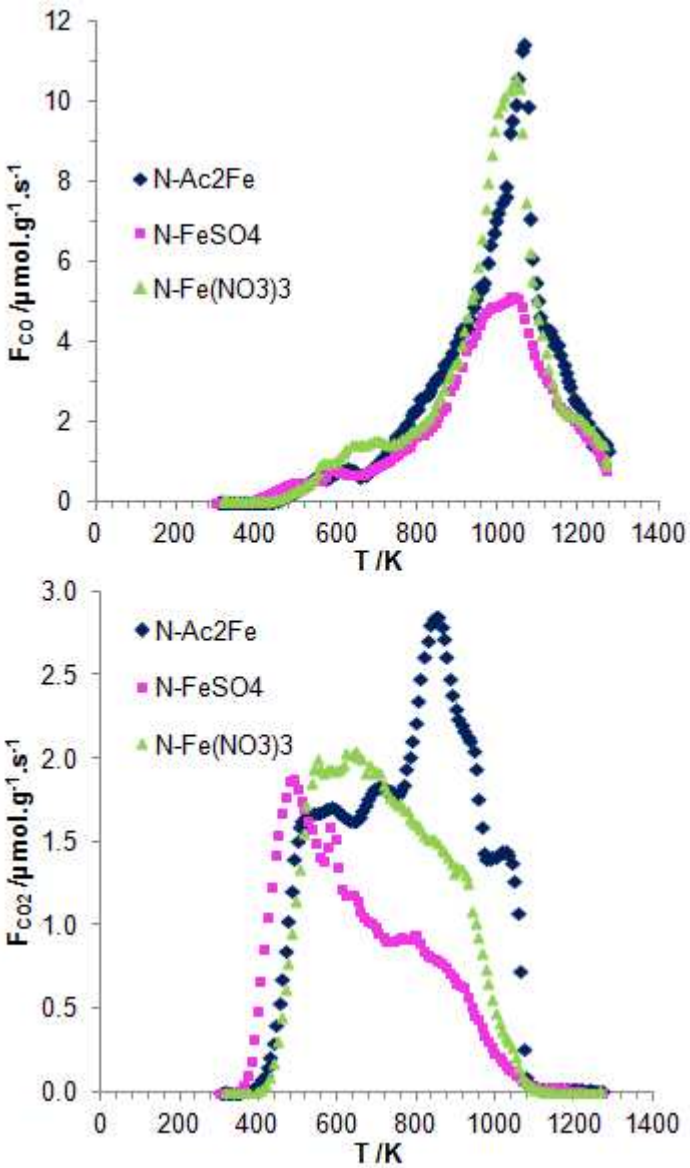

Figure 4.10 – TPD profiles of the used catalysts.

4.4. Conclusions

The main goal of this Chapter was to choose the most suitable iron precursor to be used for impregnation of a commercial AC for the degradation of the model azo dye Orange II by the heterogeneous Fenton-like process. It was observed that different iron precursors led to different catalyst properties, with different iron particles size and located in different porosity ranges of the AC.

Using iron acetate as precursor, the catalyst presented a good dispersion with small Fe-particles located inside (blocking) the narrowest micropores while larger Fe-particles located on larger micropores/mesopores were found using $FeSO_4$ (thus, more externally on the AC support). An intermediate behaviour is detected when $Fe(NO_3)_3$ is used. In spite of having lower discoloration rates, N-Ac_2Fe catalyst led to higher TOC removals, which are favoured by a higher adsorption capacity and a greater oxidation activity provided by the good iron dispersion, with the iron particles located inside the micropores increasing the oxidation products residence time (and thus their mineralization).

A series of experiments using simultaneously supported and dissolved iron as catalysts pointed out that iron in solution promotes the discoloration, but can somehow prevent the TOC removal (which also occurs by adsorption), independently of the iron salt.

Characterization of fresh and used samples revealed different textural transformations, which occurred in accordance with the different catalytic performances. The stronger pore blockage corresponds to the most active catalyst in terms of TOC removal. TPD experiments proved that there was a deeper oxidation of the dye pollutant and its oxidation products in the case of N-Ac_2Fe catalyst, forming smaller and more acidic by-products.

In this way, this work reinforces the importance of the heterogeneous contribution for dyes degradation by the Fenton-like process. Moreover, iron acetate was considered the most promising salt, thanks to the lower leaching and higher oxidation levels yielded by the N-Ac_2Fe catalyst.

References

[1] F. Duarte, F.J. Maldonado-Hódar, A.F. Pérez-Cadenas, L.M. Madeira, Fenton-like degradation of azo-dye Orange II catalyzed by transition metals on carbon aerogels, Appl. Catal., B 85 (2009) 139-147.

[2] S. Navalon, A. Dhakshinamoorthy, M. Alvaro, H. Garcia, Heterogeneous Fenton Catalysts Based on Activated Carbon and Related Materials, ChemSusChem 4 (2011) 1712-1730.

[3] F. Duarte, F.J. Maldonado-Hódar, L.M. Madeira, Influence of the characteristics of carbon materials on their behaviour as heterogeneous Fenton catalysts for the elimination of the azo dye Orange II from aqueous solutions, Appl. Catal., B 103 (2011) 109-115.

[4] F. Duarte, F.J. Maldonado-Hódar, L.M. Madeira, Influence of the particle size of activated carbons on their performance as fe supports for developing fenton-like catalysts, Ind. Eng. Chem. Res. 51 (2012) 9218-9226.

[5] A. Rey, M. Faraldos, J.A. Casas, J.A. Zazo, A. Bahamonde, J.J. Rodríguez, Catalytic wet peroxide oxidation of phenol over Fe/AC catalysts: Influence of iron precursor and activated carbon surface, Appl. Catal., B 86 (2009) 69-77.

[6] D. Cazorla-Amoros, J. Alcañiz-Monge, M.A. De la Casa-Lillo, A. Linares-Solano, CO_2 as an adsorptive to characterize carbon molecular sieves and activated carbons, Langmuir 14 (1998) 4589-4596.

[7] J.H. Ramirez, F.J. Maldonado-Hódar, A.F. Pérez-Cadenas, C. Moreno-Castilla, C.A. Costa, L.M. Madeira, Azo-dye Orange II degradation by heterogeneous Fenton-like reaction using carbon-Fe catalysts, Appl. Catal., B 75 (2007) 312-323.

[8] C.D. Wagner, W.M. Riggs, L.E. Davis, J.F. Moulder, G.E. Muilenberg, Handbook of X-Ray Photoelectron Spectroscopy, Perkin-Elmer Corp., Physical Electronics Division, Eden Prairier, Minnesota, 1978.

[9] A.P. Grosvenor, B.A. Kobe, M.C. Biesinger, N.S. McIntyre, Catalytic wet peroxide oxidation of phenol over Fe/AC catalysts: Influence of iron precursor and activated carbon surface, Surf. Interface Anal. 36 (2004) 1564-1574.

[10] J.L. Figueiredo, M.F.R. Pereira, M.M.A. Freitas, J.J.M. Orfão, Modification of the surface chemistry of activated carbons, Carbon 37 (1999) 1379-1389.

[11] L. Abramian, H. El-Rassy, Adsorption kinetics and thermodynamics of azo-dye Orange II onto highly porous titania aerogel, Chem. Eng. J. 150 (2009) 403-410.

[12] K. Bourikas, M. Stylidi, D.I. Kondarides, X.E. Verykios, Adsorption of Acid Orange 7 on the Surface of Titanium Dioxide, Langmuir 21 (2005) 9222–9230.

[13] F. Duarte, F.J. Maldonado-Hódar, L.M. Madeira, New insight about orange II elimination by characterization of spent activated carbon/Fe Fenton-like catalysts, Appl. Catal., B 129 (2013) 264-272.

[14] G. Zhang, J. Qu, H. Liu, A.T. Cooper, R. Wu, $CuFe_2O_4$/activated carbon composite: A novel magnetic adsorbent for the removal of acid orange II and catalytic regeneration, Chemosphere 68 (2007) 1058-1066.

[15] M.H. Do, N.H. Phan, T.D. Nguyen, T.T.S Pham, V.K. Nguyen, T.T.T. Vu, T.K.P. Nguyen, Activated carbon/Fe_3O_4 nanoparticle composite: Fabrication, methyl orange removal and regeneration by hydrogen peroxide, Chemosphere 85 (2011) 1269-1276.

CHAPTER 5 - New insight about Orange II elimination by characterization of spent activated carbon/Fe Fenton-like catalysts

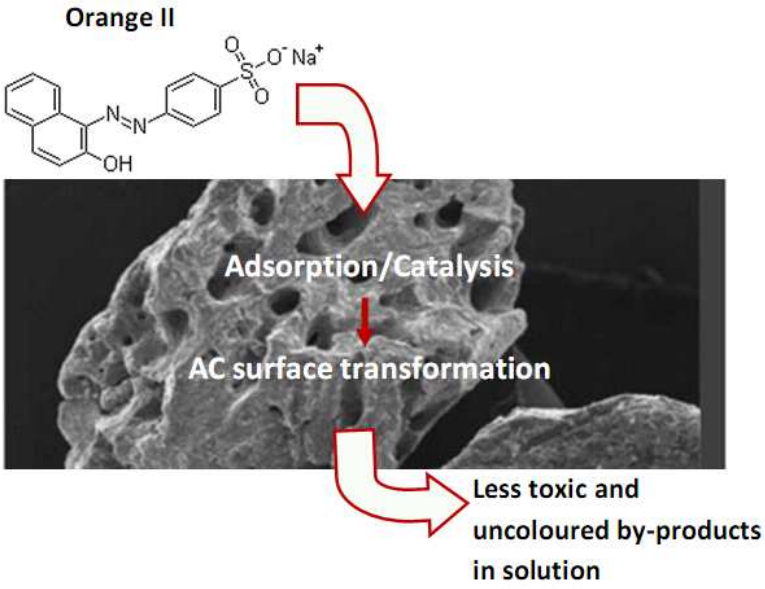

Chapter 5. New insight about Orange II elimination by characterization of spent activated carbon/Fe Fenton-like catalysts *

Abstract

This Chapter is focused on the characterization of heterogeneous Fe-based catalysts supported on activated carbons (ACs) that are used in elimination of the azo-dye Orange II (OII) from an aqueous solution. The main goal is to clarify the process of OII removal by analyzing textural and chemical surface properties of the fresh and spent activated carbon and Fenton-like catalysts upon using as adsorbents and/or catalysts. Textural changes were analyzed based on the corresponding N_2 adsorption isotherms and the nature of the adsorbed products by thermogravimetry and temperature-programmed desorption. It was found that OII was adsorbed filling the microporosity without degradation, although interactions between OII molecules and the AC surface groups have been detected. The total organic carbon (TOC) removal is complete in adsorption experiments. In the catalytic experiments using different H_2O_2 concentrations (in the range 6 – 24 mM) the TOC elimination was never complete and got worse when increasing the H_2O_2 load. The OII molecules were partially oxidized and the adsorption of these products also led to some blockage of the porosity; higher blockage and higher TOC removals was noticed after experiments carried out with the lowest H_2O_2 concentration. The different TOC removal was related to the interactions of the oxidation products with the carbon surface. When using the highest concentration of the oxidant (24 mM), the highest biodegradability and the lowest toxicity of the treated solution were reached, corroborating again the different nature of the oxidation by-products formed in each case.

* Adapted from: F. Duarte, F.J. Maldonado-Hódar, L.M. Madeira, Appl. Catal., B 129 (2013) 264-272.

5.1. Introduction

The knowledge of the different factors that influence dyes removal when using heterogeneous catalysts in Fenton-like processes can help the optimization of their properties, maximizing their performance and minimizing deactivation and Fe-leaching. Such factors include adsorption and catalysis, co-existent phenomena in this heterogeneous advanced oxidation processes (AOPs). In both, apart from other properties (like the textural ones), the surface chemistry of the activated carbon support/catalyst and the nature of the parent molecule or oxidation products determine the performance reached in their removal from water. Moreover, the properties of the catalyst, which change during the adsorption/reaction, also play an important role. Such study was the main goal of this Chapter.

So, the elimination of the azo dye Orange II (OII) by adsorption or by catalytic Fenton reaction was analyzed using the AC/Fe catalyst previously selected (Norit RX 3 Extra impregnated with iron (II) acetate). The performances of each water purification method and the influence of some experimental conditions (as the H_2O_2 concentration) are presented. Special attention is given to the characterization of spent samples and their physical and chemical transformation with the OII elimination process. The correlation of the removal performances with the variation of porous and chemical characteristics of samples is presented, looking for information about the OII elimination in adsorption or catalytic processes. The toxicity / biodegradability of the effluents obtained was also analysed.

5.2. Material and methods

The AC/Fe catalyst (N-Fe) was obtained by the same procedure as described previously, in section 2.2 – Chapter 2 (using Norit RX 3 Extra as support, diameter < 0.15 mm, and iron (II) acetate as the iron salt precursor). The materials were characterized by N_2 adsorption at 77 K, temperature programmed desorption (TPD) and thermogravimetric analysis (TG-DTG) following the procedures detailed in section 2.3 (Chapter 2).

Adsorption and catalytic tests were performed according to section 2.4.1 of Chapter 2. For the assessment of the support's performance in a second cycle of adsorption, the AC was recovered by filtration after the first cycle of adsorption (24 h) and reused under the same operating conditions. After all the experiments, the solid adsorbent or catalyst were recovered by filtration and analyzed as above mentioned.

The analytical techniques described in section 2.5 were again employed (UV-Vis spectrophotometry for dye quantification, TOC analysis for total organic carbon removal and atomic absorption for iron leaching assessment). Moreover, the biodegradability of the treated solutions (after 24 h of reaction) was assessed by respirometry following the O_2 decay along time, in a YSI model 5300 Biological Oxygen Monitor, by comparing the oxygen consumption rate of the sample with that of a biodegradable standard (sodium acetate) - linear decay along time was observed in both cases. So, two parallel experiments were carried out to determine such consumption rates (*m*), in both cases using biomass obtained in a WWT activated sludge reactor that treats domestic and textile effluents: i) 1 ml biomass + 5 ml sample (m_{sample}); ii) 5 ml distilled water + 1 ml biomass + sodium acetate at the right concentration to get the same TOC as the sample ($m_{sodium\ acetate\ 1}$). The biodegradability (expressed in percentage) of the sample was calculated according to Eq. (5.1) [1, 2]:

$$\%\ biodegradability = \frac{m_{sample}}{m_{sodium\ acetate\ 1}} \times 100 \qquad (5.1)$$

It is worth noting that the *m* parameters above-mentioned refer to the values after subtracting the *m* value from endogenous respiration. For the toxicity evaluation, the solution obtained after protocol i) was aerated to restore initial dissolved oxygen level, fed with sodium acetate (again at the right concentration to get the same TOC as the sample) and $m_{sodium\ acetate\ 2}$ was obtained similarly. Then, Eq. (5.2) was applied [1, 2]:

$$\%\ toxicity = \frac{m_{sodium\ acetate\ 1} - m_{sodium\ acetate\ 2}}{m_{sodium\ acetate\ 1}} \qquad (5.2)$$

5.3. Results and discussion

5.3.1. Adsorption on the AC support and characterization of the spent material

In a first approach, the behaviour of the AC support as adsorbent was studied. The reason behind this is that in heterogeneous Fenton oxidation both phenomena (adsorption and catalysis) co-exist; so, adsorption was firstly investigated in the carbon support. The results of the OII elimination in terms of discoloration (followed by absorbance) are illustrated in Fig. 5.1 for two consecutive adsorption cycles, which showed that the AC adsorption capacity is nearly saturated after the first adsorption cycle. Thus, the AC support used in a single cycle as adsorbent will be called N-sat henceforward, meaning that its surface is almost completely saturated by dye molecules. TOC analysis were also done during the first cycle and revealed a similar tendency as described for the discoloration curve, i.e., almost total TOC removal was achieved by OII adsorption in these experimental conditions (slight differences are due to analytical uncertainties, more evident at low TOC levels); discoloration and TOC removal seem to be therefore produced simultaneously by the same phenomenon (adsorption).

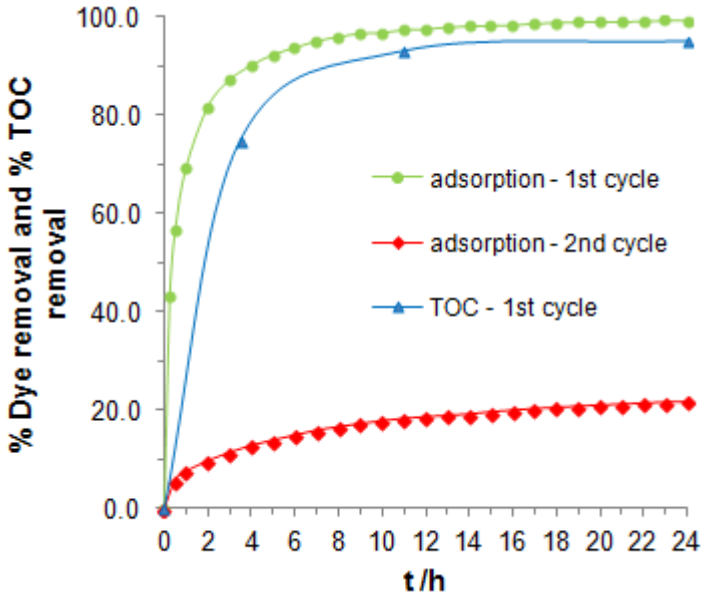

Figure 5.1 – OII removal in the first and second cycles of adsorption on the AC surface and TOC removal along the 1st cycle of adsorption (C_{OII}= 0.1 mM, C_{AC}= 0.1 g.L^{-1}, T = 30 ºC, pH 3).

To analyse the textural consequences of the support saturation, the N_2 adsorption isotherms were determined (Figure 5.2) for fresh and saturated samples, being noteworthy the strong decrease of the adsorption capacity. The BET surface area, micropore volume (W_0, computed by applying the Dubinin-Raduskevich equation) and micropore width (L_0) obtained from the isotherms analysis are shown in Table 5.1. It was observed a BET surface area (S_{BET}) decrease from 1405 to 317 $m^2.g^{-1}$ after the first cycle of adsorption. On the other hand, the blockage of the micropore volume allows inferring that the OII adsorption took place mainly into the narrow micropores, pointed out also by the increase of the L_0 values.

Table 5.1 – Textural properties of fresh and OII-saturated AC support.

Sample	S_{BET} ($m^2.g^{-1}$)	W_0 ($cm^3.g^{-1}$)	L_0 (nm)
N	1405	0.62	1.70
N-sat	317	0.14	2.13

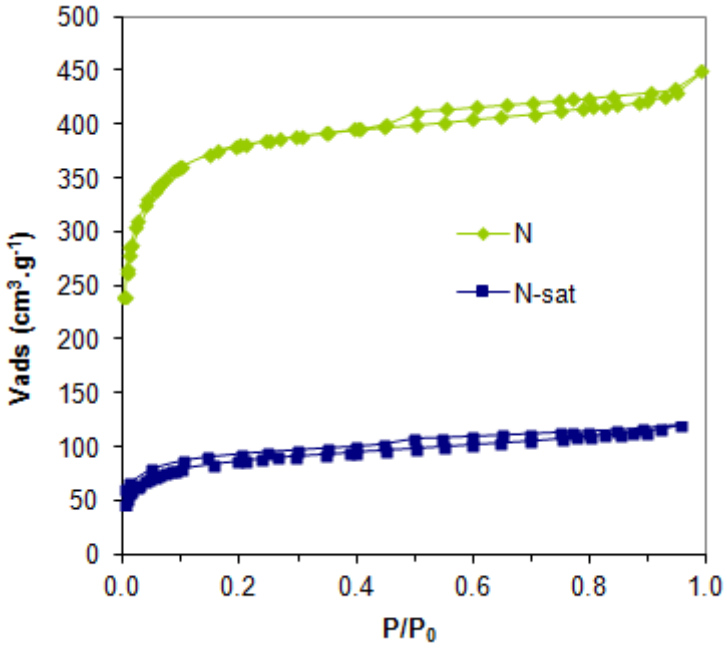

Figure 5.2 – N_2 adsorption/desorption isotherms of the AC fresh support (N) and the same sample after the first cycle of saturation with OII (N-sat).

Samples of fresh and saturated AC were analyzed by TG-DTG and the results compared with the TG-DTG of pure OII in order to look for information about the nature of the adsorbed products and the interactions between the solid and the dye molecules. The TG-DTG profile of pure OII is shown in Figure 5.3. The dye underwent a 63% of weight loss (WL) by heating in inert atmosphere up to 1200 K, with a main decomposition process at 604 K. Moreover, different decomposition processes inducing less important weight losses were observed at different temperatures, namely at around 820 K or 1020 K. This is a relevant result, because after the thermal degradation of OII in these conditions around 40% remained as solid residue.

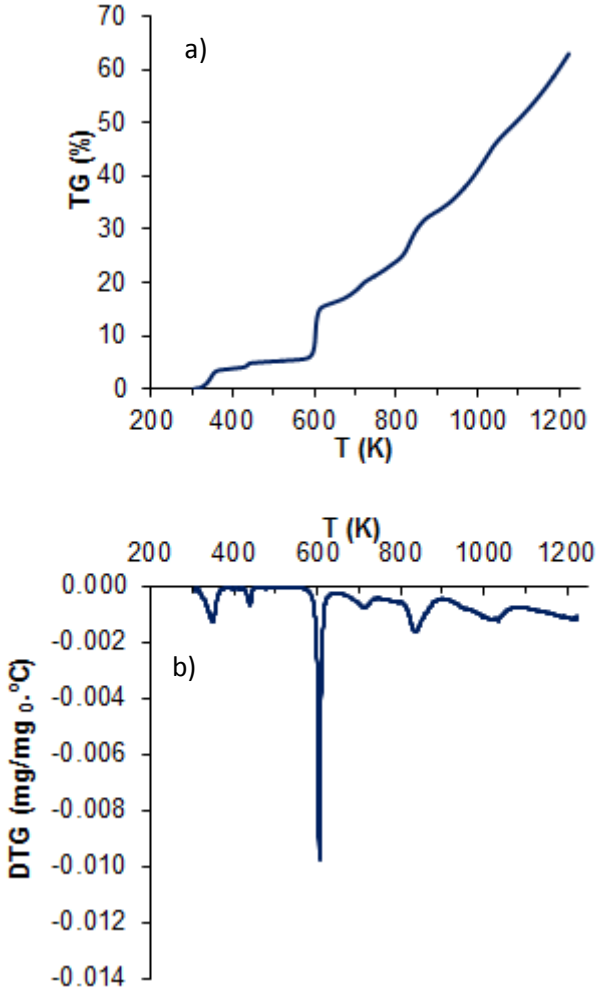

Figure 5.3 – TG (a) and DTG (b) profiles of pure OII.

The same thermal treatment in TG for the fresh AC yielded a WL of 6.5%, while for the sample of AC saturated with OII by adsorption this parameter increased to 16% -

Fig. 5.4a. In the case of fresh AC, the WL is due only to drying and decomposition of oxygenated surface groups. The main DTG peak (Fig. 5.4b) at low temperature (around 373 K) was associated with the removal of physisorbed water, although this assumption can mask also certain thermal dehydration of the OII molecule in the saturated sample (according to Figure 5.3). Clearly, the other two peaks only existing on the DTG profile of N-sat at around 600 and 820 K correspond to the decomposition of the adsorbed compound. One should note that the decomposition of adsorbed molecules took place at similar temperatures as for pure OII (cf. Fig. 5.3b). These results, together with the similar evolution of the OII elimination curves determined by discoloration or TOC values, suggest that OII is adsorbed directly without any degradation, filling the micropores of the AC and leading to the observed S_{BET} decrease.

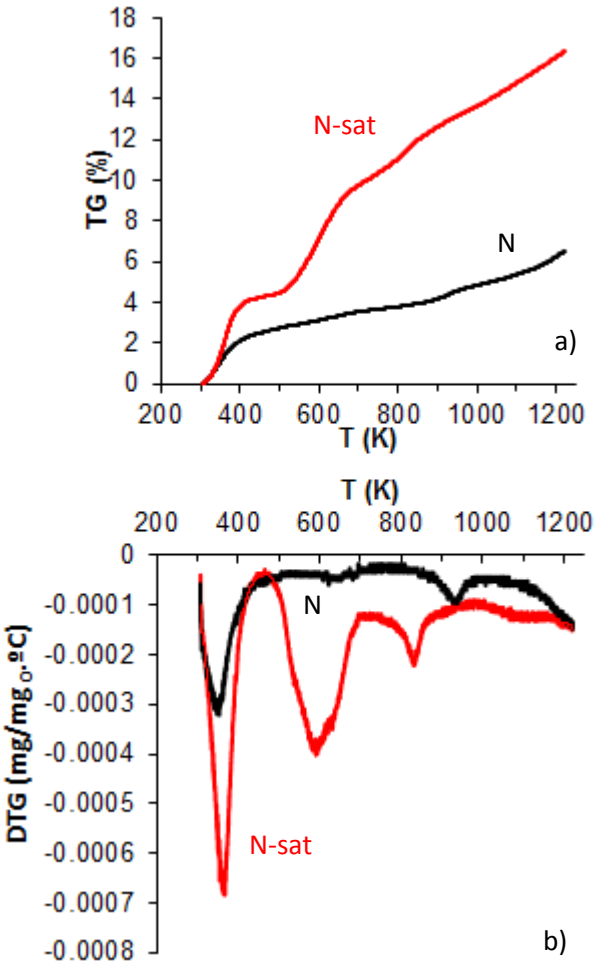

Figure 5.4 – TG (a) and DTG (b) profiles of fresh AC support (N) and after adsorption with OII (N-sat).

Temperature programmed desorption (TPD) is one of the most powerful and extensively used techniques for the characterization of surface groups in carbon materials [3, 4]. The nature and amount of these surface groups can be quantified, which was done by integration of the TPD areas. Thus, this information complements the results obtained from the TG-DTG experiments. The TPD profiles of hydrogen, water, CO and CO_2 evolving from fresh and saturated AC are shown in Figure 5.5, while the oxygen content, calculated from the amount of CO and CO_2 evolved, is compiled in Table 5.2. The total oxygen content increased from 1.8 to 3.6 % after the OII adsorption, changing also significantly the corresponding TPD profiles. This increase is mainly due to the higher CO desorption from the N-sat sample, obviously produced by decomposition of the adsorbed dye molecules (Table 5.2 and Fig. 5.5).

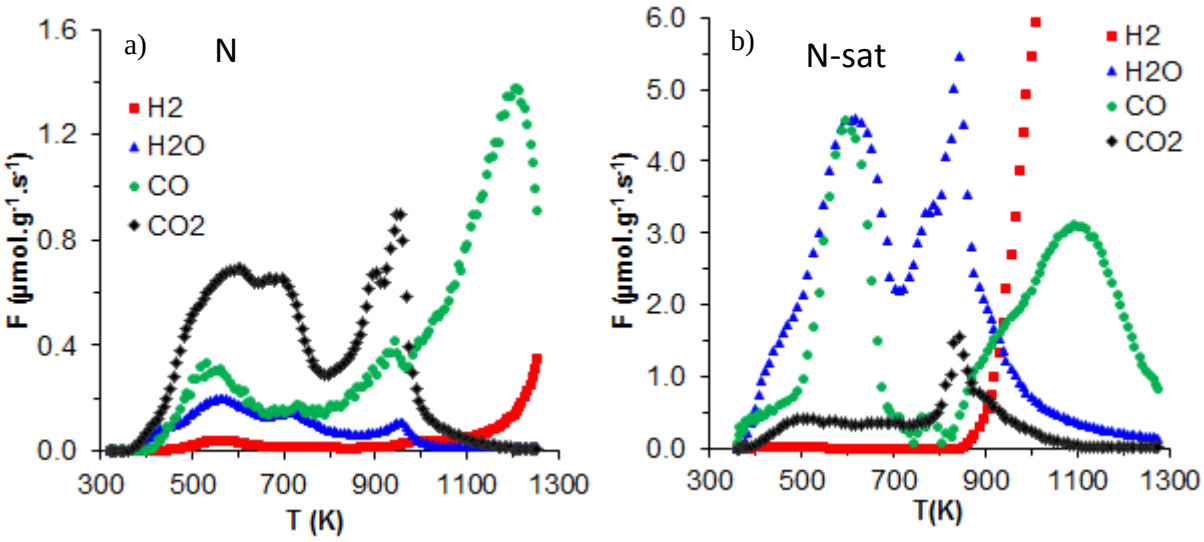

Figure 5.5 – TPD profiles obtained for fresh (a) and OII-saturated AC support (b).

Table 5.2 – Oxygen content of fresh and saturated AC support obtained by TPD experiments.

Sample	**O (wt.%)**	**CO (µmol .g $^{-1}$)**	**CO_2 (µmol .g $^{-1}$)**
N	1.8	455	346
N-sat	3.6	1640	307

The oxygen content of the fresh sample is low, according to the nature of untreated ACs. The different oxygenated surface groups were evolved as CO or CO_2 while increasing the temperature. The assignation of the peaks to the different types of

surface groups was carried out according to the bibliography. Regarding fresh AC, the CO_2 evolution took place mainly in two temperature intervals: between 300-800 and 800-1100 K, and in both ranges, the CO_2 profiles presented two maxima, located in the first temperature range at 600 and 700 K and at 900 and 950 K in the second temperature interval. The CO profile presented the maximum desorption rate at 1213 K, although one smaller peak at around 550 and a clear shoulder at 950 K are coincident with those previously described for CO_2. In the case of the N-saturated sample, it is evident that the CO_2 evolving peak at 850 K was clearly favoured regarding those appearing at lower temperatures, as compared to the N sample. However, the contrary behaviour was observed for CO, where the maximum desorption rate shifted to lower temperature, occurring in this case at 600 K *vs*. 1213 K in the N-sample. The water desorption profile is clearly associated to the decomposition of the new oxygenated surface groups, showing maxima simultaneously to those observed for CO and CO_2 (550 K and 850 K), in both cases. Finally, the H_2 evolution started at 900 K while in the fresh sample this occurred only at 1100 K. These changes are therefore due to the thermal decomposition of adsorbed molecules.

These variations were quantified and summarized in Table 5.2. As commented, after saturation with OII there was a strong increase in the amount of CO desorbed, while the CO_2 slightly decreased. Because the adsorption experiments were carried out in the absence of any additional oxidant, these variations should be associated only with the decomposition of adsorbed species. Three processes are susceptible to contribute to this behaviour: (i) the decomposition of the phenol / carbonyl groups of the dye molecule, (ii) the reduction of SO_2 evolved by the carbon matrix, forming CO-evolving groups, and (iii), some CO_2 evolving groups (*e.g.* carboxylic groups) of the AC surface can interact with the OII dye molecule, favouring a chemical adsorption leading to intermediate oxygenated complexes that also evolved as CO. Either the SO_2 release or the OII chemisorption on the AC surface were suggested by Zhang *et al.* [5]. Taking into account the amount of adsorbed OII (350 mg / g AC, 35% by weight), the increase in the oxygen content should be of 6.4% instead 1.8 %. This difference is mainly to the fact that the oxygen content shown in Table 5.2 is obtained only from the CO and CO_2 evolved during the TPD experiments (*e.g.* H_2O was not considered).

By comparison of the TPD profiles, it can clearly be seen that the peaks corresponding to the decomposition of the carboxyl groups at around 600 K in the N-

sample disappeared from the CO_2-TPD profile of N-sat sample, favouring, however, a strong CO-desorption peak in this temperature range. Simultaneously, the formation of anhydrides is also favoured, as denoted by the simultaneous evolution of CO and CO_2 at higher temperature. However, the nature of these anhydrides is also influenced by the presence of the adsorbed species, thus, in the saturated sample the CO_2-TPD peaks appear at lower temperature (850 *vs*. 950 K). Similarly, the second maximum for CO-desorption occurred at around 1100 K, versus 1213 K observed in the fresh sample.

These TG / TPD results clearly showed that the OII molecule is chemisorbed on the AC surface, mainly through the original carboxylic groups present in the fresh AC support. This fact generates the formation of intermediate oxygenated surface complexes that evolve as CO. Thus, the amount of CO evolved increased while the CO_2 decreases. The new complexes formed present a very low thermal stability, being mainly evolved at low temperature (600 K), but also, the original COx-evolving groups are clearly destabilized, and both anhydrides (CO_2–TPD maxima) and semiquinone (CO-TPD maxima) shifted to lower temperatures. Thus, the previous modification of the surface chemistry of the support can be appropriate to control this kind of interactions in future works.

5.3.2. Catalytic behaviour and nature of adsorbed products

In spite of the high efficiency of AC as OII adsorbent, this process only transfers the pollutants to the adsorbent. So, the main objective is to develop heterogeneous catalysts able to oxidize pollutants by a Fenton-like process. Firstly, a blank experiment showed that the H_2O_2, used as oxidant, is not able to eliminate the dye by its own. Then, the catalytic role of the AC surface by itself was checked by different experiments. Remembering what was observed in Chapter 3, it was found that the discoloration rate is independent of the presence of H_2O_2 in solution (Fig. 5.6), indicating that in these experimental conditions adsorption on AC is faster than the catalytic removal. Therefore, to estimate the ability of the carbon surface to activate H_2O_2 for the dye oxidation, the adsorptive component was eliminated by a previous saturation of the AC

with OII, and then, a catalytic run was carried out in the same experimental conditions. The results obtained (Figure 5.6) showed that the AC surface is clearly active as catalyst.

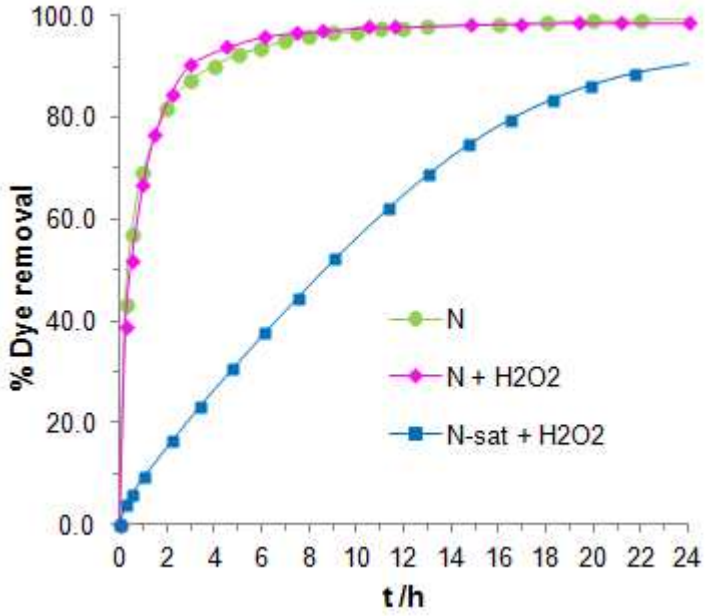

Figure 5.6 – Comparison of adsorption and catalytic activity of the fresh and OII saturated support (C_{OII}= 0.1 mM, C_{AC}= 0.1 g.L^{-1}, C_{H2O2}= 6 mM – when used, T = 30 ºC, pH 3).

Iron is the most active and selective metal in Fenton-like reactions [6, 7] and the AC used as support in this work (Norit RX 3 Extra) has already demonstrated good characteristics to develop supported catalysts, which were successfully applied in very different processes with environmental (*e.g.* previous Chapters and [8, 9]) or fuel chemistry (*e.g.* [10, 11]) aims, for instance. The catalytic behaviour of N-Fe catalyst towards OII elimination was checked in different experimental conditions, namely increasing the oxidant (H_2O_2) concentrations. Evolution of discoloration and TOC removal using different oxidant dosages is presented in Figures 5.7a) and 5.7b). Leaching levels were also assessed along the experiment with the best TOC removal levels (6 mM of H_2O_2). It was observed an increase of the iron concentration in solution with the reaction time, with values of 0.029, 0.081 and 0.345 ppm after 1, 6 and 24 h. To evaluate the contribution for the colour removal of the homogeneous process in this

experiment, an additional run was carried out with the iron concentration found in solution after 6h of reaction (0.081 ppm corresponding to 0.25 ppm of iron acetate), when total discoloration was already achieved in the heterogeneous process and the TOC removal had also nearly stabilized. . It is observed that the homogeneous reaction removes ca. 26 % of colour in 6 h (Fig. 5.7a), but it is noteworthy that the iron amount used in this experiment does not correspond to the iron concentration present in solution in the heterogeneous process from the beginning of the reaction. Concerning to the influence of the initial H_2O_2 concentration, and as it was already mentioned in Chapter 3, it was observed that the dye degradation rate was almost not affected when using H_2O_2 concentrations between 6 and 24 mM (Fig. 5.7a). The TOC data clearly pointed out that the increase of initial H_2O_2 content is far to improve the mineralization degree, on the contrary, being the TOC removal obtained progressively lower (Figure 5.7b). This fact can be due to scavenging reactions (parallel reactions) of the hydroxyl radical due to the presence of excess hydrogen peroxide. The determination of the residual H_2O_2 was carried out by a simple colorimetric method [12] after 24 h of reaction under the conditions of Fig. 5.7, using the extreme H_2O_2 initial concentrations: 6 mM and 24 mM. The results showed that in the first case nearly all the oxidant was consumed, while with 24 mM of initial H_2O_2 concentration, the reactant is in excess, and approximately 9 mM remained in solution in spite that around 63% of the initial TOC were not removed (Figure 5.7b). Thus, a progressively higher amount of by-products remained in solution, i.e. their nature changed with the operational conditions, and/or they are more resistant to the oxidation and were not adsorbed as easily as the dye molecules. Therefore, the solid catalysts were analyzed looking for information about the cause of this behaviour.

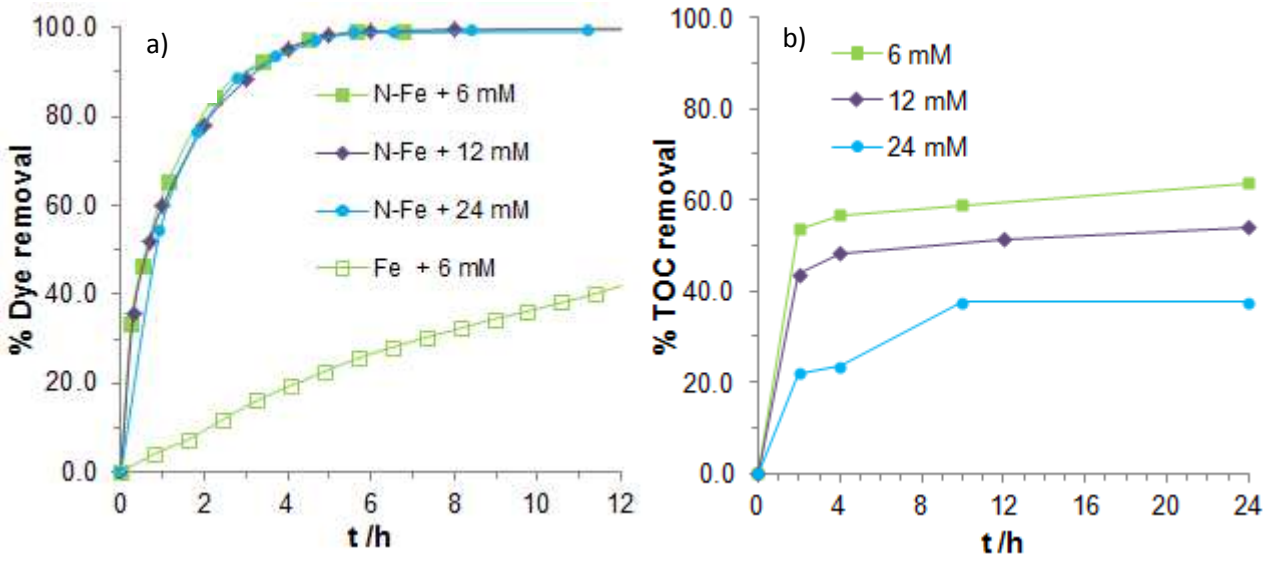

Figure 5.7 – OII elimination in terms of discoloration (a) and TOC removal (b) using N-Fe / Fe catalysts with different oxidant concentrations (C_{OII}= 0.1 mM, $C_{N\text{-}Fe}$= 0.1 g.L^{-1}, C_{Fe}= 0.081 mg.L^{-1}, T = 30 ºC, pH 3).

Analysing the textural characteristics of the fresh catalyst (Table 5.3), it is observed a certain decrease of the BET surface area regarding the AC support, because the Fe-phase partially blocked the AC porosity [13, 14] (cf. Chapter 3). This surface blockage represents only 5% of the total S_{BET} surface, and consequently, cannot justify that by-products were not adsorbed and remained in solution (TOC removal was not complete, as above mentioned). Regarding the used catalysts, it is observed that the decrease of S_{BET} is not as strong as the one observed after adsorption experiments (cf. Table 5.1 and Table 5.3), and that the evolution of the S_{BET} values is clearly related with the evolution of the TOC removal data (Fig. 5.7b): the higher TOC removal (corresponding to the use of 6 mM of H_2O_2) yielded the stronger S_{BET} decrease, which induces to think that TOC removal might be also due to a greater adsorption of OII or OII by-products rather than a greater mineralization.

Table 5.3 – Textural parameters of N support, the fresh N-Fe catalyst and the used catalyst samples with 6 and 24 mM of oxidant.

Sample	S_{BET} **($m^2.g^{-1}$)**	***Wo*** **(N_2) ($cm^3.g^{-1}$)**	***Lo*** **(nm)**
N	1405	0.62	1.70
N-Fe	1328	0.58	1.74
N-Fe + 6 mM	577	0.26	1.96
N-Fe + 24 mM	673	0.30	1.90

There are two characteristics of ACs that control their adsorption capacity: the textural properties and the surface chemistry. Obviously, to be adsorbed, the porosity should be accessible to the adsorbate (relation between the pore size of the adsorbent and the adsorbate molecular size), while the surface chemistry controls the interactions between both phases. This last characteristic of the adsorbent is strongly important mainly in adsorption carried out in aqueous solution and was extensively analyzed previously (*e.g.* [15]). In our catalytic system, the porosity of the AC support is clearly accessible even to the OII original molecule, because a total elimination of OII by adsorption was detected even by TOC values (cf. section 5.3.1). It is expected that the uncoloured by-products remaining in solution after the catalytic runs were smaller than the original OII molecule, being therefore also accessible into the AC microporosity. Therefore, chemical interactions should be responsible for this unexpected lower adsorption capacity, which also depends on the oxidation products formed.

Our preliminary studies aiming to identify the intermediate products showed that the primary degradation products might be benzene sulfonate and naftoquinone, i.e. the fractions formed by breakage of the OII molecule by the N=N azo-bond. Also, the main oxidation products detected were benzoic, phtalic and oxalic acids. Nevertheless, the identification of a large amount of additional smaller peaks, the quantification of all the species and the closure of the mass balance, requires a deeper analysis and the application of complementary analytical techniques. Even so, it is worth noting that these results are in agreement with those described in the literature for the OII degradation products, although mainly TiO_2-based catalysts were used for the OII photo-oxidation. According to Stylidi *et al.* [16], naphthalene-type compounds may be considered as primary degradation products of the dye, originated from oxidative cleavage of the molecule. Several breakdown products of OII including coumarin, 2-

naphthol, 2-hydroxy-1,4-naphthoquinone and 1,4-naphthoquinone were identified by GC/MS. From these compounds, a large list of 22 products, progressively smaller and more oxidized, starting by aromatic intermediates containing a six and a five-atom ring, such as phthalic anhydride, were also detected. Bauer *et al.* [17], by using FTIR spectroscopy, revealed the presence of C_2 carboxylic aliphatic acids, carbonates and oxygenated sulfur compounds on TiO_2 surfaces. Oxalate, acetate, carbonates and oxygenated sulfur compounds were identified as the final degradation products. The oxidation of Orange II by hydrogen peroxide catalyzed by iron (III) complexes in aqueous solutions at pH 9–11 led to CO_2, CO, phthalic acid and smaller aliphatic carboxylic acids as major mineralization products [18].

Obviously, the degree of mineralization, concentration and ratios of intermediate products, etc. will be strongly influenced either by the catalysts characteristics as by the experimental conditions. So, looking for information about properties of the used catalysts, TPD profiles were obtained for fresh and spent catalysts – Figure 5.8 – and the amount of products evolved determined and compiled in Table 5.4.

Regarding the characterization of fresh catalyst (pre-treated at 300 ºC = 573 K), it is observed that the TPD profiles are quite similar to those of the original AC support (cf. Fig. 5.5), except by the strong CO desorption peak observed at 1060 K (Fig. 5.8). At this temperature, there is simultaneously a small CO_2-desorption peak. The strong CO peak is associated with the reduction of the iron oxide particles (the only difference regarding the support). The calculated oxygen content of the catalyst increased 2.8% regarding the bulk AC (Table 5.4), which is also in agreement with a Fe-content of 7 wt.% (taking into account that Fe_3O_4 and/or Fe_2O_3 were found to be the principal iron species – Chapters 3 and 4).

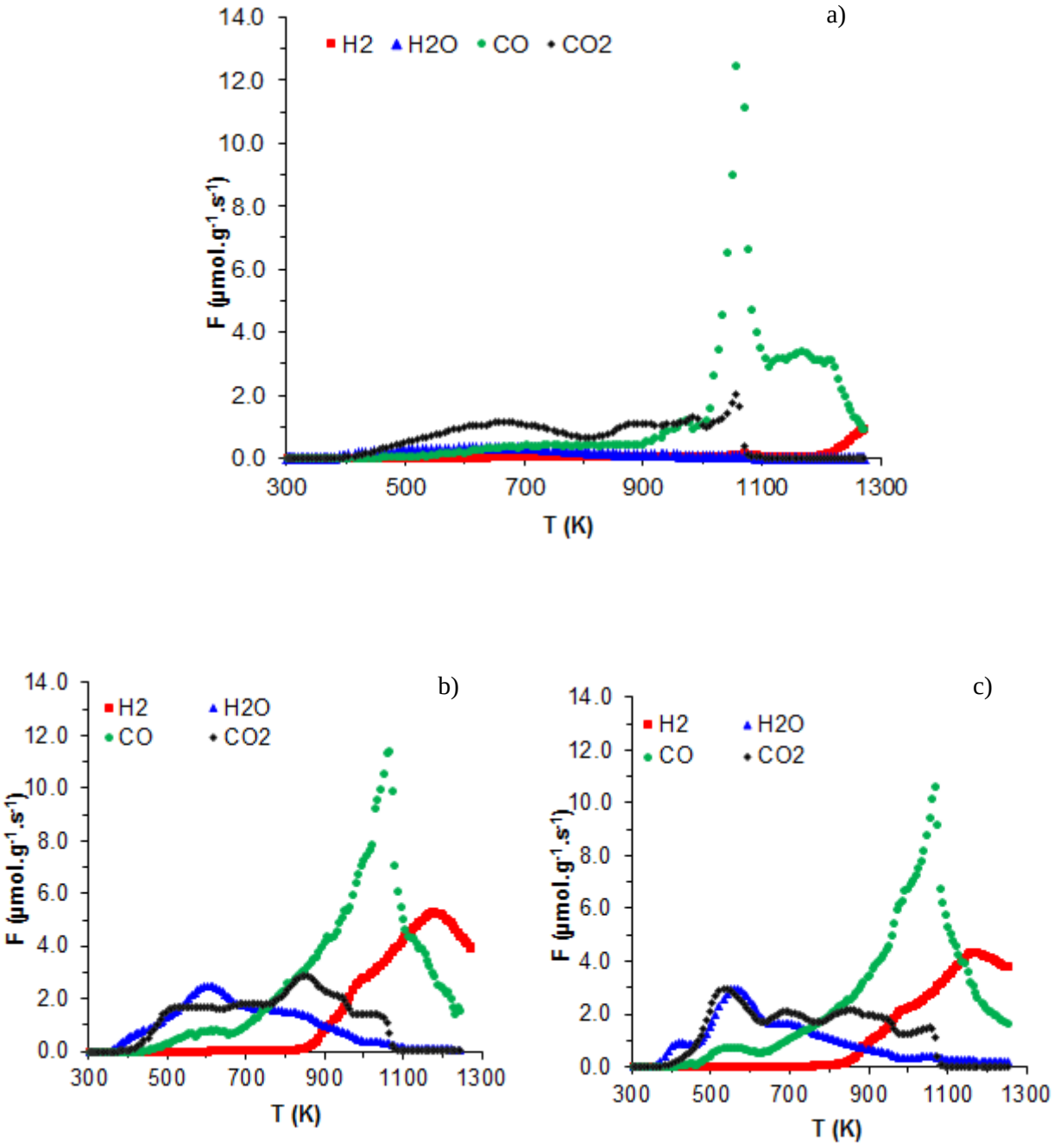

Figure 5.8 – TPD profiles of fresh (a) and used catalysts with 6 (b) and 24 mM (c) of H_2O_2.

Table 5.4 – Oxygen content obtained by TPD of the AC support, and fresh and used N-Fe catalysts with 6 and 24 mM of oxidant.

Sample	% O	CO (μmol .g $^{-1}$)	CO_2 (μmol .g $^{-1}$)
N	1.8	455	346
N-Fe	4.6	1566	647
N-Fe + 6 mM	10.6	3514	1550
N-Fe + 24 mM	10.7	3340	1661

When analyzing the TPD of used catalysts (Fig. 5.8b-c), the different nature of the adsorbed species regarding spent samples used as adsorbents (Fig. 5.5b) is observed at a glance. Thus, the TPD profiles of used catalyst also present a main CO peak associated to iron oxides reduction. Nevertheless, this peak becomes wider regarding fresh samples and clearly involves all the additional decomposition of CO-evolving groups between 700 – 1300 K associated to the decomposition of adsorbed molecules. Also, at low temperatures, where the TPD profile is not influenced by the iron oxides reduction, the main decomposition process in the N-sat sample occurred at around 560 K, being the CO-desorption preferential regarding the CO_2 one, while in the residues of catalysts the CO_2-desorption is preferential in this temperature range, although CO-desorption also occurred. The CO-TPD profile increased more or less homogeneously between 700 – 1060 K, showing small shoulders, and then, decreased similarly. The CO_2-profile showed also clearly the existence of different surface groups by some maxima with variable intensity depending on the experimental conditions used in the catalytic process, i.e., the dose of oxidant. The decay of this profile is coincident with the maximum CO-desorption probably because the iron particles are able to catalyze the oxidation of the carbon surface ($CO_2 + C = 2CO$). The H_2O profile is also clearly associated to the decomposition of carboxylic acid, in spite that the large tail and small shoulders also justified different processes such as the phenolic group decomposition. The hydrogen desorption of both spent samples showed a maximum located at 1150-1200 K; in this case, the H_2 evolution starts at a similar temperature than in spent adsorbents, but increases with smaller slope and in both cases defines a clear maxima.

In spite of the quite similar oxygen content evaluated for both catalyst residues after processes at low (6 mM) and high (24 mM) H_2O_2 concentrations (Table 5.4), the formation of carboxylic acid is clearly favoured in the later as denoted by the intense

peak observed on the CO_2-profile at 530 K with simultaneous H_2O desorption. In this case, also the amount of CO_2 evolved is slightly higher, indicating a greater oxidation degree of the adsorbed compounds on the AC surface.

This fact can clearly influence the adsorption capacity of the by-products formed. The carbon surface is amphoteric, and there is a broad bibliography regarding adsorption of pollutants on ACs as a function of pH, surface chemistry, nature of the organic pollutants, etc. All these parameters determine the attractive or repulsive interactions between both phases in solution. Dispersion (van der Walls) interactions also play an important role, thus, aromatic solutes have a high affinity for graphene layers of the AC favoured by π-π interactions. These interactions are weakened by the presence of acidic oxygenated groups on the edge of the graphene layers because serve to withdraw electrons from the π-system deactivating the ring system of AC – *e.g.* it is well known that the adsorption of phenol is retarded by the acidity of the carbons [19], but also, the aromatic ring of a solute (pollutant) is deactivated depending on the substituents (phenol, chlorophenol, dinitrophenol, etc.) [20]. Thus, increasing the H_2O_2 dose used in reaction, the total mineralization capacity is not increased, probably by the development of scavenging reactions in a greater extent; nevertheless, the by-products formed are clearly more oxidized than those formed at low H_2O_2 concentrations. The greater TOC removal observed in the latter case is therefore a consequence of a greater adsorption of by-products that provoked a greater pore blockage.

In order to check these conclusions, and also looking for some indications about the evolution of the solution biodegradability/toxicity after the different treatments, some additional experiments were carried out. It is noteworthy that the partial oxidation of organic contaminants may lead to more toxic by-products than the initial compounds [21], independently of the TOC decay. Thus, biodegradability and toxicity of the initial and treated solutions (with 6 and 24 mM of H_2O_2) were analyzed and the results proved that the present process led to an increase of effluent biodegradability, as well as to a decrease of the toxicity relatively to the initial dye solution (Table 5.5). It is observed that the process that used a higher H_2O_2 concentration presented the highest biodegradability and, accordingly, the lowest toxicity. However, it is important to note that the values for these parameters depend on the microorganisms used as well as on the method applied, which should be chosen accordingly to the final destination of the treated water [21]. The biodegradability/toxicity dependence on initial hydrogen

peroxide concentration follows a different trend as compared to TOC data. These results confirm the different nature of the by-products generated in each experimental condition, which are in clear agreement with those previously discussed.

Table 5.5 – Parameters of biodegradability and toxicity for the initial poluent solution and for the solution treated by the heterogeneous Fenton process using 6 and 24 mM of H_2O_2.

	Biodegradability (%)	**Toxicity (%)**
OII initial solution	16	80
N-Fe + 6 mM	65	60
N-Fe + 24 mM	90	34

5.4. Conclusions

This Chapter deals with the characterization of used samples after adsorption and catalytic experiments in order to clarify the process implicated in the elimination of OII from an aqueous solution by the heterogeneous Fenton advanced oxidation using an AC/Fe catalyst. It is known that this process involves the co-existence of adsorption and reaction phenomena, so adsorption experiments were firstly carried out; they allowed concluding that the OII molecules are adsorbed without any transformation, although interactions with the surface groups of the AC have been detected by TPD. The main difference detected in the AC after the adsorption was the increase of CO and the decrease of CO_2 desorption amounts, which were attributed to i) the decomposition of OII molecule groups; ii) the interaction of these molecules with the CO_2-evolving groups of the AC surface (chemical adsorption); iii) the reduction of SO_2 that came from AC and/or the OII molecules. Upon adsorption a blockage of the porosity was observed, particularly micropores where dye molecules are retained.

Catalytic runs were done with different oxidant concentrations. The higher TOC removal was obtained with a 6 mM concentration of H_2O_2. However, a significant amount of intermediate products still stayed in solution, i.e. they are not mineralized or adsorbed. Because OII molecules are easily adsorbed, this lack of by-products

adsorption is due to chemical interactions that did not favour the affinity between adsorbent-adsorbate, particularly using higher concentrations of H_2O_2 (that also favours the scavenging). The textural and chemical characterization of spent catalysts pointed out that S_{BET} decrease was stronger when using a low H_2O_2 load (6 mM). However, TPD and biodegradability experiments showed that by-products formed at higher H_2O_2 concentrations are more oxidized, which difficult their adsorption, but decreases their toxicity.

References

[1] M. Farré, M. Franch, J. Ayllón, J. Peral, X. Domènech, Biodegradability of treated aqueous solutions of biorecalcitrant pesticides by means of photocatalytic ozonation, Desalination 211 (2007) 22–33.

[2] R.C. Martins, R.M. Quinta-Ferreira, Remediation of phenolic wastewaters by advanced oxidation processes (AOPs) at ambient conditions: Comparative studies, Chem. Eng. Sci. 66 (2011) 3243–3250.

[3] J.L. Figueiredo, M.F.R. Pereira, M.M.A. Freitas, J.J.M. Orfão, Modification of the surface chemistry of activated carbons, Carbon 37 (1999) 1379-1389.

[4] S. Morales-Torres, F.J. Maldonado-Hódar, A.F. Pérez-Cadenas, F. Carrasco-Marín, Design of low-temperature Pt-carbon combustion catalysts for VOC's treatments, J. Hazard. Mater. 183 (2010) 814-822.

[5] G. Zhang, J. Qu, H. Liu, A.T. Cooper, R. Wu, $CuFe_2O_4$/activated carbon composite: A novel magnetic adsorbent for the removal of acid orange II and catalytic regeneration, Chemosphere 68 (2007) 1058-1066.

[6] R.J. Bigda, Consider Fenton´s chemistry for wastewater treatment, Chem. Eng. Prog. 92 (1995) 62-66.

[7] F. Duarte, F.J. Maldonado-Hódar, A.F. Pérez-Cadenas, L.M. Madeira, Fenton-like degradation of azo-dye Orange II catalyzed by transition metals on carbon aerogels, Appl. Catal., B 85 (2009) 139-147.

[8] I. Mesquita, L.C. Matos, F. Duarte, F.J. Maldonado-Hódar, A. Mendes, L.M. Madeira, Treatment of azo dye-containing wastewater by a Fenton-like process in a continuous packed-bed reactor filled with activated carbon, J. Hazard. Mater. 237/238 (2012) 30-37.

[9] J.P.S. Sousa, M.F.R. Pereira, J.L. Figueiredo, Catalytic oxidation of NO to NO_2 on N-doped activated carbons, Catal. Today 176 (2011) 383-387.

[10] B. Pawelec, R. Mariscal, J.L.G. Fierro, A. Greewood, P.T. Vasudevan, Carbon-supported tungsten and nickel catalysts for hydrodesulfurization and hydrogenation reactions, Appl. Catal., A 206 (2001) 295-307.

[11] S. Echeandia, P.L. Arias, V.L. Barrio, B. Pawelec, J.L.G. Fierro, Synergy effect in the HDO of phenol over Ni–W catalysts supported on active carbon: Effect of tungsten precursors, Appl. Catal., B 101 (2010) 1-12.

[12] R.M. Sellers, Spectrophotometric determination of hydrogen peroxide using potassium titanium (IV) oxalate, Analyst105 (1990) 950-954.

[13] F. Duarte, F.J. Maldonado-Hódar, L.M. Madeira, Influence of the characteristics of carbon materials on their behaviour as heterogeneous Fenton catalysts for the elimination of the azo dye Orange II from aqueous solutions, Appl. Catal., B 103 (2011) 109-115.

[14] A. Rey, M. Faraldos, J.A. Casas, J.A. Zazo, A. Bahamonde, J.J. Rodríguez, Catalytic wet peroxide oxidation of phenol over Fe/AC catalysts: Influence of iron precursor and activated carbon surface, Appl. Catal., B 86 (2009) 69-77.

[15] L.R. Radovic, C. Moreno-Castilla, J. Rivera-Utrilla, Carbon Materials as adsorbents in aqueous solutions, in Chemistry and Physics of Carbon, Vol. 27, Marcel Dekker Inc, New York, 2000.

[16] M. Stylidi, D.I. Kondarides, X.E. Verykios, Pathways of solar light-induced photocatalytic degradation of azo dyes in aqueous TiO_2 suspensions, Appl. Catal., B 40 (2003) 271-286.

[17] C. Bauer, P. Jacques, A. Kalt, Photooxidation of an azo dye induced by visible light incident on the surface of TiO_2, J. Photochem. Photobiol., A 140 (2001) 87-92.

[18] N. Chahbane, D. Popescu, D.A. Mitchell, A. Chanda, D. Lenoir, A.D. Ryabov, K. Schramma, T.J. Collins, Fe^{III}–TAML-catalyzed green oxidative degradation of the azo dye Orange II by H_2O_2 and organic peroxides: products, toxicity, kinetics, and mechanisms, Green Chem. 9 (2007) 49-57.

[19] H. Oda, M. Kishida, C. Yokokawa, Adsorption of benzoic acid and phenol from aqueous solution by activated carbons - effect of surface acidity, Carbon, 19 (1981) 243-248.

[20] F. Caturla, J.M. Martín-Martínez, M. Molina-Sabio, F. Rodriguez-Reinoso, R. Torregrosa, Adsorption of substituted phenols on activated carbon, J. Colloid Interface Sci 124 (1988) 528-534.

[21] L. Rizzo, Bioassays as a tool for evaluating advanced oxidation processes in water and wastewater treatment, Water Res. 45 (2011) 4311-4340.

CHAPTER 6 - Influence of the particle size of activated carbons on their performance as Fe supports for developing Fenton-like catalysts

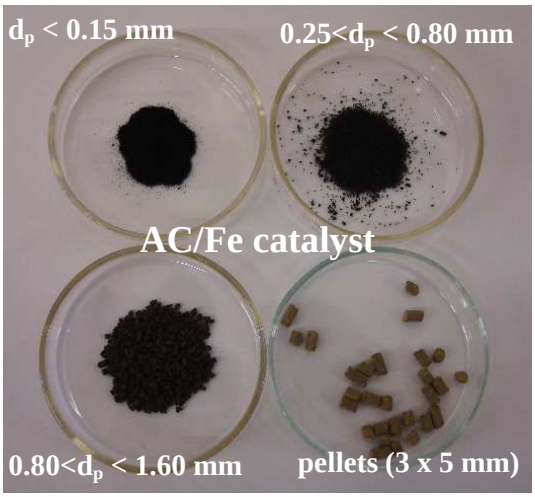

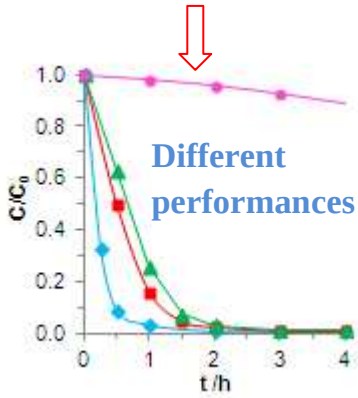

Chapter 6. Influence of the particle size of activated carbons on their performance as Fe supports for developing Fenton-like catalysts *

Abstract

In this Chapter, a commercial activated carbon (AC) impregnated with iron (7% wt. Fe/AC) is used as catalyst for the removal of the azo-dye Orange II (OII) by the heterogeneous Fenton-like process. The influence of the particle size of the AC support on adsorption and catalytic runs was evaluated, using different particle sizes below commercial pellets form (cylinders of ca. 3 × 5 mm). The characterization of the materials was carried out using several techniques (N_2 and CO_2 adsorption, X-ray diffraction and high resolution transmission electron microscopy). It was found that the porosity of the extruded AC was liberated by milling, enhancing the adsorption capacity and the adsorption rate. Nevertheless, total discoloration was achieved with the four particle sizes tested, albeit taking ca. 24 hours using pellets and only 2 hours using the powder, under tested conditions. The dispersion of iron in the Fenton-like catalysts was also improved with the decrease in AC particle size, which also favoured their catalytic activity. However, leaching increased in the same way. This trade-off between activity and stability pointed to the intermediate size of 0.80-1.60 mm as the best choice. To analyze the effect of only the support particle size on catalytic performance, catalysts were prepared with nearly the same iron dispersion (keeping the load of iron per unit of surface area constant). The smaller the support, the higher is the activity and thus the effectiveness factor, due to competition between the internal diffusion and reaction rate.

* Adapted from: F. Duarte, F.J. Maldonado-Hódar, L.M. Madeira, Ind. Eng, Chem. Res. 103 (2011) 109-115.

6.1. Introduction

In the previous Chapters 3 and 4 the runs were carried out in *slurry* batch reactors, with the powder catalyst (containing 7 wt.% of Fe) in suspension, enabling to obtain promising results, namely when using the Norit RX 3 Extra as AC support and iron (II) acetate as the precursor salt. Nevertheless, the economy of the treatment process will greatly improve with the development of continuous flow reactors, for which the use of powder catalysts is problematic.

Thus, this part of the work deals with the removal of the azo-dye Orange II, using the commercial activated carbon Norit RX 3 Extra, milled and sieved in four different particle sizes. The influence of the particle size (d_p) of the AC support on adsorption and catalytic runs was evaluated, taking into account the fact that in Fenton's oxidation both adsorption and reaction coexist. AC particle size not only influences competition between internal mass transfer and chemical reaction, but also iron dispersion, and consequently leaching and catalytic performance. The Fe-catalysts were therefore extensively characterized by different techniques and their catalytic performance related to chemical and physical properties.

6.2. Material and methods

Norit RX 3 Extra (herein called sample N), commercialized as extruded pellets of approximately 3×5 mm, was milled and sieved to obtain particles in powder form (< 0.15 mm) and within the ranges 0.25 – 0.80 mm and 0.80 – 1.60 mm. Then part of each fraction, including the original pellets, was impregnated with iron (II) sulphate heptahydrate and thermally pre-treated (as detailed in Chapter 2 – section 2.2) to obtain the N-Fe powder, N-Fe 0.25-0.80 mm, N-Fe 0.80-1.60 mm and N-Fe pellets samples. Another series of samples (series B) was synthesized in order to minimize/eliminate the variation of Fe dispersion, which was done by impregnating each support with different d_p with the same iron amount per unit of surface area as the N-Fe powder (used as reference). Therefore, the iron loading decreases proportionally to the BET surface area, from 7 wt.% for the powder till 5.5 wt.% for the pellets.

The samples were characterized by N_2 (at 77 K) and CO_2 (at 273 K) adsorption, high resolution transmission electron microscopy (HRTEM) and X-ray diffraction (XRD) techniques – see Chapter 2, section 2.3. Apparent (particle) density was measured by mercury pycnometry.

Adsorption and catalytic runs were carried out using the set-up and operating conditions (pH 3, T = 30 ºC, C_{OII} = 0.1 mM and C_{H2O2} = 6 mM) described in section 2.4.1. (Chapter 2). Analytical techniques mentioned in section 2.5. of the same Chapter were also used.

6.3. Results and discussion

6.3.1. Characterization of supports and catalysts

The textural properties of the supports were evaluated by N_2 and CO_2 adsorption at 77 and 273 K respectively, the results being summarized in Table 6.1. As previously observed, this AC is essentially a microporous material, as denoted by the shape of the N_2 adsorption isotherms (Figure 6.1). However, the large knee of the isotherms suggests notable heterogeneity in micropore size, while the slope after micropore saturation, as well as the existence of a small hysteresis cycle, are indicative of the presence of some mesoporosity. In fact, all samples have W_0 (N_2) > W_0 (CO_2) – Table 6.1, indicating the occurrence of N_2 condensation inside the larger micropores and/or mesopores.

Table 6.1 – Textural characteristics of the support in the four particle sizes used.

N support	S_{BET} ($m^2.g^{-1}$)	L_0 (N_2) (nm)	W_0 (N_2) ($cm^3.g^{-1}$)	S_{mic} (CO_2) ($m^2.g^{-1}$)	L_0 (CO_2) (nm)	W_0 (CO_2) ($cm^3.g^{-1}$)	V_{BJH} ($cm^3.g^{-1}$)	S_{BJH} ($m^2.g^{-1}$)
powder	1405	1.70	0.62	1173	0.81	0.48	0.592	1653
0.25-0.80 mm	1230	1.66	0.52	942	0.73	0.35	0.482	1339
0.80-1.60 mm	1110	1.64	0.48	893	0.72	0.32	0.430	1206
pellets	1113	1.56	0.47	984	0.73	0.36	0.358	942

S_{BET}: BET surface area obtained by N_2 adsorption; L_0 (N_2): mean micropores' size obtained by N_2 adsorption; W_0 (N_2): micropores' volume obtained by N_2 adsorption; S_{mic}: micropores' surface; L_0 (CO_2): mean micropores' size obtained by CO_2 adsorption; W_0 (CO_2): micropores' volume obtained by CO_2 adsorption; V_{BJH}: BJH pores' volume; S_{BJH}: BJH surface area.

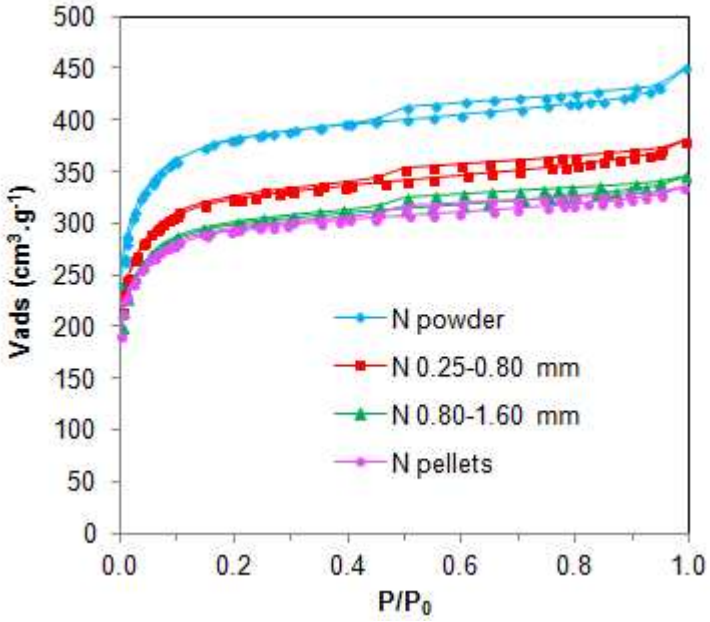

Figure 6.1 – Variation of the N_2 adsorption isotherms with the particle size of the AC support; closed symbols for adsorption, open symbols for desorption.

Clearly the accessible porosity and surface area increased with milling, i.e. from pellets to powder samples. Thus, the micropore volume (W_0), determined either by N_2 or CO_2 adsorption, progressively decreases with the increase in particle size, and simultaneously the mean micropore size (L_0) also decreases, leading to a progressive reduction in S_{BET} or S_{mic} (CO_2) values. The variation in the mesopore volume determined by the BJH method also showed the same trend. However, mesopore size distribution was not affected, as can be concluded from Figure 6.2. The diminution of the pore volume and surface area by pelletization of carbon powder has previously been described by other authors [1].

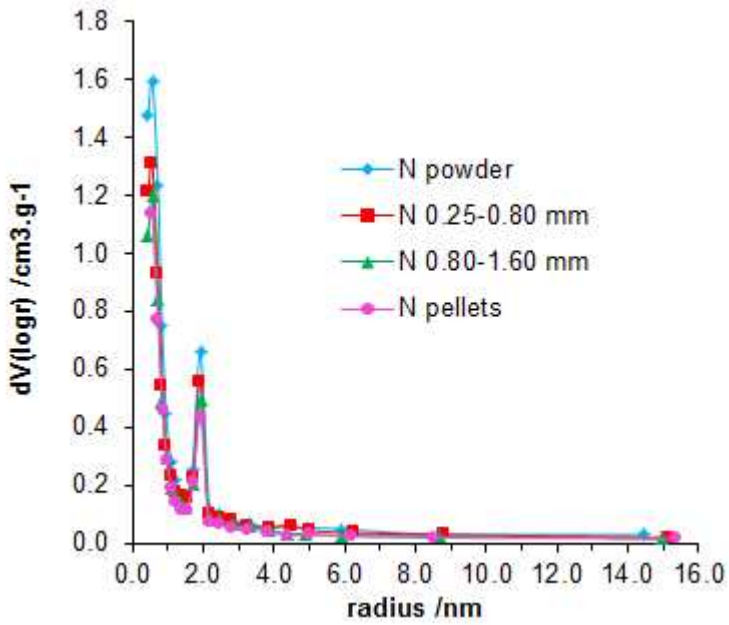

Figure 6.2 – Pore size distribution by the BJH method.

After the Fe impregnation of the supports to obtain the corresponding catalysts, the shape of the N_2-adsorption isotherms was basically maintained (data not shown). However, it produced a certain micropore blockage, indicated mainly by the decrease in the BET surface areas and the W_0 (N_2) values from the supports to the catalysts (Table 6.2). Moreover, when the support is used as a powder there is a strong decrease (of 0.12 ± 0.01 $cm^3.g^{-1}$) in the micropore volume obtained either by N_2 or CO_2 adsorption (Table 6.2). Nevertheless, when the pellets support is impregnated, W_0 (CO_2) is almost fully maintained, while W_0 (N_2) shows a decrease similar to that observed in the case of the powder. This means that the Fe-particles will be formed within a different porosity range: in the case of the powder, the small particle size and the larger mean micropore size of the support can favour access of the Fe-solution to a narrower porosity than in the case of the pellets.

Table 6.2 – Textural characteristics of the support in powder form and in pellets together with their corresponding catalysts.

Sample	S_{BET} ($m^2.g^{-1}$)	L_0 (N_2) (nm)	W_0 (N_2) ($cm^3.g^{-1}$)	S_{mic} (CO_2) ($m^2.g^{-1}$)	L_0 (CO_2) (nm)	W_0 (CO_2) ($cm^3.g^{-1}$)
N powder	1405	1.70	0.62	1173	0.81	0.48
N-Fe powder	1160	1.75	0.51	758	0.89	0.35
N pellets	1113	1.56	0.47	984	0.73	0.36
N-Fe pellets	893	1.38	0.37	923	0.70	0.33

S_{BET}: BET surface area obtained by N_2 adsorption; $L_0(N_2)$: mean micropores' size obtained by N_2 adsorption; $W_0(N_2)$: micropores' volume obtained by N_2 adsorption; S_{mic}: micropores' surface; $L_0(CO_2)$: mean micropores' size obtained by CO_2 adsorption; $W_0(CO_2)$: micropores' volume obtained by CO_2 adsorption.

Therefore, the accessibility of the iron solution used for impregnation of the support porosity strongly depends on the AC particle size, and thus the Fe distribution and dispersion change significantly among the four catalysts, decreasing in line with the corresponding increase in the support particle size (Fe particles will be formed progressively on the outer surface). This was appreciable even at a glance, because in the case of the catalyst prepared with pellets, the high iron concentration on the external surface of the pellets provokes a yellow-green hue in comparison with the black aspect of the other ones (Figure 6.3). The HRTEM images (Figure 6.4) also revealed a better dispersion of the iron particles in the case of the catalyst prepared in powder, with Fe-particle size below 20 nm, while in the case of the catalyst prepared in pellets the iron particles are more heterogeneous and form some particles larger than 100 nm.

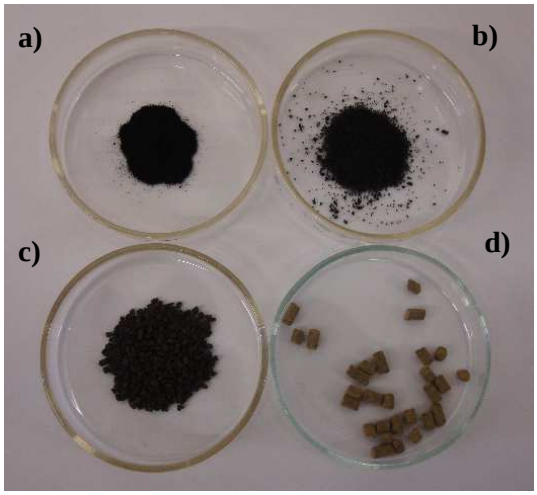

Figure 6.3 – Photos of N-Fe catalysts in the four different sizes: a) powder, b) 0.25-0.80 mm, c) 0.80-1.60 mm, d) pellets.

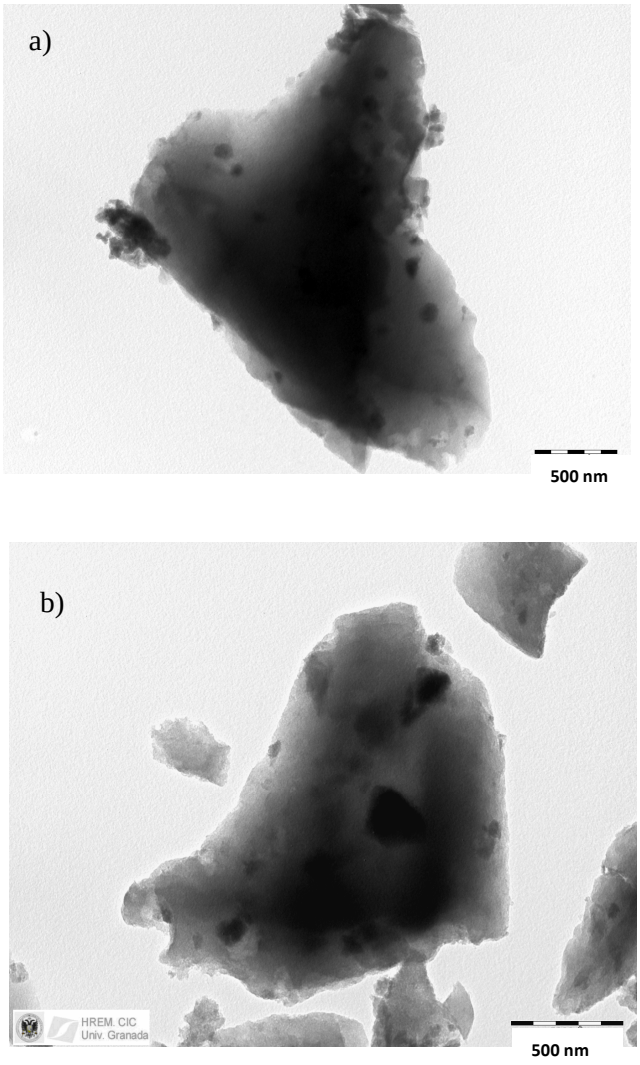

Figure 6.4 – HRTEM photos of N-Fe in powder (a) and in pellet form (b).

The XRD patterns also demonstrated this effect because the crystallinity of the Fe-phases increased progressively along with the support particle size, the peaks of the iron phases becoming noticeably more intense (Figure 6.5a).

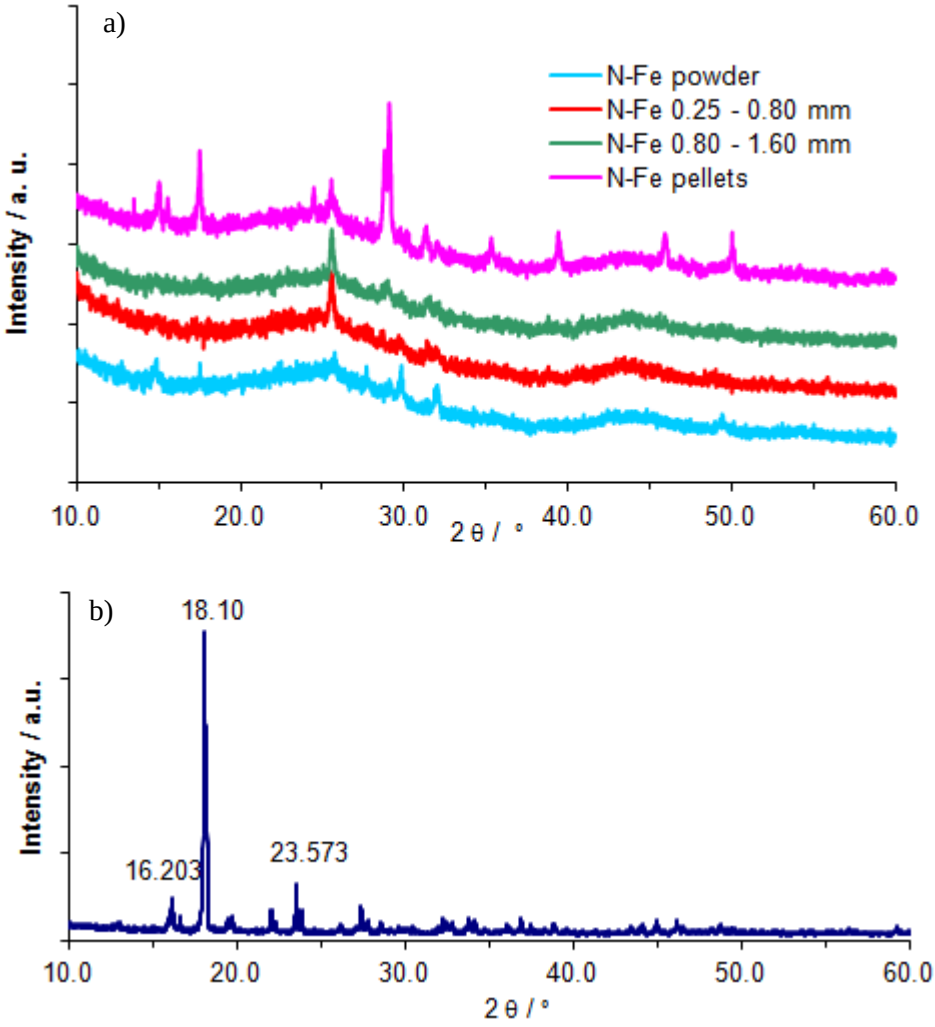

Figure 6.5 – XRD patterns of the pre-treated catalysts in N_2 flow at 300 ºC (a) and of the raw $FeSO_4.7H_2O$ (b) used as iron salt precursor.

However, the XRD patterns plotted in Figure 6.5a not only show an increase in the Fe-particle size, but also a change in the nature of the Fe-phases. Clearly, comparing the XRD patterns of the pre-treated catalysts (Figure 6.5a) with those obtained for the raw $FeSO_4.7H_2O$ used as precursor (Figure 6.5b), it is possible to conclude that the precursor salt was always decomposed. However, the assignation of the XRD diffraction peaks observed for the catalysts is a hard task because of the different oxides

500 nm

and allotropic forms. Major iron oxides include: hematite (α-Fe_2O_3), maghemite (γ-Fe_2O_3), goethite (α-FeOOH), lepidocrocite (γ-FeOOH), wustite (FeO) and magnetite (Fe_3O_4). Beta (β-Fe_2O_3) and epsilon (ε-Fe_2O_3) iron (III) oxides are less frequent polymorphs. Moreover, both are unstable, forming hematite as a product of their transformations. The thermal decomposition of iron sulphates was previously studied. According to Tagawa [2], the decomposition of hydrated $FeSO_4$ does not yield anhydrate but rather iron (III) oxide through previous oxidation to $Fe_2(SO_4)_3$, although the crystal system of Fe_2O_3 was not specified. Zboril *et al.* [3] identified the trigonal-hexagonal α-Fe_2O_3 and cubic β-Fe_2O_3 as $Fe_2(SO_4)_3$ decomposition products. Nevertheless, the ratio between both phases depends on the experimental conditions such as decomposition temperature or the initial particle size of the raw sulphate, influencing the transformation of the metastable β-Fe_2O_3 into α-Fe_2O_3. Moreover, α-Fe_2O_3 is also transformed into γ-Fe_2O_3 during the $Fe_2(SO_4)_3$ reduction process through the formation of magnetite (Fe_3O_4) as intermediate [4]. Both γ-Fe_2O_3 and Fe_3O_4 present the same inverse spinel structure, with some cation vacancies in octahedral position for the former. Finally, the XRD patterns of γ-Fe_2O_3 present different diffraction peaks according to the shape, dimensions (axial ratio) and order-disorder of the iron nanoparticle defects [4].

Thus, in our case, clearly a mixture of phases was always present. The small Fe-particles found in the N-Fe powder mainly match the peaks attributable to lepidocrocite (JCPDS file 8-98) with I_{100} at 14.2 º corresponding to the (020) diffraction. This phase also seems to be present using the pellets as support. The peak at 33.1 º in the powdered catalyst can be assigned to the I_{100} of hematite (JCPDS file 33-0664). All the samples presented a diffraction peak at around 2θ = 26 º, this being the main peak when using intermediate sizes of the AC support; however, the relative intensity with regard to the remaining peaks underwent significant change between samples. This peak can be assigned to the I_{100} (310 diffraction) of the akaneite (β-Fe_2O_3) oxide-hydroxide (JCPDS file 13-157), but can also be due to the diffraction (120) of lepidocrocite. The most intense XRD peaks in the N-Fe pellet catalyst are attributable to the maghemite (γ-Fe_2O_3) phase, with I_{100} corresponding to the (220) diffraction at around 30 º. At 35.5 º there also appears a small peak that can be attributable to the I_{100} (311) of the magnetite (Fe_3O_4) (JCPDS file 19-629).

6.3.2. Elimination of Orange II from the solution

6.3.2.1. Adsorption experiments

The elimination of OII from the solution by the heterogeneous Fenton-like process using this kind of porous samples is complex, with the co-existence of adsorption and reaction phenomena. Thus, adsorption experiments were first carried out, in the same conditions as the catalytic tests (but in the absence of H_2O_2). The adsorption rate and the amount adsorbed after 24 h showed a significant decrease with the increase in particle size (Figure 6.6). Only the support in powder form was able to decolorize the solution completely during this period, in fact after approximately 6-8 h. The evolution of the OII adsorption performance is in agreement with the smaller and narrower microporosity/mesoporosity observed with the increase in the support particle size (Table 6.1). The pore blockage by Fe particles justifies the smaller adsorption rate and capacity of the catalysts regarding their supports (cf. Table 6.2 and Fig. 6.6). This effect was more evident when the AC particle size was being reduced, because, as previously mentioned, micropores were blocked to a large(r) extent by the greater accessibility of the Fe-solution in the smaller particles.

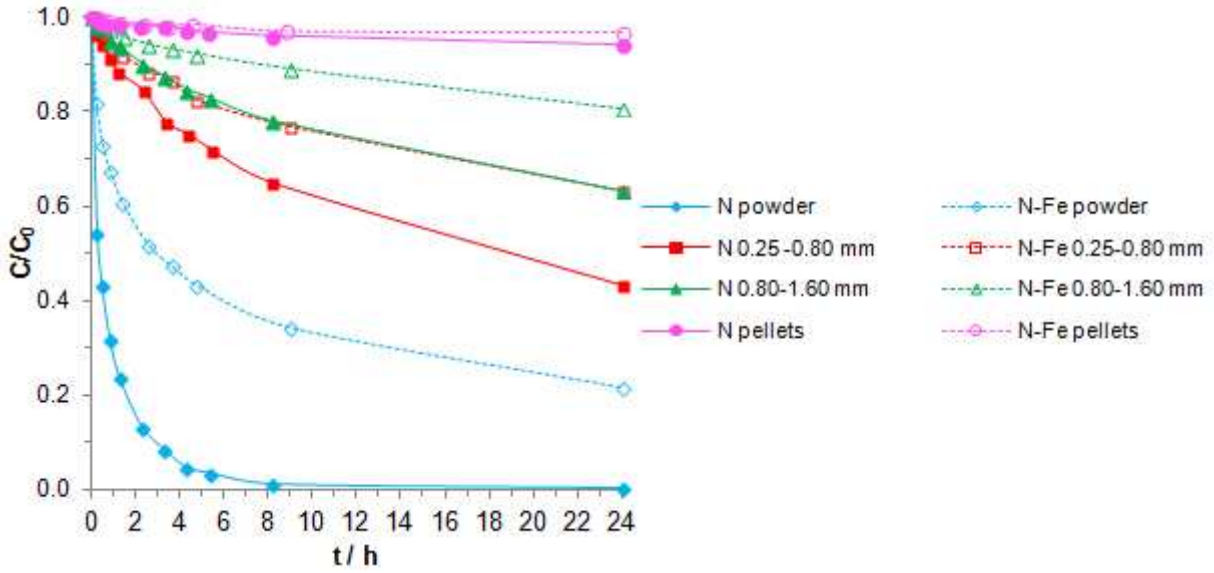

Figure 6.6 – OII removal by adsorption using N supports (closed symbols) and N-Fe catalysts (open symbols) with different particle sizes (C_{OII}= 0.1 mM, C_{solid}= 0.1 g.L^{-1}, pH 3, T = 30 ºC).

6.3.2.2. Catalytic Fenton-like oxidation experiments

The catalytic behaviour of the four prepared catalysts is determined by their different porosity, the nature of the iron species and their dispersion. During the heterogeneous process the reactants should be adsorbed on the catalyst surface, which varies markedly depending on the support particle size, as previously described. Although the process is quite complex and is determined by several factors, it was already proved the importance of the iron distribution and dispersion in the catalytic performance of Fe-catalysts in previous studies [5, 6] (cf. Chapter 3). This clearly justifies the catalytic behaviour summarized in Figure 6.7. The catalyst prepared by impregnation of N-powder is therefore the most efficient in terms of the dye oxidation rate, although the differences in discoloration ability were smaller between the three catalysts with smaller particle sizes than in the adsorption experiments (Figure 6.6), confirming that in these conditions the OII removal was due mainly to catalytic oxidation and not to the adsorption process. The poor ability of the pellets to disperse the Fe species was therefore the key factor with regard to the significant difference reported. The three catalysts with smaller support sizes decolorized the solution in 2h, while the conversion obtained at this reaction time using the catalyst in pellet form is

almost negligible. Nevertheless, total discoloration was also obtained in this case, but only after 24 h of reaction.

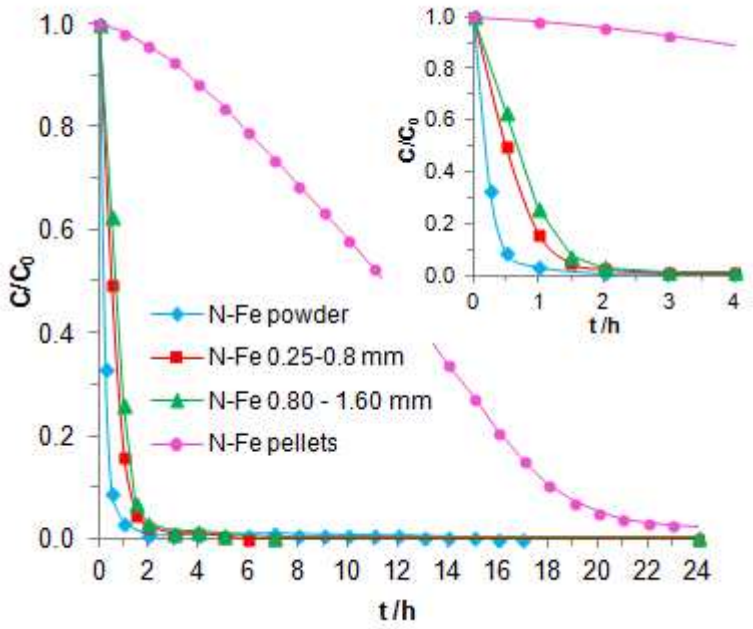

Figure 6.7 – OII removal by heterogeneous Fenton reaction using the N-Fe catalyst in the four particle sizes (C_{OII}= 0.1 mM, C_{H2O2}= 6 mM, C_{solid}= 0.1 g.L^{-1}, pH 3, T = 30 ºC).

In addition to dye degradation, quantification of the mineralization degree (i.e. level of oxidation) is also important. The TOC analyses (Figure 6.8a) showed that a large proportion of the degradation products remained in solution after 24 h, indicating a high stability of the intermediates/degradation products, i.e. a high refractory character, and also that they were not adsorbed. Once again the most effective catalyst was the most well dispersed one – N-Fe in powder form. However, leaching also presented the same trend (Figure 6.8b), and the less stable catalyst therefore corresponded to that supported on the powder, compromising its reutilization. In fact, the smaller Fe-particles (better dispersion) lead to more active catalysts, but also favoured Fe leaching. Nevertheless, this parameter can be improved, for instance using another iron salt precursor or more drastic thermal treatments, which will be the subject of future study. In any case, the final iron concentration found in solution was just slightly above the European Legislation values (2 ppm) [7] in the worst cases, and

below that threshold for the supported catalysts of d_p > 0.80-1.60 mm. Of course, if reaction is not prolonged for 24 h, iron leached into solution is even smaller.

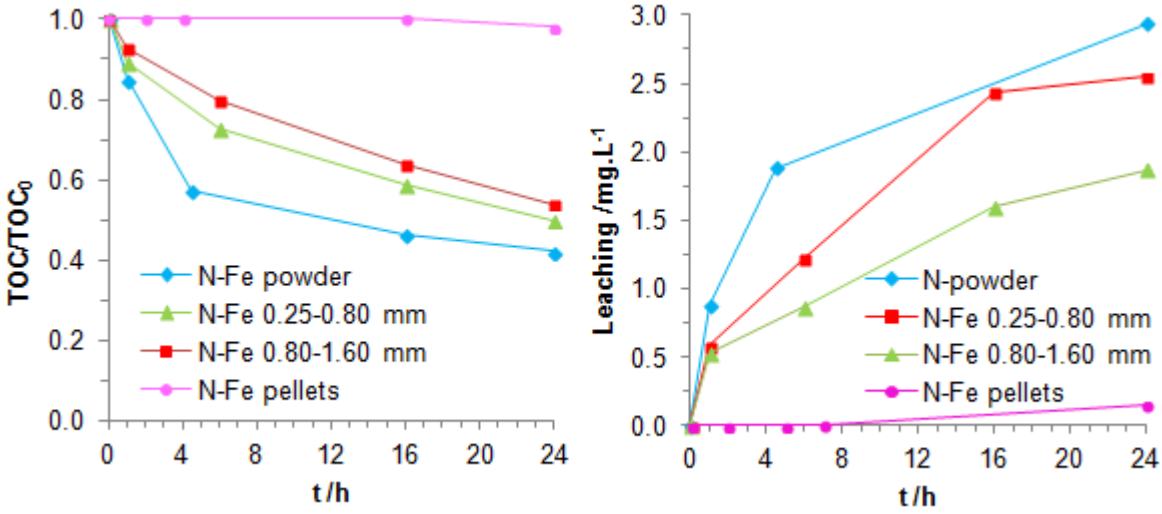

Figure 6.8 – Mineralization degree (a) and leaching values (b) achieved along 24 h of reaction for the different samples (experimental conditions as in Fig. 6.7).

The levels of dissolved iron increased progressively over time, as leaching from the supports proceeded. Homogeneous experiments performed with a ferrous salt employing the maximum values reported in Fig. 6.8b (i.e., after 24 h of reaction) as initial load provided a TOC removal degree ca. 20 % smaller, showing that the homogenous contribution cannot be discarded and under such conditions both processes were important. However, at the early stages of reaction the process was exclusively heterogeneous because there was no iron in solution.

A suitable balance between dye degradation, TOC removal and leaching has to be made in the choice of the best particle size. The results suggested that intermediate sizes can be a good option, particularly in the case of the catalyst with 0.80 < d_p < 1.60 mm, which also complied with the legislated value for iron in the final effluent.

The catalytic performance of heterogeneous Fenton catalysts is related to their ability to decompose H_2O_2 molecules into hydroxyl radicals. For that, a colorimetric method [8] was used for the determination of the hydrogen peroxide concentration remaining in solution after 4 and 24 hours of reaction without dye. The H_2O_2 conversions are compiled in Table 6.3 and showed an increase in H_2O_2 consumption

with a decrease in d_p due to the improvement in iron dispersion which, together with the adsorptive behaviour of the samples previously described, justifies the differences in the performances of the catalysts towards OII elimination.

Table 6.3 – H_2O_2 conversion achieved using the four catalysts after 4 and 24 h of the Fenton reaction.

Sample	**X_{H2O2} after 4 h (%)**	**X_{H2O2} after 24 h (%)**
N-Fe powder	91	99
N-Fe 0.25-0.80 mm	58	99
N-Fe 0.80-1.60 mm	28	84
N-Fe pellets	14	23

The reported decrease in the discoloration rate with increasing particle size (d_p) may be due to the higher resistance to mass transfer (diffusion of the dye molecules within catalyst pores). In order to obtain the kinetic and mass transport parameters, of importance for reactor design (*e.g.* in packed-bed applications), the effectiveness factors η were calculated [9, 10]:

$$\eta = \frac{r_{obs}}{r_{v,s}} \tag{6.1}$$

where r_{obs} is the observed reaction rate and $r_{v,s}$ stands for the true reaction rate, under catalyst surface conditions (both in $mol.s^{-1}.g_{cat}^{-1}$). It is noteworthy that oxidation experiments with particles of d_p < 0.10 mm, carried out in the same conditions as Fig. 6.7, proved that the catalyst of d_p < 0.15 mm (powder sample) is in chemical regime, since hardly any differences for OII concentration histories were detected (data not shown). Thus, in this case, there are no internal resistances to mass transfer, so that η = 1 ($r_{obs} = r_{v,s}$), and thus $k_{obs} = k_v$, where k_{obs} and k_v are the observed and true rate constants for dye consumption, respectively.

To determine the observed rate constants and the apparent reaction orders (n_{obs}) with respect to the dye for each run, the differential method [10] was used for the experiments carried out with the three catalysts of smaller particle sizes. Pellets were excluded from this study because of their extremely low reaction rates, particularly at

the beginning of the experiments, making the analysis for the extraction of significant parameters difficult. A power rate law was thus assumed ($r = kC_{OII}^{n}$), and from the logarithmic plot of r_{obs} *vs.* C_{OII} the observed reaction order and kinetic constant were computed, as well as the initial r_{obs} (based on the initial dye concentration). Table 6.4 shows the results obtained, wherein the reported rate constants include the radicals concentration, which are assumed to be constant (pseudo-steady-state approach) [10, 11]. As expected, there was a significant decrease in the observed rate constants, as well as in the initial rates, with the increase in particle size. For the powder sample, which is in the chemical regime, the effectiveness factor is 1, and a reaction order of 1.4 was obtained. For the larger particles, which are in intermediate/diffusion regime, the effectiveness factors are progressively lower, as well as the observed order of reaction. This is in line with the well-known falsification of the kinetics when competition between reaction and mass transfer becomes significant within catalyst particles, leading to a decreased n_{obs} [9].

Based on the computed effectiveness factors, the generalized Thiele's modulus (ϕ_g) can then be obtained [9, 10]:

$$\eta = \frac{\tanh \phi_g}{\phi_g} \tag{6.2}$$

and finally the characteristic time constants, De/r^2:

$$\phi_g = \frac{V_p}{A_p}\sqrt{\frac{n+1}{2}\frac{\rho_{ap} k_v C_{OII,s}^{\,n-1}}{D_e}} \tag{6.3}$$

where:

V_p – volume of the catalyst particle, in cm^3;

A_p – area of the catalyst particle, in cm^2;

$C_{OII,s}$ – OII concentration at the catalyst's surface conditions, in $mol.cm^{-3}$;

D_e - effective OII diffusion coefficient, in $cm^2.s^{-1}$;

ρ_{ap} – catalyst apparent density, in $g.cm^{-3}$;

r – radius of the spherical catalyst particle, in cm.

k_v – true rate constant, in $(mol.g_{cat}^{-1}.s^{-1}).(cm^3.mol^{-1})^n$

In this study, spherical geometry was considered for the catalysts; thus, in Eq. (6.3), $V_p/A_p = r/3$. As already mentioned (section 6.2), apparent densities were measured by mercury pycnometry. The apparent density almost did not change with particle size, so a mean value of 0.60 ± 0.03 $g.cm^{-3}$ was used.

As indicated in Table 6.4, there was a clear loss of catalytic efficiency from the powder to the 0.80-1.60 mm sample, this being related to the increase in the Thiele modulus. It is also in line with the decrease in D_e/r^2 from the sample with $0.25 < d_p <$ 0.80 mm to that with $0.80 < d_p < 1.60$ mm, which justifies the poorer performance of the latter (Fig. 6.7). The slight differences in the effective diffusion coefficients can be related to the changes in the textural properties from sample to sample, as well as to the iron dispersion, as discussed in section 6.3.1.

Table 6.4 – Kinetic parameters of the three samples with the smaller particle sizes.

Sample	**d_p (cm)***	**k_{obs} $((mol.g^{-1}.s^{-1})(cm^3.mol^{-1})^n)$**	**n_{obs}**	**Initial r_{obs} $(mol.g^{-1}.s^{-1})$**	**η**	**ϕ_g**	***De*** **$(cm^2.s^{-1})$**	**D_e/r^2 (s^{-1})**
N-Fe powder	1.4×10^{-2}	1.0×10^{4}	1.4	1.6×10^{-6}	1.00	___	_____	____
N-Fe 0.25 – 0.80 mm	6.2×10^{-2}	8.4×10^{0}	1.0	5.2×10^{-7}	0.33	3.0	3.2×10^{-8}	3.3×10^{-5}
N-Fe 0.80 – 1.60 mm	1.2×10^{-1}	3.6×10^{-1}	0.9	2.9×10^{-7}	0.18	5.4	3.8×10^{-8}	1.0×10^{-5}

* d_p - average particle size diameters of powder and $0.25 < d_p < 0.80$ mm samples were measured by a LS 230 Laser Diffraction Particle Size Analyzer from Beckman Coulter; for the sample with $0.80 < d_p < 1.60$ mm, it is an average of the extremes values of d_p.

As mentioned above, besides particle size, the Fe dispersion (and type of iron species) also varies from catalyst to catalyst. To minimize/eliminate this aspect, new samples were synthesized (identified henceforth with a B) with the same iron amount per unit of surface area as the N-Fe powder (used as reference). Therefore, the iron loading decreases proportionally to the BET surface area, from 7 wt.% for the powder until 5.5 wt.% for the pellets. It is worth mentioning that the XRD patterns obtained for

all samples (not shown for brevity's sake) are equal to the one reported in Fig. 6.5 for the powder, i.e. iron species are the same. Even with the pellets, no new XRD peaks were observed, contrary to what happened with the samples with the same iron load of 7 wt.%.

Discoloration curves obtained with the new samples are shown in Fig. 6.9. Again, the discoloration rate increased with the decrease in the d_p. However, in this case, the differences found in the OII elimination are due to particle size only, since the iron dispersion and nature are nearly the same in every sample. It is nevertheless remarkable that even though the amount of iron in each sample was reduced, compared with the previous ones that contain 7 wt.% of Fe (except in the powder one), their activities were increased as a consequence of improved iron dispersion. This is particularly noteworthy for the pellets, which led to a dye conversion of ca. 70% after 2 h of reaction *vs.* <5 % in the previous sample (cf. Fig. 6.7).

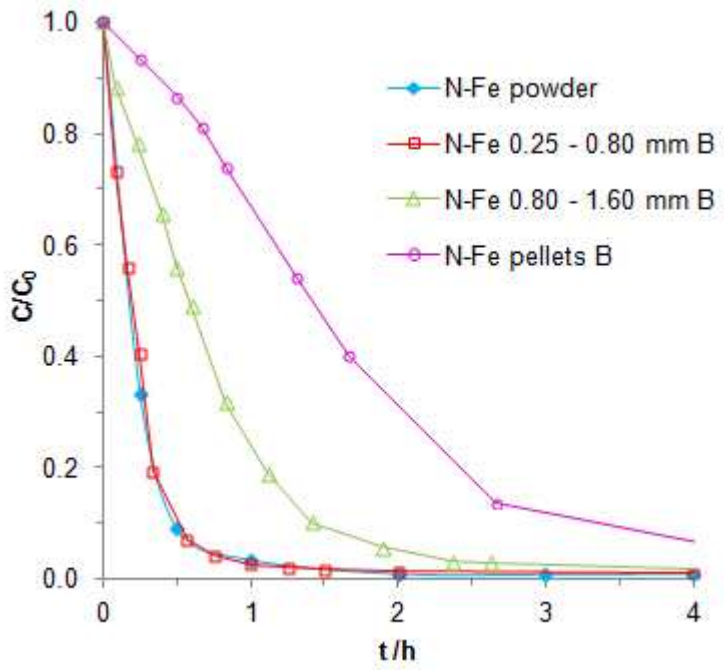

Figure 6.9 – OII discoloration histories using the Fe-AC catalysts with the same iron dispersion (wt.% Fe/S_{BET} ratios; experimental conditions as in Fig. 6.7).

Similar curves were now observed for N-Fe powder and N-Fe 0.25-0.80 mm B samples (Fig. 6.9), which means that, with the same Fe/S_{BET} ratio, these catalysts are in

the chemical regime (where the performances are independent of particle size due to the absence of internal resistances to mass transfer, i.e. η = 1). A kinetic analysis was also performed for the new samples B, except for the pellets, for the reasons mentioned above. As a consequence of the improved activity in the new samples, their effectiveness factors are higher (Tables 6.5 and 6.4, respectively).

Table 6.5 – Kinetic parameters of the three samples with the smaller particle sizes and the same iron dispersion (wt.% Fe/S_{BET} ratios).

Sample	**d_p (cm)***	**k_{obs} (mol.g^{-1}.s^{-1}) (cm^3.mol^{-1})^n)**	**n_{obs}**	**Initial r_{obs} (mol.g^{-1}.s^{-1}))**	**η**	**ϕ_g**	***De*** **(cm^2.s^{-1})**	**D_e/r^2 (s^{-1})**
N-Fe powder	1.4×10^{-2}	1.0×10^{4}	1.4	1.6×10^{-6}	1.00	___	____	____
N-Fe 0.25 – 0.80 mm B	6.2×10^{-2}	1.0×10^{4}	1.4	1.6×10^{-6}	1.00	___	____	____
N-Fe 0.80 – 1.60 mm B	1.2×10^{-1}	5.2×10^{-1}	0.9	3.6×10^{-7}	0.23	4.4	4.5×10^{-8}	1.2×10^{-5}

In spite of now having the same iron dispersion as the other two samples, the N-Fe 0.80-1.60 mm catalyst presented significantly lower k_{obs}, n_{obs} and initial r_{obs} values (Table 6.5), as was also verified for samples with different Fe/S_{BET} ratios (Table 6.4), but now as a consequence of the larger particle size only. Compared to the original sample, *De* of the referred catalyst did not remain exactly the same, since the samples have different textural properties due to the different iron loads.

6.4. Conclusions

This Chapter deals with azo dye Orange II removal by heterogeneous Fenton-like reaction using an activated carbon as iron support, impregnated with 7 wt.% of Fe in four different particle sizes: powder (d_p < 0.15 mm), 0.25 < d_p < 0.80 mm, 0.80 < d_p < 0.60 mm and pellets (approx. 3 × 5 mm). Adsorption of gases showed that this AC is a microporous material, with a high heterogeneity in micropore size, and with some mesopores. It was observed that the grinding produced an increase in the BET area and in the pore volume, and that the iron dispersion in the catalysts also increased from pellets to the powder form. The textural properties of the powder AC explain the best

performance in removal of the dye by adsorption, the adsorption rate increasing from pellets to powder. Catalytic Fenton-like experiments also showed an increase in the activity of the catalyst with a decrease in particle size, attributed not only to the better performance for adsorption, but mainly to the increase in iron dispersion.

The performance of the catalysts was also evaluated by TOC removal and leaching levels, which confirmed N-Fe powder as the best catalyst in terms of mineralization, with higher TOC conversions. However, leaching values also increased from pellets to powder. Thus, intermediate sizes can be the best option, since compared with the powder, they presented only slightly lower TOC removal values and significantly lower leaching levels, particularly in the case of the $0.80 < d_p < 1.60$ mm catalyst.

Kinetic parameters were determined, showing a much higher initial reaction rate for the powder. However, the decreased effectiveness factors with d_p are also a consequence of the worst iron dispersion. Samples prepared with the same iron load per unit surface area (thus, nearly the same iron dispersion and iron oxide species, as determined by XRD) showed increased effectiveness factors, as a consequence of the improved catalyst dispersion. For the latter samples, the differences found in the OII elimination performances are due to the different support particle sizes, because molecules are subjected to increased internal mass transfer resistances when d_p increases. Even so, for $d_p < 0.80$ mm, catalysts operate in chemical regime.

References

[1] R. Ubago-Pérez, F. Carrasco-Marín, D. Fairén-Jiménez, C. Moreno-Castilla, Granular and monolithic activated carbons from KOH-activation of olive stones, Microporous Mesoporous Mater. 92 (2006) 64-70.

[2] H. Tagawa, Thermal decomposition temperatures of metal sulphates, Thermochim. Acta 80 (1984) 23-33.

[3] R. Zboril, M. Mashlan, D. Krausova, P. Pikal, Cubic β-Fe_2O_3 as the product of the thermal decomposition of $Fe_2(SO_4)_3$, Hyperfine Interact. 120/121 (1999) 497-501.

[4] M.P. Morales, C. Pecharroman, T.G. Carreñ, C.J. Serna, Structural Characteristics of Uniform γ-Fe_2O_3 Particles with Different Axial (Length/Width) Ratios, J. Solid State Chem. 108 (1994) 158-163.

[5] F. Duarte, F.J. Maldonado-Hódar, L.M. Madeira, Influence of the characteristics of carbon materials on their behaviour as heterogeneous Fenton catalysts for the elimination of the azo dye Orange II from aqueous solutions, Appl. Catal., B 103 (2011) 109-115.

[6] F. Duarte, F.J. Maldonado-Hódar, A.F. Pérez-Cadenas, L.M. Madeira, Fenton-like degradation of azo-dye Orange II catalyzed by transition metals on carbon aerogels. Appl. Catal., B 85 (2009) 139-147.

[7] S. Sabhi, J. Kiwi, Degradation of 2,4-dichlorophenol by immobilized iron catalysts, Water Res. 35 (2001) 1994-2002.

[8] R.M. Sellers, Spectrophotometric determination of hydrogen peroxide using potassium titanium (IV) oxalate, Analyst 105 (1980) 950-954.

[9] G.F. Froment, K.B. Bischoff, Chemical Reactor Analysis and Design, John Wiley & Sons, New York, 1979.

[10] H.S. Fogler, Elements of Chemical Reaction Engineering, 4th Ed., Prentice Hall, Massachusetts, 2005.

[11] J.C. Crittenden, R.R. Trussell, D.W. Hand, K.J. Howe, G. Tchobanoglous, Water Treatment: Principles and Design, 2nd Ed., John Wiley & Sons, New Jersey, 2005.

CHAPTER 7 - Treatment of textile effluents by the heterogeneous Fenton process in a continuous packed-bed reactor using Fe/activated carbon as catalyst

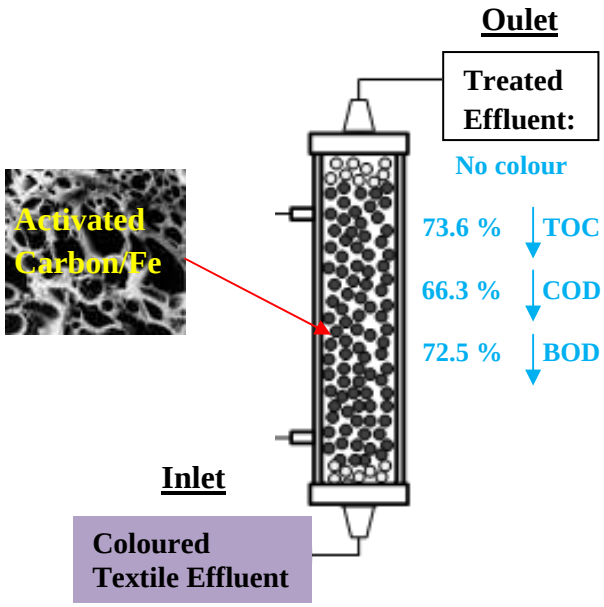

Chapter 7. Treatment of textile effluents by the heterogeneous Fenton process in a continuous packed-bed reactor using Fe/activated carbon as catalyst *

Abstract

This Chapter deals with the treatment of textile effluents by the heterogeneous Fenton-like process in a fixed-bed reactor filled with a catalyst based on activated carbon impregnated with iron (AC/Fe). In a preliminary stage it was used the dye Alcian Blue (A,B,C,D-tetrakis(Pyridiniomethyl) Cu(II) phthalocyanine chloride), AB, as model compound. The catalyst is essentially microporous, with large micropores and some mesopores, able to partially adsorb the dye. The stability of the catalyst was checked with 5 consecutive runs, without significant loss of activity (less than 5 %). Then, the effect of the main operating conditions was analyzed, and the H_2O_2 dose, pH and temperature optimized; the best conditions found using $C_{AB,feed}$ = 0.01 mM and a contact time of 3.3 g.min.ml^{-1} were: $C_{H2O2,feed}$ = 30 mM, pH 2.5 and T = 50 ºC, with which it was achieved, at steady-state, 93.2 % of discoloration and 54.1 % of total organic carbon (TOC) removal. It was verified that pH had a preponderant effect in the oxidation performance. Finally, the selected catalytic system was applied to the treatment of a real textile effluent used in the cotton dyeing. It was achieved almost total discoloration (96.7 %) and a strong abatement of the TOC – 73.6 %, as well as of the chemical oxygen demand (COD) – 66.3 %, and biochemical oxygen demand (BOD_5) – 72.5 %. The iron leached reached very low levels in every run, which is a crucial factor for the catalyst long-term use.

* Adapted from: F. Duarte, F.J. Maldonado-Hódar, L.M. Madeira, 2013, submitted.

7.1. Introduction

Different parameters like the activated carbon (AC) support characteristics, iron precursor salt, support particle size, among others, were already studied in this thesis in order to optimize the AC/Fe Fenton-like catalysts. Besides, in the literature, this heterogeneous process has already been deeply studied in batch mode, analyzing the influence of the main important operation conditions, but very few works employed a continuous system, in spite of having several advantages regarding batch reactors. Moreover, none has applied such heterogeneous catalytic reactors to the treatment of real textile effluents.

Thus, this part of the work covers the treatment of textile effluents by the heterogeneous Fenton process in a continuous packed-bed reactor filled with the AC/Fe catalyst previously selected (AC Norit RX 3 Extra, d_p between 0.80 and 1.60 mm, impregnated with iron (II) acetate). The main operating conditions (H_2O_2 dose, pH and temperature) were optimized using the Alcian Blue (A,B,C,D-tetrakis(Pyridiniomethyl) Cu(II) phthalocyanine chloride) dye (herein simply called AB) as model compound, and the stability of the AC packed-bed was also checked. Then, the optimized system was applied to the treatment of a real textile effluent generated during the cotton dyeing stage.

7.2. Materials and methods

The catalyst was prepared as has being described throughout this thesis, using the AC Norit EX 3 Extra as support (Chapter 3), with particles' diameter in the range of 0.80 – 1.60 mm (Chapter 6) and iron (II) acetate as the salt precursor (Chapter 4). N_2 (77 K) adsorption and XRD techniques were used to characterize the catalyst – further details of the techniques are given in Chapter 2, section 2.3.

Catalytic runs were carried out in the set-up described in section 2.4.2. (Chapter 2), using a fixed-bed reactor. The model dye compound used was the commercially named Alcian Blue-tetrakis(methylpyridinium) chloride (AB) - 0.01 mM in the feed, supplied by Sigma-Aldrich and widely used in the textile industry. It has a dark blue

colour and it is a large molecule (Fig. 7.1), with molecular weight of 1086.38 $g.mol^{-1}$. The molecular dimensions were estimated by using the appropriate software of molecular modelling (Hyperchem). As observed in Fig. 7.1, the final aromatic rings of the ligands are rotated regarding the main plane of the chemical structure, avoiding the flat shape of the molecule and increasing the molecular dimension up to 0.69 nm.

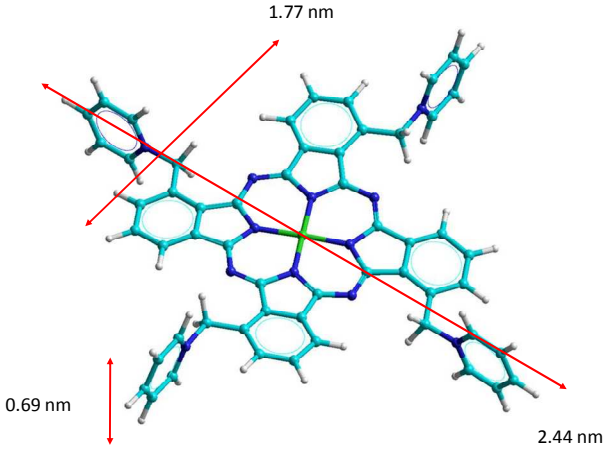

Figure 7.1 – Alcian Blue (A,B,C,D-tetrakis(Pyridiniomethyl) Cu(II) phthalocyanine chloride) structure and dimensions.

As this study was focused on the results in the steady state, experiments were initiated with the saturation of the AC/Fe bed with AB dye; this way, the time of the oxidation reactions is shortened. Between experiments the catalyst bed was flushed with distilled water to remove the inter-particle dye in excess and make the absorbance turn to zero.

Dye concentration was followed by UV/Vis spectrophotometry at 609 nm (characteristic wavelength of AB). Besides, in all oxidation experiments, samples were regularly taken for total organic carbon analysis (TOC) and to determine the iron leached (iron left from the support); it was also analysed the H_2O_2 concentration at the reactor outlet (by application of the colorimetric method developed by Sellers [1]). Eq. (7.1) was employed to estimate the iron loss ($Fe_{leached}$):

$$Fe_{leached} = \int_0^t C_{Fe} Q dt \qquad (7.1)$$

where C_{Fe} is the iron concentration at the time t and Q stand for the volumetric flow rate.

The real textile effluent (λ_{max} = 600 nm) was supplied by Têxteis Luís Simões and characterized in terms of the biochemical oxygen demand (BOD_5) and the chemical oxygen demand (COD), which were evaluated following the Standard Methods [2]. In short, BOD_5 was determined by the method of dilutions and it is expressed by the oxygen needed by aerobic organisms to degrade the biodegradable organic matter during 5 days, at 20 ºC - Method 5210 B. COD was determined by acidic digestion (open reflux) method at 150 ºC for 2 hours, using potassium dichromate as oxidant, followed by a titration with iron (II) sulphate and ammonia – Method 5220 B. Both COD and BOD_5 were measured in duplicate.

7.3. Results and discussion

7.3.1. Catalyst characterization and dye adsorption

Table 7.1 shows the results of the activated carbon support and iron-impregnated catalyst textural characterization. In spite that the deposition of the Fe particles on the carbon surface (N-Fe catalyst) led to certain pore blockage concerning the support (N – Norit activated carbon), the Fe-catalyst maintained a high micropore volume and surface area values. The micropore width (L_0) also decreased, indicating that the Fe-particles can be located inside this porosity range. By analyzing the shape of the N_2 adsorption isotherms (Figure 7.2), it is clear that the support is eminently a microporous material, although the large knee of the isotherm denotes a heterogeneous microporosity. Moreover, the small hysteresis cycle denotes the existence of certain mesoporosity. The microporosity was assessed by applying the DR equation, as previously described (section 2.3.1. – Chapter 2). A broad pore size distribution was obtained also by analyzing the N_2 adsorption isotherms in different adsorption ranges: $0.0 < P/P_0 < 0.1$ corresponds to the adsorption into primary micropores (smaller than 0.8 nm), $0.1 < P/P_0 < 0.4$ into secondary micropores (0.8 – 2.0 nm), and $0.4 < P/P_0 < 0.95$ corresponds to the adsorption in mesopores [3].

Table 7.1. Textural characteristics of the N (Norit activated carbon) support and N-Fe catalyst.*

Sample	S_{BET} ($m^2.g^{-1}$)	W_0 ($cm^3.g^{-1}$)	L_0 (nm)	V_{meso} ($cm^3.g^{-1}$)
N	1110	0.48	1.64	0.06
N-Fe	966	0.41	1.58	0.05

* S_{BET}: BET surface area; W_0: micropores' volume; L_0: mean micropores' size; V_{meso}: mesopores' volume.

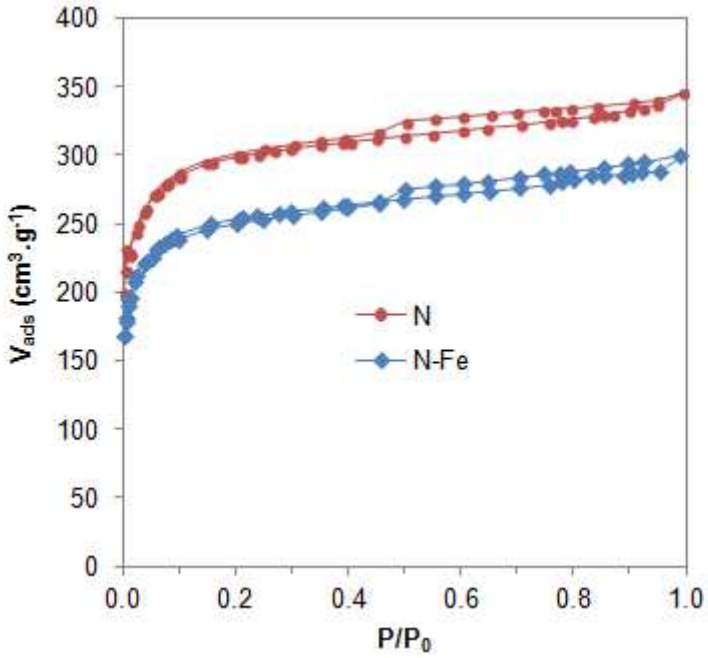

Figure 7.2 – N_2 adsorption/desorption isotherm of the N support and N-Fe catalyst.

The XRD pattern of the N-Fe catalyst – Fig. 7.3 – presented peaks with I_{30} at 30.1 º (220 reflection), I_{100} at 35.5 º (311 reflection), I_{30} at 56.8 º (511 reflection) and I_{40} at 62.2 º (440 reflection), showing the presence of magnetite (Fe_3O_4, JCPDS 88-0866). The low intensity of the diffraction peaks are indicative of the small Fe-particle size (high dispersion) reached on the support porosity.

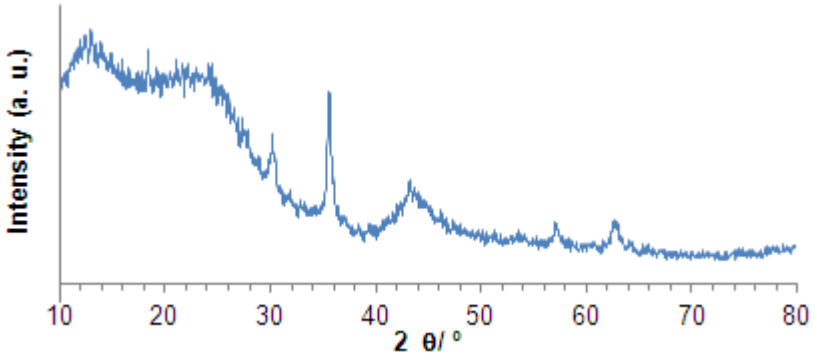

Figure 7.3 – XRD pattern of the N-Fe catalyst.

As mentioned above (section 7.2), the AC/Fe column was saturated with AB before the catalytic runs. The adsorption capacity calculated by integrating the breakthrough adsorption curve was 2.93 mg AB / g of catalyst (W_{cat}/Q = 3.3 g.min.ml^{-1} – data not shown). These results confirm that in spite of the large size of the dye molecules they are adsorbed on the larger micropores and mesopores of the support, denoting the slit-shape of porosity where the dye molecules can be adsorbed taking into account the minimal molecular dimension (0.69 nm). The adsorption capacity is a relative low value comparing to other adsorption AC/dyes systems (*e.g.* [4]). Nevertheless, these results are in agreement with Mesquita *et al.* [5], whom have used a similar flow rate (2.5 ml.min^{-1}) and reported an adsorption capacity value of 2.88 mg of the Chicago Sky Blue dye (molar mass similar to the one of AB) per gram of a similar catalyst (Norit RX 3 Extra impregnated with iron (II) sulphate).

7.3.2. Stability of the AC/Fe catalyst

Activity loss might happen in the system employed due to different phenomena (iron leaching, porosity blockage, etc.). To check whether this could be of relevance for the parametric study, five consecutive catalytic runs were firstly carried out (up to steady-state, lasting in each case ca. 180 minutes). The runs were performed under the same operating conditions (pH 3, T = 30 ºC, and $C_{H2O2,\ feed}$= 1.75 mM). The stoichiometric amount of H_2O_2 to oxidize one mole of AB is 161 moles ($C_{56}H_{40}Cl_4CuN_{12} + 161H_2O_2 \rightarrow 56CO_2 + 174H_2O + 4HCl + Cu(NO_3)_2 + 10HNO_3$).

So, to degrade 0.01 mM of AB is necessary at least a 1.61 mM H_2O_2 solution. An excess of oxidant feed concentration was used in this section: 1.75 mM, (ratio of 1.09).

It was verified very small differences between the experiments (less than 5 %), both in terms of discoloration (Fig. 7.4a) and TOC removal (Fig. 7.4b). In the last run, it was achieved at steady-state 30 % and 26 % of colour and TOC removal, respectively. On the other hand, very low levels of leaching were obtained in every run, varying between 0.003 and 0.063 mg of Fe leached, corresponding to only 0.033 % (cumulative value) of the total iron present in the bed. These facts confirm the stability of the catalyst under the used conditions and, on the other hand, validate the further results in the parametric study.

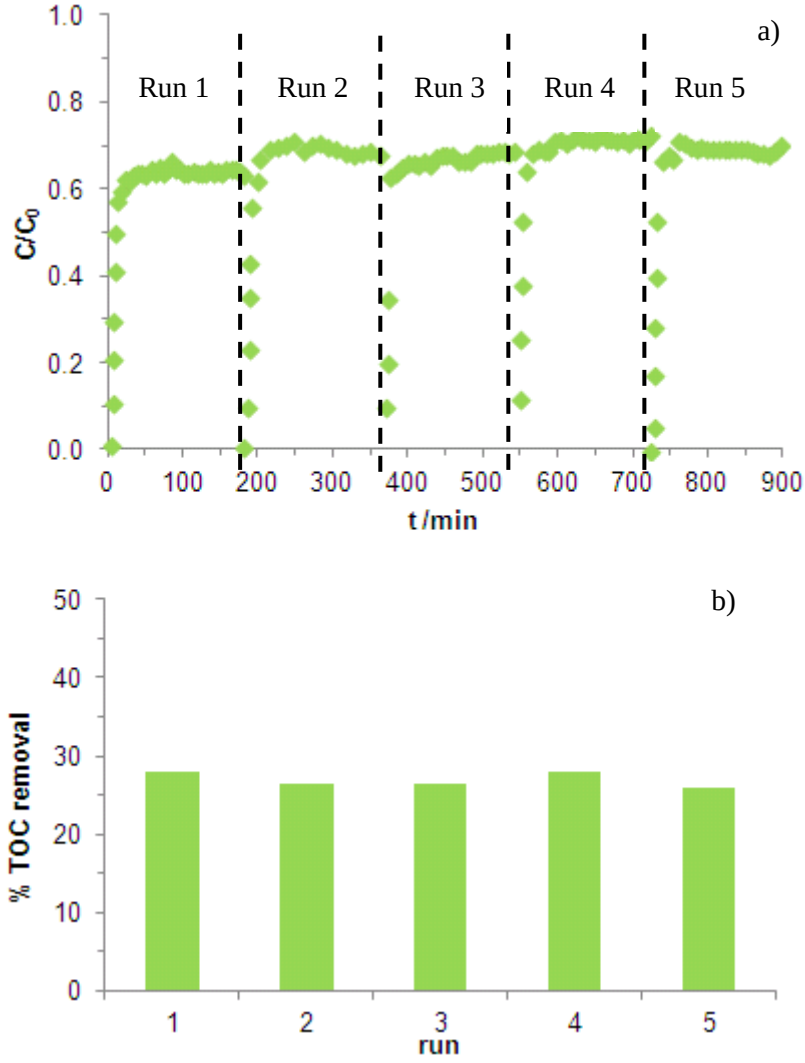

Figure 7.4 – AB elimination in terms of discoloration (a) and TOC removal (b) by the heterogeneous Fenton oxidation in 5 consecutive runs ($C_{H2O2,\,feed}$= 1.75 mM, pH 3, T = 30 ºC, W_{cat}/Q = 3.3 g.min.ml^{-1}).

7.3.3. Optimization of the H_2O_2 dose

As it was previously referred, it is necessary a H_2O_2 concentration of 1.61 mM to degrade a 0.01 mM AB solution. Because hydrogen peroxide participates in parallel reactions that do not produce the active species (hydroxyl radicals), particularly through a scavenging effect (Eq. 7.2), the dosage used is often quite above the stoichiometric one. So, the H_2O_2 feed concentration was varied in the range of 1.75 – 40 mM (ratios in the range of 1.09-24.84 *vs*. the stoichiometric dose) - Figure 7.5.

$$H_2O_2 + HO^{\bullet} \rightarrow HO_2^{\bullet} + H_2O \qquad (7.2)$$

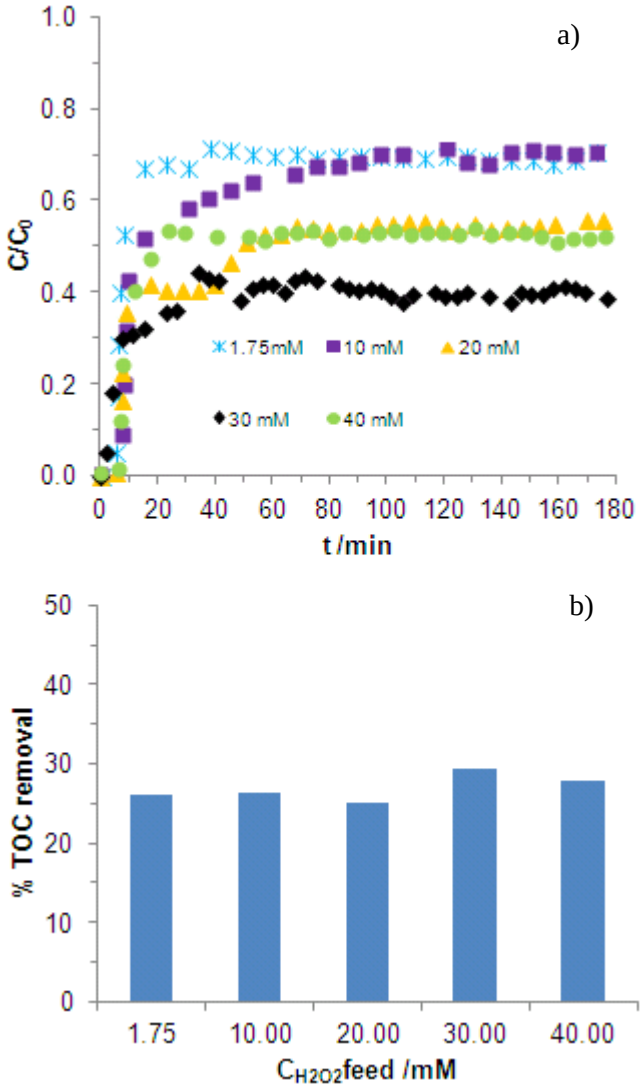

Figure 7.5 – Effect of the H_2O_2 feed concentration in the discoloration (a) and TOC removal (b) of the AB solution (pH 3, T = 30 ºC, W_{cat}/Q = 3.3 g.min.ml^{-1}).

Figure 7.5a shows that for the lower doses of oxidant (1.75 – 10.00 mM), dye removal under steady-state was only about 30 %, the conversion increasing for a 20.00 mM and particularly for a 30.00 mM dose of peroxide. As it can be observed, there is an optimum value for the H_2O_2 feed concentration, which is 30.00 mM (60 % of discoloration and 30 % of TOC removal were achieved), in spite of being more evident in terms of discoloration (Fig. 7.5a) rather than in terms of TOC removal (Fig. 7.5b). These results are in agreement with the literature, where is generally accepted that, as it was referred, the stoichiometric amount of oxidant is not enough, but on the other hand excess of H_2O_2 can lead to the scavenger effect. In such conditions, hydroxyl radicals are consumed in an undesirable way (Eq. 7.2) [6], contributing for the decrease of the Fenton's process efficiency [7-9]. It is noteworthy that Eq. 7.2 shows the production of another radical, but its oxidation potential is significantly lower than that of the hydroxyl radical one [10, 11]. As a consequence, for a 40.00 mM H_2O_2 feed concentration dye conversion decreases for the same level observed at a 20.00 mM dosage (Fig. 7.5a).

Concerning to iron leaching, it was not found a direct relation between the leaching levels reached and the H_2O_2 concentration. The leaching in these runs varied in the range of 0.009-0.142 mg of Fe, corresponding to a cumulative iron loss (i.e. in the 5 runs) of 0.08 % of the total iron initially present in the column.

Thus, further experiments were carried out with 30.00 mM of H_2O_2 in the reactor feed.

7.3.4. Effect of the pH

Experiments to optimize the pH were carried out in the range of 2.0 - 4.0. In fact, homogenous Fenton reactions usually run under acidic conditions (pH from ca. 2 to 4) because it leads to the optimum rate of free radicals generation [12-15].

In this study, it was observed an efficiency decrease of the heterogeneous Fenton reaction with the increase of the pH (Fig. 7.6a and 7.6b). This is probably related to the smaller stability of the oxidant at higher pH values that favour the decomposition of H_2O_2 into molecular oxygen instead of generating active species [16, 17]. A

significantly improved performance was noticed when the medium was strongly acidified. Actually, pH 2 improved significantly both the discoloration (93 % of colour removal) and TOC reduction (48 %). However, in terms of leaching, it was verified that more acidic conditions favoured the iron loss from the catalyst – Table 7.2. This fact was also observed by other authors [16, 18]. The total iron lost in this series of experiments was 0.64 % of the iron initially present inside the column reactor.

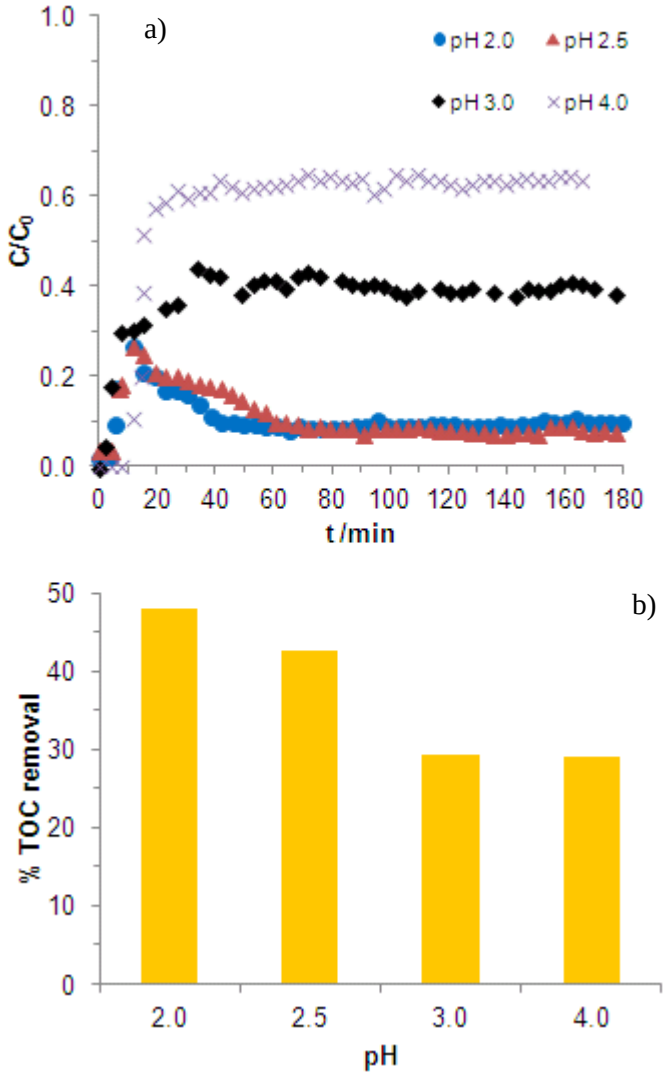

Figure 7.6 – Effect of the pH in the discoloration (a) and TOC removal (b) of the AB solution ($C_{H2O2}feed$ = 30 mM, T = 30 ºC, W_{cat}/Q = 3.3 g.min.ml^{-1}).

Table7. 2 – Iron leached after 3 hours for different pH values (experimental conditions as in Fig. 7.6).

pH	Fe leached (mg)	% Fe*
2.0	2.280	0.4914
2.5	0.455	0.0981
3.0	0.024	0.0052
4.0	0.197	0.0425

* Concerning to the total iron load present in the reactor.

Thus, after analyzing the trade-off between catalytic performances and leaching levels, pH 2.5 was considered as the best value, once colour elimination and TOC removal achieved at these conditions were very similar to pH 2.0 but the leaching obtained after 3 hours was significantly reduced (by a factor of 5).

7.3.5. Effect of the temperature

Temperature effect was also analysed in order to find the optimum value for this Fenton's reaction. A range of 10 – 70 ºC was used and the results are shown in Fig. 7.7. In a first stage, the pH of reference for Fenton's reactions was set (pH 3), but later on the optimal pH condition found in the previous section (pH 2.5) was employed together with the optimal temperature. It is observed that in the range 10 – 50 ºC, higher temperatures improved the process both in terms of colour and TOC removal, which is in agreement with the Arrhenius law either for radical's generation or for their attack to the organic molecules. In spite of that, at 70 ºC the oxidation is not further improved, and in terms of mineralization; a decrease was even clearly noticed (as compared to results at 50 ºC – Fig. 7.7b). The reason is that at high temperatures the decomposition of hydrogen peroxide into O_2 and H_2O is favoured, jeopardizing the HO• production, and, as consequence, the organics degradation. Thus, the optimal temperature was 50 ºC, which led to 74 % of discoloration and 37 % of TOC removal at steady-state. However, this optimal temperature did not lead to a significant degradation of the dye as that achieved at low pH. In fact, the pH seems to have a greater influence in this process than the temperature.

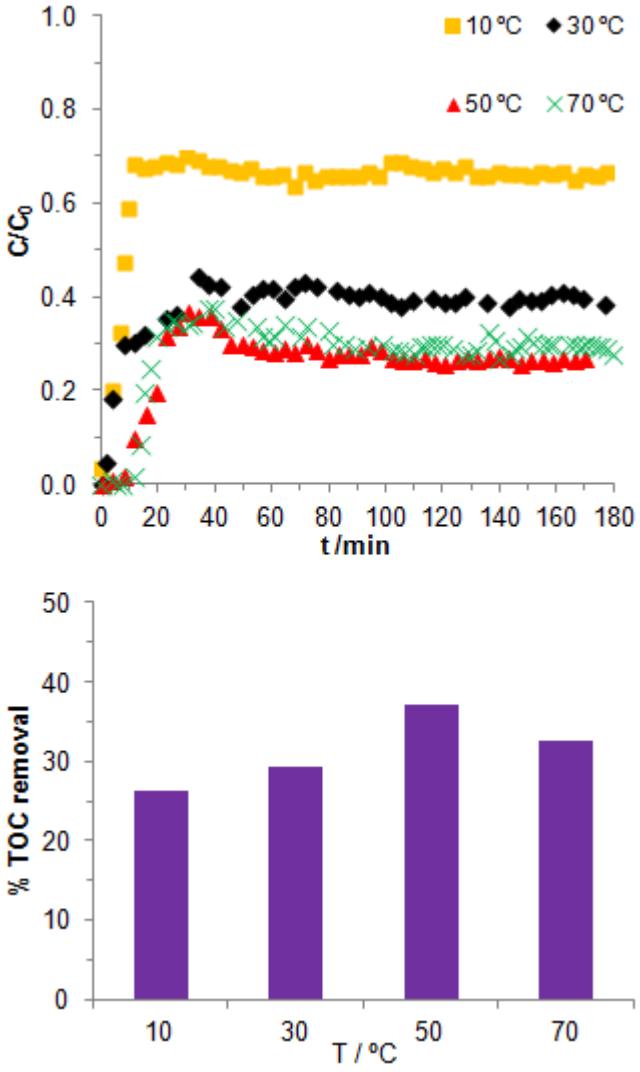

Figure 7.7 – Effect of the temperature in the discoloration (a) and TOC removal (b) of the AB solution ($C_{H2O2,feed}$ = 30 mM, pH 3, W_{cat}/Q = 3.3 g.min.ml^{-1}).

The runs at different temperatures led again to a very low iron leaching, in the range of 0.024 – 0.065 mg (0.04 % of total iron was lost in the 4 experiments together), and, curiously, no relation could be established between iron leaching and the reaction temperature, as it was observed in other works [16, 19].

The optimal conditions found of H_2O_2 feed concentration (30 mM), pH (2.5) and temperature (50 ºC) were then employed for the AB degradation (and also for the treatment of a real textile effluent - following section).

The history of colour elimination of the AB solution was very similar to those obtained using pH 2.0 and pH 2.5, at 30 ºC (Fig. 7.6a). However, at a temperature of 50

ºC, 93.2 % of colour removal was reached after 3 hours. TOC removal was the highest obtained (54.1 %), and iron leached did not exceed the 0.1 % of the total iron load present in the fresh AC/Fe bed. These results confirm the preponderance of the pH effect in the process efficiency.

7.3.6. Treatment of a real textile effluent

Finally this catalytic system ($C_{H2O2,feed}$ = 30 mM, pH 2.5, T = 50 ºC and W_{cat}/Q = 3.3 g.min.ml^{-1}) was applied to a real textile effluent generated by the dyeing process of cotton. The main characteristics of the effluent before and after treatment are resumed in Table 7.3. It is noteworthy that this experiment produced only a leaching of 0.36 % of the total iron (in 3 hours).

Table 7.3 – Textile effluent characterization and oxidation process efficiency.

Parameter	**Initial effluent**	**Treated effluent**	**% Removal** *
Absorbance (a.u.)	0.548	0.009	96.7
TOC (mg.L^{-1})	174.7	23.1	73.6
COD (mg.L^{-1})	495.0 ± 0.5	83.3 ± 0.3	66.3
BOD_5 (mg.L^{-1})	127.5 ± 3.2	17.5 ± 1.4	72.5

* Removal by oxidation alone, excluding the dilution effect caused at the reactor inlet.

As can be observed from Table 7.3, besides almost total discoloration of the real effluent, high removals of TOC, COD and BOD were achieved. Further work could include a parametric study for the optimization of the main operating conditions to treat the real textile effluent, namely the H_2O_2 dose, from which largely depends the cost of the process. Particularly, one should take into account that this could be significantly decreased for this particular effluent, which was used herein merely as a case-study to prove the concept.

Although the real effluent has a high organic load, it was possible to oxidize and mineralize it efficiently (cf. Table 7.3). This is probably due to the nature of the organic molecules present therein.

It is noteworthy that no H_2O_2 was detected in the reactor outlet in any experiment included in this Chapter, which means that in every situation the oxidant was totally consumed during the oxidation, in effective (production of active species) or non-effective ways. Moreover, the total mineralization was never achieved, even under the optimal conditions, which means that there were intermediate products that were not mineralized. After 60 h in operation, only ca. 1.25 % of the total Fe was left from the catalyst.

7.4. Conclusions

The aim of this Chapter was to treat a real textile effluent by the heterogeneous Fenton reagent in a packed-bed reactor filled with AC/Fe catalyst. Although this AOP has been much described in the literature for the degradation of dyes, very few studies reported the operation in the continuous mode.

N_2 adsorption/desorption showed that the catalyst is essentially microporous, with large micropores and some mesopores, and is able to partially adsorb the dye. The catalytic study began with the use of a model dye compound (AB) solution. The stability of the catalyst was proved with five consecutive runs without significant differences between catalytic performances (less than 5 %). At pH 3, T = 30 ºC and $C_{H2O2,feed}$ = 1.75 mM, 30 % of discoloration and 26 % of TOC removal was achieved in the 5th run at steady state, each one lasting ca. 3 h. The H_2O_2 dose used in these experiments showed to be scarce, being the optimal feed concentration 30.00 mM. Hydrogen peroxide concentrations above this threshold led to scavenger effects.

The oxidation reactions were jeopardized by high pH values and low temperatures, being the optimal values pH 2.5 and T = 50 ºC. Reaction pH seems however to have a stronger effect in the process performance, but it also affected significantly the iron leaching, with the acidic medium favouring the iron loss from the AC support. The optimal conditions (pH 2.5, T = 50 ºC and $C_{H2O2,feed}$ = 30.00 mM) were employed for the AB solution oxidation and also for the treatment of a real textile effluent. In the first case, 93 % of discoloration and the highest TOC removal (54 %) were achieved at steady state. The real textile effluent was treated with success, with an abatement of 73.6, 66.3 and 72.5 % of TOC, COD and BOD_5, respectively, and with an

almost complete discoloration (96.7 %). It is noteworthy that iron leaching was very low along all the study, with only 1.25 % of the total Fe initially present being left from the catalyst in 60 hours of operation.

References

[1] R.M. Sellers, Spectrophotometric determination of hydrogen peroxide using potassium titanium (IV) oxalate, Analyst 105 (1990) 950-954.

[2] APHA, AWWA, WEF, Standard Methods for the Examination of Water and Wastewater, 20th ed., American Public Health Association, AmericanWater Works Association, Water Pollution Control Federation, Washington DC, 1998.

[3] C.A. Moreno-Castilla, M.A. Alvarez-Merino, M.V. Lopez-Ramon, J. Rivera-Utrilla, Cadmium adsorption on different carbon adsorbents from aqueous solutions. Effect of surface chemistry, pore texture, ionic strength and dissolved natural organic matter, Langmuir, 20 (2004) 8142–8148.

[4] P.C.C. Faria, J.J.M. Órfão, M.F.R. Pereira, Adsorption of anionic and cationic dyes on activated carbons with different surface chemistries, Water Res. 38 (2004) 2043–2052.

[5] I. Mesquita, L.C. Matos, F. Duarte, F.J. Maldonado-Hódar, A. Mendes, L.M. Madeira, Treatment of azo dye-containing wastewater by a Fenton-like process in a continuous packed-bed reactor filled with activated carbon, J. Hazard. Mater. 237-238 (2012) 30-37.

[6] C. Walling, Fenton's reagent revisited, Acc. Chem. Res. 8 (1975) 125-131.

[7] M. Rodrígez, V. Sarria, S. Esplugas, C. Pulgarin, Photo-Fenton treatment of a biorecalcitrant wastewater generated in textile activities: biodegradability of the photo-treated solution, J. Photochem. Photobiol., A 151 (2002) 129-135.

[8] L. Núnez, J.A. García-Hortal, F. Torrades, Study of kinetic parameters related to the discoloration and mineralization of reactive dyes from textile dyeing using Fenton and photo-Fenton processes, Dyes Pigm. 75 (2007) 647-652.

[9] J.H. Ramirez, C.A. Costa, L.M. Madeira, Experimental design to optimize the degradation of the synthetic dye Orange II using Fenton's reagent, Catal.Today 107-108 (2005) 68-76.

[10] R.J. Bigda, Consider Fenton´s chemistry for wastewater treatment, Chem. Eng. Prog. 91(1995) 62-66.

[11] S.F. Santos, A. Alves, L.M. Madeira, Paraquat removal from water by oxidation with Fenton's reagent, Chem. Eng. J. 175 (2011) 279-290.

[12] F.J. Rivas, V. Navarrete, F.J. Beltran, J.F. Garcia-Araya, Simazine Fenton's oxidation in a continuous reactor, Appl. Catal., B 48 (2004) 249-258.

[13] E. Neyens, J. Baeyens, A review of classic Fenton's peroxidation as an advanced oxidation technique, J. Hazard. Mater. 98 (2003) 33-50.

[14] R.J. Watts, B.C. Bottenberg, T.F. Hess, M.D. Jensen, A.L. Teel, Role of reductants in the enhanced desorption and transformation of chloroaliphatic compounds by modified Fenton's reactions. Environ. Sci. Technol. 33 (1999) 3432-3437.

[15] E. Neyens, J. Baeyens, M. Weemaes, B.De Heyder, Pilot-scale peroxidation (H_2O_2) of sewage sludge, J. Hazard. Mater. 98 (2003) 91-106.

[16] J.H. Ramirez, F.J. Maldonado-Hódar, A.F. Pérez-Cadenas, C. Moreno-Castilla, C.A. Costa, L.M. Madeira, Azo-dye Orange II degradation by heterogeneous Fenton-like reaction using carbon-Fe catalysts, Appl. Catal., B 75 (2007) 312 - 323.

[17] J. Guo, M. Al-Dahhan, Catalytic wet oxidation of phenol by hydrogen peroxide over pillared clay catalyst, Ind. Eng. Chem. Res. 42 (2003) 2450-2460.

[18] J. Feng, X. Hu, P.L. Yue, Effect of initial solution pH on the degradation of Orange II using clay-based Fe nanocomposites as heterogeneous photo-Fenton catalyst, Water Res. 40 (2006) 641-646.

[19] F. Duarte, L.M. Madeira, Fenton- and photo-Fenton-like degradation of a textile dye by heterogeneous processes with Fe/ZSM-5 zeolite, Sep. Sci. Technol. 45 (2010) 1512-1520.

CHAPTER 8 - Conclusions and Future Work

Chapter 8. Conclusions and future work

8.1. Conclusions

This final part of the thesis provides a general overview of the work done, remarking the main results and achievements, as well as the most relevant conclusions.

The heterogeneous Fenton process was proposed to treat dye-containing solutions, as an alternative to the conventional physical and chemical ones, which have shown to be inefficient in dealing with complex and toxic substances, as dyes. Moreover, in some cases they simply transfer the pollutants to another phase, not destroying them. In addition, and as compared to the homogeneous Fenton process, with the used approach the formation of iron-containing sludge is avoided. Activated carbons (ACs) were chosen as the iron support because they are cheap materials, have high surface areas and highly developed porosity, and can be easily modified by suitable treatments.

The choice of the AC/Fe catalyst is fundamental for the good performance of the process and thus it has to be analysed carefully. In this thesis a deep study of the influence of several parameters regarding the development of AC/Fe catalysts was carried out in batch reactors, having in mind the implementation of a fixed-bed reactor to treat textile effluents in a continuous way. However, in the first stages, an azo-dye (Orange II – OII) was adopted as model compound.

The first remark goes to the influence of the AC support in the OII elimination from water. Three different commercial activated carbons were tested – Norit (N), Merck (M) and Kynol (K) – and it was found that high surface areas and the presence of large micropores/mesopores favoured the iron dispersion, leading however to opposite effects: the increase of catalytic activity and the decrease of catalyst stability (due to iron leaching). The N material was selected as the best AC support because it led to the most efficient catalyst, thanks to its textural properties. The surface of N support is catalytic active and it was shown that the oxidation reaction can take place both on the external surface of this AC and inside the micropores, which enables its regeneration by H_2O_2. However, its corresponding catalyst (N-Fe) showed to have a higher catalytic

ability towards the OII elimination, leading to 90 % of discoloration in ca. 4 h and a total organic carbon (TOC) removal of 61 % in 24 h.

After selecting the most promising AC support, the influence of the iron precursor salt in the development of AC/Fe catalysts was studied, using iron acetate, iron sulphate and iron nitrate to impregnate the Norit RX 3 Extra support. Depending on the interaction established between the iron precursor solution and the AC surface, different catalysts were obtained, with different textural porosities, different active phases and distinct Fe dispersions / locations. It was verified that iron particles located more externally in the ACs porous structure favoured the colour removal, but jeopardized the mineralization (observed for the case of N-$FeSO_4$ catalyst), while the iron particles located inside the micropores promote the TOC removal (due to a higher residence time of the oxidation reaction intermediates). This was the case of the N-Ac_2Fe catalyst, chosen as the best sample also due to the limited leaching levels observed. Characterization of the used samples corroborated the conclusions described, with the TPD experiments confirming the deeper oxidation of the dye and its by-products when using the N-Ac_2Fe catalyst.

To better understand the processes involved in the elimination of OII by the heterogeneous Fenton-like reagent using the catalyst previously selected (N support in the powder form impregnated with iron acetate), a deeper attention was paid to the spent samples, used both in adsorption and oxidation reactions. In the absence of H_2O_2, the TOC was completely removed and the OII molecules were adsorbed without degradation in the micropores. Regarding catalytic runs, different H_2O_2 doses were employed (in the range of 6-24 mM) but in all cases significant amounts of intermediate products stayed in solution, namely when using the highest oxidant concentration. As the dye is easily adsorbed, this fact should be assigned to the lower affinity between adsorbent-adsorbate (oxidation products). In spite of the better performance of the experiment using the lowest H_2O_2 initial concentration in terms of TOC removal, TPD and biodegradability experiments showed a higher mineralization of the by-products (more oxidized) when using the highest H_2O_2 dose (24 mM), which prevented their adsorption but decreased their toxicity.

Having in mind to implement later on a fixed-bed reactor to treat textile effluents, the AC particle size was also optimized (once the use of the catalyst in the powder form is not recommended in such columns). Catalysts were then prepared

(using the previously selected Norit RX 3 Extra as support and iron sulphate as a cheap salt precursor) in four size ranges – powder (< 0.15 mm), 0.25 – 0.80 mm, 0.80 – 1.60 mm and pellets (ca. 3 × 5 mm, as received). It was observed that the accessibility into the porosity of AC supports depends on the particle size. Decreasing the particle diameter (d_p) of the AC, the porosity is opened, favouring both the reagents accessibility and the Fe-dispersion and minimizing the mass transfer resistances. However, the leaching phenomenon was also promoted in this sense (pellets < 0.80-1.60 mm < 0.80-1.60 mm < powder). Thus, the intermediate sizes were considered the best option, particularly the catalyst with 0.80-1.60 mm, because it presented only slightly lower TOC removal values, but significant lower leaching levels. When a series of samples was prepared with the same Fe dispersion (same % Fe/S_{BET}), it was observed an increase in the effectiveness factors due to the better Fe dispersion on these samples. Here, the differences found in the OII elimination were only due to the increase of internal mass transfer resistances when d_p increases.

Finally a fixed-bed reactor filled with the AC/Fe previously selected (Norit RX 3 Extra, 0.80 < d_p < 1.60 mm, impregnated with iron acetate) was designed, tested and implemented with success. The effect of the main operating conditions was analysed in a wide range, including temperature (10 – 70 ºC), pH (2.0 – 4.0) and H_2O_2 dose (1.75 – 40.00 mM in the feed), using the Alcian Blue-tetrakis(methylpyridinium) chloride dye as model compound. It was found that pH has a preponderant effect on the process. Five consecutive runs under the same operating conditions (pH 3, T = 30 ºC, $C_{H2O2\ feed}$ = 1.75 mM and W_{cat}/Q = 3.3 g.min.ml^{-1}) were carried out without significant loss of activity (less than 5 %), confirming the stability of the catalyst under these conditions. The optimal conditions – T = 50 ºC, pH 2.5 and $C_{H2O2\ feed}$ = 30.00 mM – were applied to the treatment of a real textile effluent (proceeding from the cotton dyeing industry) in order to proved the concept. Almost total discoloration was achieved – 96.7 % and it was verified a strong abatement of TOC, chemical oxygen demand (COD) and biochemical oxygen demand (BOD_5): 73.6, 66.3 and 72.5 %, respectively. It is very important to retain that only 1.25 % of the total Fe initially present in the AC/Fe bed was lost from the support during the whole study using the fixed-bed reactor, i.e. in 60 hours of operation.

8.2. Suggestions for future work

There are still some important issues that should be covered in the future, following this work. In this section some suggestions are mentioned concerning the development of Fenton catalysts, the reactor configuration and the process/effluents to be treated.

8.2.1. Fenton catalysts

The study of the ability to regenerate the catalysts by suitable treatments is a key point. The catalysts should present insignificant or even no iron leaching and these treatments intend to recovery the blocked porosity by oxidation by-products. Several treatments – chemical, thermal and extraction - have already been employed for the regeneration of adsorbents. In Chapter 3 it was already shown that H_2O_2 is able to regenerate the activated carbon (AC) support and this treatment should be deeper studied once the oxidant is the same as used in the Fenton process and has already shown good results in regenerating other AC materials [1]. However, other chemical agents can also be applied (e.g. Co^{2+}/oxone [2]). Thermal treatments showed to be efficient in the recovery of ACs porosity too [3, 4] and, in the case of extraction, methanol can be a good option.

As it was already mentioned, the stability of the catalysts is crucial for their long term use. In this sense, strategies to eliminate the iron leaching should be further investigated. For instance, the study of thermal pre-treatment temperature (during the preparation of the catalysts) on their stability is a possibility, once it was verified the decrease of the iron leaching with the increase of the pre-treatment temperature in preliminary studies.

On the other hand, this thesis was mainly focused on finding correlations between textural properties of ACs and their ability to originate catalysts with good performances. However, the manipulation of the surface chemistry of the supports can also be used to improve the materials' behaviour. Several treatments have already been employed for ACs surface chemistry modification (cf. Cap. 1, section 1.2.2.3.), namely

oxidation with chemical agents to introduce surface groups and thermal treatments to remove selectively these groups. It has already been proved that the ACs surface chemistry plays an important role in the adsorption of dyes [5] and it should be determinant for the materials' performance as Fenton catalysts because this process involves both adsorption and catalysis phenomena.

Another point to be addressed would be the development of activated carbon-based Fenton catalysts from residues (agricultural, plastics, etc), which can be very interesting either in terms of valorisation of residues or process cost (cheap materials).

8.2.2. Reactor configuration

This thesis presented experimental work carried out firstly in batch reactors, but the main goal was to employ a fixed-bed reactor for the continuous treatment of effluents. However, other configurations can be tested, namely using a continuous stirred-tank reactor (CSTR) as a basket reactor. Such configurations can be useful because i) they allow to use smaller catalysts' particles, that lead to higher efficiency factors, avoiding the pressure's drop along the catalysts bed, and ii) the problem of the formation of gas bubbles during the treatment of strongly loaded effluents with organic matter is overcome.

8.2.3. Process / effluents

It would be important to test other real textile effluents or even wastewater coming from different industries particularly with high organic loads such as olive oil and cork cooking – two critical activities (among others) from the environmental point of view in Portugal, where they are intensively exploited. Moreover, it would be interesting to couple biological systems after the Fenton's treatment for such toxic/non-biodegradable effluents in order to reduce the H_2O_2 doses and, consequently, the operating costs of the process. On the other hand, the stability of the catalyst should be tested in long-term runs.

References

[1] M.H. Do, N.H. Phan, T.D. Nguyen, T.T.S. Pham, V.K. Nguyen, T.T.T. Vu, T.K.P. Nguyen, Activated carbon/Fe_3O_4 nanoparticle composite: Fabrication, methyl orange removal and regeneration by hydrogen peroxide, Chemosphere 85 (2011) 1269-1276.

[2] G. Zhou, H. Tian, H. Sun, S. Wang, C.E. Buckley, Synthesis of carbon xerogels at varying sol-gel pHs, dye adsorption and chemical regeneration, Chem. Eng. J. 171 (2011) 1399-1405.

[3] H.H. Tseng, M.Y. Wey, Study of SO_2 adsorption and thermal regeneration over activated carbon-supported copper oxide catalysts, Carbon 42 (2007) 2269-2278.

[4] G. Zhang, J. Qu, H. Liu, A.T. Cooper, R. Wu, $CuFe_2O_4$/activated carbon composite: A novel magnetic adsorbent for the removal of acid orange II and catalytic regeneration, Chemosphere 68 (2007) 1058-1066.

[5] M.F.R. Pereira, S.F. Soares, J.J.M. Órfão, J.L. Figueiredo, Adsorption of dyes on activated carbons: Influence of surface chemical groups, Carbon 41 (2003) 811-821.